DRYING OF NATURAL ZEOLITE POWDERS IN VIBRATED FLUIDIZED BEDS

A THESIS SUBMITTED TO
THE GRADUATE SCHOOL OF NATURAL AND APPLIED SCIENCES
OF
MIDDLE EAST TECHNICAL UNIVERSITY

BY

CİHAN ÖCAL

IN PARTIAL FULFILLMENT OF THE REQUIREMENTS
FOR
THE DEGREE OF MASTER OF SCIENCE
IN
CHEMICAL ENGINEERING

AUGUST 2013

Approval of the thesis:

DRYING OF NATURAL ZEOLITE POWDERS IN VIBRATED FLUIDIZED BEDS

Submitted by **Cihan Öcal** in partial fulfillment of the requirements for the degree of **Master of Science in Chemical Engineering Department, Middle East Technical University** by,

Prof. Dr. Canan Özgen _____
Dean, Graduate School of **Natural and Applied Sciences**

Prof. Dr. Deniz Üner _____
Head of Department, **Chemical Engineering**

Assoc. Prof. Dr. Görkem Külah _____
Supervisor, **Chemical Engineering Dept., METU**

Examining Committee Members

Prof. Dr. Nevin Selçuk _____
Chemical Engineering Dept., METU

Assoc. Prof. Dr. Görkem Külah _____
Chemical Engineering Dept., METU

Assoc. Prof. Dr. Murat Köksal _____
Mechanical Engineering Dept., Hacettepe University

Asst. Prof. Dr. Serkan Kıncal _____
Chemical Engineering Dept., METU

Assoc. Dr. Burcu Akata Kurç _____
Micro and Nanotechnology Dept., METU

Date: 28/08/2013

I hereby declare that all information in this document has been obtained and presented in accordance with academic rules and ethical conduct. I also declare that, as required by these rules and conduct, I have fully cited and referenced all material and results that are not original to this work.

Name, Last Name: Cihan Öcal

Signature:

ABSTRACT

DRYING OF NATURAL ZEOLITE POWDERS IN VIBRATED FUIDIZED BEDS

Öcal, Cihan

M.Sc., Department of Chemical Engineering

Supervisor: Assoc. Prof. Dr. Görkem Külah

August 2013, 108 pages

The objectives of this study were to characterize the fluidization behavior and the drying performance of a vibrated fluidized bed dryer operating with animal feed additive 'Clinoptilolite' bed material with a mean particle size of 3 microns, and determine the efficient operating conditions for the drying process. For this purpose, two fully equipped vibrated fluidized bed systems were designed and constructed for the analyses related to hydrodynamic and drying tests, respectively.

The hydrodynamic test results showed that the fluidization quality increased with both vibration strength and vibration frequency. Moisture content of the bed material was found to be very important on hydrodynamic parameters. Among the experimental conditions used in the hydrodynamic tests, the vibration strength of 1.8 and the vibration frequency of 40 Hz were chosen as the most effective vibration conditions for a high quality fluidization of the clinoptilolite powders. On the basis of the results of batch drying tests, drying curves indicated that the drying rate increased with the inlet gas temperature and superficial gas velocity. Based on a rough estimate of operating cost considering the electrical energy need for heating the drying gas, the conditions of 90 °C temperature and 10.5 mm/s gas velocity were recommended for a cost-effective continuous drying operation of clinoptilolite powders.

Keywords: Vibrated Fluidized Bed, Drying, Clinoptilolite

ÖZ

DOĞAL ZEOLİT TOZLARININ TİTREŞİMLİ AKIŞKAN YATAKTA KURUTULMASI

Öcal, Cihan

Yüksek Lisans, Kimya Mühendisliği

Tez Yöneticisi: Doç. Dr. Görkem Külah

Ağustos 2013, 108 sayfa

Bu çalışmanın amacı; ortalama parçacık boyutu 3 mikron olan hayvan yemi katkı maddesi 'Klinoptilolit' yatak malzemesi ile işletilen titreşimli bir akışkan yatağın akışkanlaşma davranışını ve kurutma performansını incelemek ve kurutma prosesinin ekonomik olarak gerçekleşmesini sağlayacak işletim koşullarını belirlemektir. Bu amaçla, hidrodinamik ve kurutma deneyleri ile ilgili analizleri gerçekleştirebilmek için iki adet tam donanımlı titreşimli akışkan yatak sisteminin tasarımı ve imalatı yapılmıştır.

Gerçekleştirilen hidrodinamik deneylerin sonuçları, titreşim uygulanmadığı koşulda yatak malzemesinin akışkanlaştırılamadığını göstermiştir. Titreşim uygulandığında ise yatağın akışkanlaşma kalitesi hem titreşim gücü hem de titreşim frekansı ile artmıştır. Yatak malzemesinin nem içeriğinin hidrodinamik parametreleri önemli ölçüde etkilediği tespit edilmiştir. Uygulanan diğer titreşim parametrelerinin arasında 1.8 titreşim gücü ve 40 Hz titreşim frekansı, ince toz haldeki klinoptilolit tozlarının kurutulması prosesinde yüksek akışkanlaşma kalitesinin elde edilebilmesi için en etkili koşullar olarak seçilmiştir. Kesikli kurutma deneylerinin sonuçları temel alındığında, kurutma eğrileri kurutma hızının gaz giriş sıcaklığı ve gaz hızı ile arttığını göstermiştir. En uygun işletim koşullarını belirlemek amacıyla, kurutucu gazı ısıtmak için sarf edilen elektrik enerjisi düşünülerek kabaca bir gider analizi yapılmış ve klinoptilolit tozlarının sürekli bir işletim ile ekonomik bir şekilde kurutulması için 90 °C sıcaklıktaki ve 10.5 mm/s gaz hızındaki işletim koşullarının uygulanması önerilmiştir.

Anahtar Kelimeler: Titreşimli Akışkan Yatak, Kurutma, Klinoptilolit

Dedicated to the memory of my beloved grandmother, Melek Öcal

ACKNOWLEDGEMENTS

I would like to express my sincere gratitude to my supervisor Assoc. Prof. Dr.Görkem Külah for her invaluable guidance and support throughout this work.

I am grateful to Assoc. Prof. Dr. Murat Köksal for his thoughtful guidance, extensive knowledge and valuable suggestions.

My sincerest appreciation goes out to Hasan Çelikli who has made a significant contribution to this work by providing technical services, always being ready whenever I was in need as well as his invaluable friendship which will last a lifetime.

I must say a special thank to my mother and brother for their endless support, tolerance and confidence throughout this study. I am also grateful to my love Dila for her patience and motivation.

I am greatly indebted to Zafer Çıplak and Kamil Gülsoy for their precious friendship and encouragement.

I must say a special thank to Burcu Gökbudak, Gökhan Çelik, Duygu Gerçeker, Tarık Yücel, Okan Özkök, Canan Şener, Melda Eskitoros, İlker Tezsevin, Atalay Çalışan, Mustafa Yasin Aslan, Seval Gündüz and Necip Berker Üner for their invaluable friendship and all the enjoyable times we spent together.

It is a pleasure for me to thank to Assoc. Prof. Dr. Haluk Külah and Burak Eminoğlu for their assistance in connection of microelectromechanical accelerometer device to my experimental set-up.

Thanks are due to Rota Mining Corporation for supplying animal feed additive zeolite mineral and personal communications.

I would like to thank to METU research fund BAP-03-04-2012-008 for the financial support of this study.

I would also like to acknowledge TÜBİTAK for providing research scholarship through the project 112M231.

TABLE OF CONTENTS

ABSTRACT v
ÖZ vi
ACKNOWLEDGEMENTS viii
TABLE OF CONTENTS ix
LIST OF TABLES xi
LIST OF FIGURES xii
LIST OF SYMBOLS xv
CHAPTERS 1
1. INTRODUCTION 1
1.1 Use of Natural Zeolites as Animal Feed Additive 1
1.2 Drying Phenomenon 3
1.2.1 General 3
1.2.2 Heating Methods 4
1.2.3 Drying of Powders 5
1.3 Fluidization Technology 7
1.3.1 Fundamentals of Fluidization 7
1.3.2 Geldart's Classification of Particles 8
1.3.3 Interparticle Forces Affecting Powder Fluidization 9
1.3.3.1 Van der Waals Forces 10
1.3.3.2 Electrostatic Forces 11
1.3.3.3 Capillary Forces 11
1.3.4 Effects of Cohesive Forces on Fine Particles 12
1.4 Drying Process in Fluidized Bed Dryers 13
1.5 Vibrated Fluidized Bed (VFB) Drying 14
2. LITERATURE SURVEY 17
2.1 Basic Concepts 17
2.2 Hydrodynamics of Vibrated Fluidized Beds 18
2.2.1 Effect of Vibration on Pressure Drop Across the Bed 25
2.2.2 Effect of Vibration on Minimum Fluidization Velocity 30
2.2.3 Effect of Vibration on Bed Expansion and Bed Voidage 31
2.3 Drying Characteristics of Vibrated Fluidized Beds 32
2.3.1 Effect of Vibration Parameters 37
2.3.2 Effect of Gas Inlet Temperature and Superficial Gas Velocity 37
2.3.3 Effect of Static Bed Height 38
2.3.4 Effect of Initial Surface Moisture Content 38
3. EXPERIMENTAL 39
3.1 Experimental Set-Up 39
3.1.1 Vibration System 39

3.1.2 Experimental Set-Up and Method for Hydrodynamic Tests 40
3.1.3 Experimental Set-Up and Method for Drying Tests 45
3.2 Properties of Clinoptilolite Particles 51
4. RESULTS AND DISCUSSION 55
4.1 Hydrodynamic Tests 55
4.1.1 Effect of Vibration on Pressure Drop Across the Bed 55
4.1.2 Effect of Vibration Parameters on Minimum Fluidization Velocity 59
4.1.3 Effect of Vibration Parameters on Bed Expansion Ratio 61
4.1.4 Agglomerate Size 66
4.2 Drying Tests 68
4.2.1 Reproducibility 68
4.2.2 Determination of Drying Curves 70
4.2.3 Effects of Operating Conditions on Drying Curves 75
4.2.3.1 Superficial Gas Velocity 75
4.2.3.2 Inlet Gas Temperature 80
4.2.4 Drying Time and Cost Analysis 82
5. CONCLUSIONS 85
5.1 Hydrodynamics 85
5.2 Drying 85
5.3 Suggestions for Future Work 86
REFERENCES 87
APPENDICES 93
A. CALIBRATION 93
B. DRYING CURVE GENERATION CODE IN MATLAB 97
C. REPRODUCIBILITY OF DRYING TESTS 99
D. SAMPLE CALCULATION FOR COST ANALYSIS 107

LIST OF TABLES

TABLES

Table 1.1 Comparison of dryer types operating with powders 6

Table 2.1 Major experimental studies on hydrodynamics of vibrated fluidized beds 19
Table 2.2 Major experimental studies on vibrated fluidized bed drying 33

Table 3.1 Operational conditions used in hydrodynamic tests 44
Table 3.2 Operational conditions used in drying tests 50

Table 4.1 Effect of operating conditions on drying times to obtain dry product with 8% (w.b.) moisture content 82
Table 4.2 Daily cost of drying operation to obtain dry product with 8% (w.b.) moisture content in a continuous VFB dryer of 1000 kg/h capacity (Bed areas are given in parenthesis) 83

LIST OF FIGURES

FIGURES

Figure 1.1 Photographs of clinoptilolite powders A) Standard B) SEM 2
Figure 1.2 Types of moisture content (Based on [13]) 4
Figure 1.3 Different regimes of fluidization: (A) Fixed Bed (B) Minimum Fluidization (C) Bubbling Fluidization (D) Slugging (E) Turbulent Fluidization (F) Pneumatic Transport (Based on [16]) 7
Figure 1.4 Geldart's classification of particles 8
Figure 1.5 Liquid bridge between two spherical particles 12
Figure 1.6 Transfer mechanisms in a fluidized bed dryer 13
Figure 1.7 Characteristic curves of convective drying (modified from [14]) 14

Figure 2.1 An ideal pressure drop curve of fluidization 25
Figure 2.2 Variations of fluidization index curves in real cases of vibrated fluidization 26
Figure 2.3 ΔP-U_0 diagram of a vibrated fluidized bed (Modified from [41]) 27
Figure 2.4 Types of pressure drop-velocity curves in fluidized beds (FB) and vibrated fluidized beds (VFB) (Modified from [42]) 28

Figure 3.1 Mechanical vibration system 40
Figure 3.2 Fluidized bed apparatus used in hydrodynamic experiments 41
Figure 3.3 Experimental set-up: 1) N_2 Tube 2) Rotameter 3) DC Supply 4) Inverter 5) Vibro-motor 6) Pressure Transducer 7) Accelerometer 8) Fluidized Bed 9) Bag Filter 10) Data Acquisition Card 11) Computer 12) Digital Camera 42
Figure 3.4 Sintered porous metal gas distributor 43
Figure 3.5 Block diagram of LabVIEW program for hydrodynamic tests 45
Figure 3.6 Virtual interface of LabVIEW program for hydrodynamic tests 45
Figure 3.7 Fluidized bed dryer 46
Figure 3.8 A photograph of the vibrated fluidized bed dryer system 47
Figure 3.9 Experimental set-up: 1) N_2 Tube 2) Rotameter 3) DC Supply 4) Inverter 5) Vibro-motor 6) Pressure Transducer 7) Accelerometer 8) Fluidized Bed 9) Exhaust Duct 10) Data Acquisition Card 11) Computer 12) Heater 13) PID controller TC: Thermocouple, RH-T: Relative Humidity and Temperature Sensor 48
Figure 3.10 Block diagram of LabVIEW program for drying tests 50
Figure 3.11 Virtual interface of LabVIEW program for drying tests 51
Figure 3.12 X-Ray Diffraction pattern of clinoptilolite 52
Figure 3.13 Quantitative analysis of clinoptilolite by reference intensity ratio method 52
Figure 3.14 Thermogravimetric analysis of clinoptilolite 53
Figure 3.15 Particle size analysis of clinoptilolite 53
Figure 3.16 Scanning electron micrograph used for determination of sphericity 54

Figure 4.1 Fluidization index curves for bed material of 9 % moisture content a) No vibration b) Λ= 1.8, f=20 Hz 56
Figure 4.2 Fluidization index curves for bed material of 15 % moisture content (Λ=1.8, f=20 Hz) 57
Figure 4.3 Effect of vibration strength on fluidization index curves (X= 9 %) (a)f=30 Hz, (b)f=40 Hz..... 58
Figure 4.4 Fluidization index with different vibration conditions for decreasing gas velocity (Λ=1.8, X= 9 %) 59
Figure 4.5 Fluidization index with different vibration conditions for decreasing gas velocity (Λ =1.8, X= 15 %) 59
Figure 4.6 Determination of minimum fluidization velocity (Λ=1.8, f=30 Hz, X= 15 %). 60
Figure 4.7 Effects of vibration conditions on minimum fluidization velocity (X= 9 %) 61
Figure 4.8 Effects of frequency and moisture content on minimum fluidization velocity (Λ=1.8) 61
Figure 4.9 Effect of vibration frequency on bed expansion ratio (X= 9 %) (a) Λ=1.5, (b) Λ=1.8..... 62
Figure 4.10 Effects of vibration strength on bed expansion ratio (f=40 Hz, X= 9 %) 63
Figure 4.11 Effects of frequency and moisture content on bed expansion ratio (Λ=1.8).... 64
Figure 4.12 Effects of vibration parameters on bed voidage at minimum fluidization 65
Figure 4.13 Effects of frequency and moisture content on bed voidage at minimum fluidization 66
Figure 4.14 Effect of moisture content on agglomerate size 67
Figure 4.15 Effect of vibration conditions on agglomerate size 67
Figure 4.16 Reproducibility of drying tests (T_{in}=60 °C, T_{out}=55°C, U_o=15.8 mm/s) 69
Figure 4.17 Reproducibility of the drying tests in terms of moisture content (T_{in}=60 °C, T_{out}=55°C, U_o=10.5 mm/s)..... 70
Figure 4.18 Comparison of drying curves obtained from intermittent bed material sampling and continuous exhaust *RH* measurements (T_{in}=60 °C) 72
Figure 4.19 Comparison of drying curves obtained from intermittent bed material sampling and continuous exhaust *RH* measurements (T_{in}=80 °C) 73
Figure 4.20 Comparison of drying curves obtained from intermittent bed material sampling and continuous exhaust *RH* measurements (T_{in}=90 °C) 74
Figure 4.21 Moisture content and bed temperature profiles (T_{in}=60 °C)..... 75
Figure 4.22 Moisture content and bed temperature profiles (T_{in}=80 °C)..... 76
Figure 4.23 Moisture content and bed temperature profiles (T_{in}=90 °C)..... 76
Figure 4.24 Drying curves of clinoptilolite (T_{in}=60 °C, U_0=21 mm/s)..... 77
Figure 4.25 Effect of gas velocity on drying rate (T_{in}=60 °C)..... 78
Figure 4.26 Effect of gas velocity on drying rate (T_{in}=80 °C)..... 79
Figure 4.27 Effect of gas velocity on drying rate (T_{in}=90 °C)..... 79
Figure 4.28 Effect of temperature on moisture content profiles 81

Figure A.1 Calibration graph of PX142-005D5V model pressure transducer (V_{offset} =1.018) 93

Figure A.2 Calibration graph of Keller 0-160mbar model pressure transducer (V_{offset} =1.918 Volt) 94
Figure A.3 Calibration graph of PCMini52 model relative humidity sensor (V_{offset}=0.007 Volt) 95
Figure A.4 Calibration graph of PCMini52 model temperature sensor (V_{offset}=2.152 Volt) 95
Figure A.5 Calibration graph of MEMs accelerometer (V_{offset}=2.38 Volt) 96

Figure C.1 Reproducibility of drying tests (T_{in}=60 °C, T_{out}=55°C, U_o=10.5 mm/s) 99
Figure C.2 Reproducibility of drying tests (T_{in}=60 °C, T_{out}=55°C, U_o=21 mm/s) 100
Figure C.3 Reproducibility of drying tests (T_{in}=80 °C, T_{out}=77°C, U_o=10.5 mm/s) 101
Figure C.4 Reproducibility of drying tests (T_{in}=80 °C, T_{out}=77°C, U_o=15.8 mm/s) 102
Figure C.5 Reproducibility of drying tests (T_{in}=80 °C, T_{out}=77°C, U_o=21 mm/s) 103
Figure C.6 Reproducibility of drying tests (T_{in}=90 °C, T_{out}=85.5°C, U_o=10.5 mm/s) 104
Figure C.7 Reproducibility of drying tests (T_{in}=90 °C, T_{out}=85.5°C, U_o=15.8 mm/s) 105
Figure C.8 Reproducibility of drying tests (T_{in}=90 °C, T_{out}=85.5°C, U_o=21 mm/s) 106

LIST OF SYMBOLS

A	Cross-sectional or effective surface area, m^2
a	Vibration amplitude, m
Ar	Archimedes number, -
b	A specific constant dependent on particle properties, -
C_P	Heat capacity, kJ kg^{-1} K^{-1}
$Cost$	Electrical energy cost for heating ambient air, Kr
D	Effective moisture diffusivity, m^2 s^{-1}
D_0	Arrhenius factor, m^2 s^{-1}
d_a	Mean agglomerate size, m
d_p	Mean particle size, m
E	Activation energy for diffusion, kJ $kmol^{-1}$
E_c	Cohesive force effect
E_g	Gravitational force effect
F_c	Interparticle cohesive force, N
F_E	Electrostatic force, N
F_l	Capillary force, N
F_v	van der Waals force, N
f	Vibration frequency, Hz
g	Gravitational acceleration, m s^{-2}
H	Bed height, m
H_0	Initial bed height, m
H_{mf}	Bed height at minimum fluidization, m
h_H	Interphase heat transfer coefficient, kW m^{-2} K^{-1}
h_M	Interphase mass transfer coefficient, kg m^{-2} s^{-1}
J	Mass transfer rate, kg s^{-1}
m	Mass of the bed material, kg
$\dot{M}_g$	Mass flow rate of dry gas, kg s^{-1}
M_s	Mass hold-up of dry solid, kg
$\dot{M}_s$	Mass flow rate of dry solid, kg s^{-1}
N	Drying rate, kg kg^{-1} s^{-1}
N_c	Constant drying rate, kg kg^{-1} s^{-1}
P	Pressure, Pa
P_{sat}	Saturated water vapor pressure, Pa
P_v	Partial pressure of water vapor, Pa
Q	Heat transfer rate, kJ s^{-1}
R	Specific gas constant, J mol^{-1} K^{-1}
RH	Relative humidity, %

R_g	Specific gas constant of drying gas, J mol^{-1} K^{-1}
R_v	Specific gas constant of water vapor, J mol^{-1} K^{-1}
r	Radius, m
Re	Reynolds number, -
Re_{mf}	Reynolds number at minimum fluidization, -
S	Hamaker constant, J
T	Temperature, K
T_{amb}	Ambient temperature of drying gas, K
T_{in}	Gas inlet temperature, K
T_{out}	Gas outlet temperature, K
T_s	Solid temperature at the interface, K
t	Time, s
t_R	Mean particle residence time, s
U_0	Superficial gas velocity, m s^{-1}
U_{mb}	Minimum bubbling velocity, m s^{-1}
U_{mf}	Minimum fluidization velocity, m s^{-1}
U_{mf}	Minimum fluidization velocity, m s^{-1}
V	Volume, m^3
W	Electrical energy cost for industrial site, Kr kW^{-1} h^{-1}
X	Moisture content of the bed material, kg kg^{-1}
X_{air}	Bulk moisture content of air, kg kg^{-1}
X_c	Critical moisture content, kg kg^{-1}
X_s	Moisture content of air at the interface, kg kg^{-1}
X^*	Equilibrium moisture content, kg kg^{-1}
$\bar{X}$	Average moisture content of the bed material, kg kg^{-1}
Y	Humidity, kg kg^{-1}
Y_{in}	Humidity of inlet drying gas, kg kg^{-1}
Y_{out}	Humidity of exhaust drying gas, kg kg^{-1}
z	Separation distance between spheres, m

Greek symbols

ΔP	Pressure drop across the bed, Pa
ΔP_{max}	Maximum pressure drop, Pa
ΔP_{mf}	Pressure drop at minimum fluidization, Pa
Λ	Vibration strength, -
α_0	Dielectric constant, F m^{-1}
δ	Liquid surface tension, N m^{-1}
ε	Bed voidage, -
ε_{mf}	Bed voidage at minimum fluidization, -
θ	Contact angle, °

μ	Viscosity of the fluid, Pa s
ρ	Density, kg m^{-3}
ρ_a	Apparent density of the bed, kg m^{-3}
ρ_{ab}	Aerated bulk density of the bed, kg m^{-3}
ρ_f	Density of fluid, kg m^{-3}
ρ_g	Density of fluidizing gas, kg m^{-3}
ρ_p	Particle density, kg m^{-3}
ρ_{tb}	Tapped bulk density of the bed, kg m^{-3}
$\sigma_{1,2}$	Charge densities, C m^{-2}
ω	Angular frequency of vibration, rad s^{-1}
Φ_s	Sphericity of particle, -

CHAPTER 1

INTRODUCTION

1.1 Use of Natural Zeolites as Animal Feed Additive

Mycotoxins are toxic byproducts of mold species which grows on stocked grains, feeds and some types of meadow grass. They are highly toxic, carcinogenic, teratogen (inhibiting standard growing up of fetus and causing various anomalies) and mutagen (causing mutations on DNA and RNA) substances. Thus, taking mycotoxic product directly or through meat and dairy products of the animals which eat mycotoxic feeds is too risky for health. Some of the bacteria in the feed are secreted inside the feed and some of them are secreted by the animals' organism after eating it [1].

In recent years, natural zeolites which adsorb the toxic substances inside of the feeds and have no bad effect (nontoxic) on animal health have acquired popularity [2–6]. Besides, natural zeolites adsorb ammonia, enhance the quality of dairy products and prohibit several animal diseases [7,8].

Zeolites are hydrated alumina silicates in crystalline form. The framework of zeolites consists of three dimensional networks of SiO_4 and AlO_4 tetrahedrals linked to each other via sharing oxygen atoms. This structure forms channels and consistent voids occupied by water molecules and cations to balance the charge of the whole framework. Due to mobility of the cations, zeolites have a high ion-exchange capacity. They are commonly used as commercial adsorbents and often named as the mineral of 21^{th} century. The pore size of zeolite minerals is in molecular size dimensions, and in fact, they are often called as 'molecule sieves' because of their small zeolitic pores. Water molecules leave a zeolitic structure by heating easily or can be adsorbed again.

The most commonly used zeolite type is a natural mineral 'Clinoptilolite'. In Figure 1.1, size and shape properties of typical clinoptilolite powders are clearly shown in a standard and an SEM photograph. Owing to its microporous structure and high ion-exchange capacity, it has a wide range of application fields such as agriculture, animal husbandry, radioactive and other contamination cleanups [7,9].

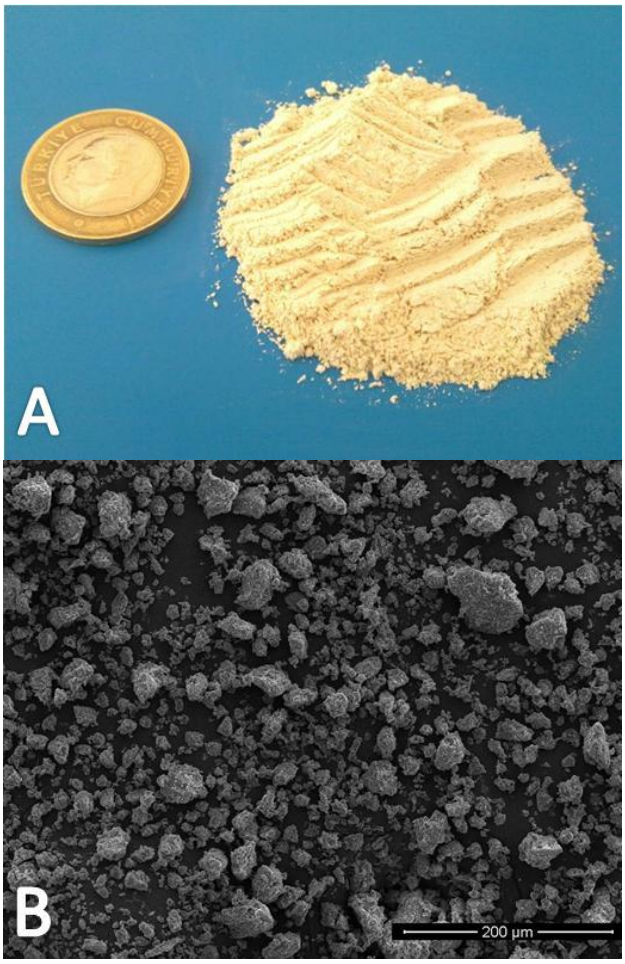

Figure 1.1 Photographs of clinoptilolite powders A) Standard B) SEM

Although it is not possible to exactly report the zeolite reserves in the world, it is known that a typical zeolite mining company in the USA, Canada and Europe produces 20000-50000 tons/year by surface mining. And the prices are up to 300 $ per ton depending on product quality [10].

The Western Anatolia region is very rich in clinoptilolite deposits. The most important clinoptilolite mineral fields, Manisa-Gördes and Balıkesir-Bigadiç, have 20 million and 500 million tons of ore deposits, respectively. In addition, it is estimated that total reserves in other fields of the region are almost 50 billion tons [11].

Usage of natural zeolite 'Clinoptilolite' is approved by European Feed Commission's instruction '70/524/EEC' as animal feed additives as mycotoxin binder in European Union on 16th June, 1999. In addition, it is approved in Turkey by Ministry of Agriculture and Rural Affairs with 'Organic Farming Procedures and Applications Instruction' on 10th June, 2005, according to the code 25841-article Appendix7/ D.6 [12].

Using clinoptilolite in a reliable way as an animal feed additive requires drying it after mining and milling to below 100 μm particle size in order to prevent growth problems of microorganisms in feed stocks. In Turkey, clinoptilolite is generally mined through surface mining in Manisa, Gördes in summer months and total moisture content of the mineral is in the range of 16 % - 20 %. To be able to use natural zeolite as animal feed additive, moisture content of zeolite should be reduced to approximately 8 % [12].

1.2 Drying Phenomenon

1.2.1 General

Drying is generally described as a mass transfer process of removing moisture to yield a dry solid product which possesses desirably low moisture content. Certain terms used to describe the moisture content of solid substances are summarized below:

Moisture content (wet basis): The moisture content of a solid is usually described in terms of weight percent moisture and unless otherwise qualified this is ordinarily understood to be expressed on the wet basis, i.e., as (kg moisture/kg wet solid)x100=[kg moisture/(kg dry solid + kg moisture)]x100.

Moisture content (dry basis): This is expressed as kg moisture/kg dry solid.

Equilibrium moisture (X^*): This is the moisture content of a substance when at equilibrium with a given partial pressure of the water vapor of the surroundings which can change as a function of relative humidity and temperature. The moisture of a substance cannot be removed further beyond this point.

Bound moisture: Due to their high polarity, water molecules can easily bond to charged surfaces of micropores or capillaries within a hygroscopic solid. They can also be in contact with neighboring molecules even as water of crystallization or as hydrates. Therefore, the removal of these molecules is much harder than the rest of the water in the solid. This type of moisture exerts an equilibrium vapor pressure lower than that of the pure water at the same temperature.

Unbound moisture: This is the moisture which is in excess of bound moisture in a hygroscopic solid. This type of moisture exerts an equilibrium vapor pressure equal to that of the pure water at the same temperature and commonly is designated as surface moisture.

Free moisture: This is the moisture consisted of unbound and some bound moisture in excess of the equilibrium moisture. During a drying process, only free moisture can be evaporated. The free moisture content of a solid depends on the water vapor concentration in the gas.

The relations are shown graphically in Figure 1.2 for a solid of moisture content X exposed to a gas of relative humidity Z % [13].

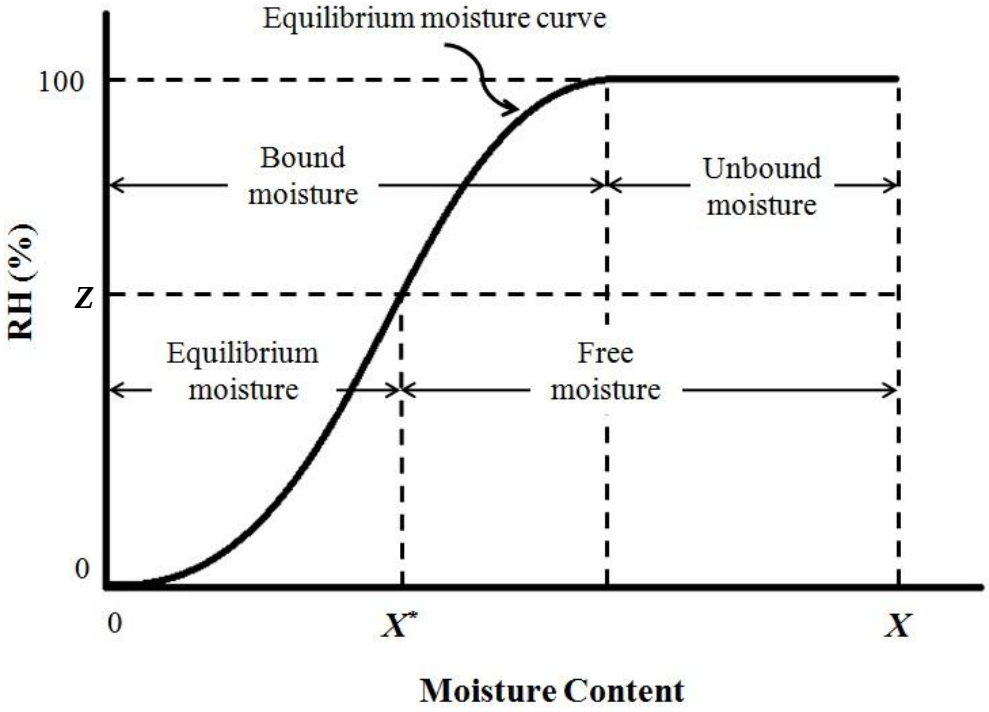

Figure 1.2 Types of moisture content (Based on [13])

During a drying process, initially, the heat transfer from surrounding environment evaporates the unbound moisture. Then, bound moisture moves to the surface of the solid and subsequently evaporates due to being in contact with surrounding environment.

The removal of surface moisture depends on several conditions such as temperature, relative humidity and flow rate of air, contact area and pressure. The transfer of bound moisture is a function of temperature, moisture content and dominantly the physical nature of the solid. The physical form and heat sensitivity of the wet material plays a dominant role in the selection of convenient dryer [14].

1.2.2 Heating Methods

Heat can be transferred in three different modes: convection, conduction and radiation. In a drying operation, the most convenient heating method for a specific wet material can be chosen by considering several characteristics of the material, operating costs and product quality.

Convection: In many industrial applications, convection is the most common method of heating in a drying process of particulate solids. During convective drying, heated air (most common drying gas) flows over the surface of the wet solid and evaporates the unbound moisture. Then, evaporated moisture is carried away with the exhaust gas leaving the dryer. Fluidized bed, flash, rotary and spray dryers are typical examples for convective dryers [14].

Conduction: Conduction is generally used for very wet materials and the heat is supplied from heated surfaces. The wet material is not in contact with heating resource directly. The resource heats the contacting surface, and then the material is dried by contacting the heated surface. Conductive dryers are energy efficient due to minimized energy loss through exhaust gas. Furthermore, indirect dryers reduce the discharge of fines, hence they are very suitable for handling dusty materials.

Radiation: Sources of heating by radiation include the wavelengths between solar spectrum and microwave (0.2 m - 0.2μm) [14]. Drying materials by using radiation (commonly radio frequency and microwave) generally means heating them volumetrically. The water molecules inside wet materials absorb heat energy selectively, thus radiation yields a bulk drying. Microwave heating method yields fast drying operation, uniform heating, easy process control and high-quality products. However, the conversion efficiency of electricity to microwave energy is up to 50% and with additional losses (waveguide, applicator, dc supply etc.) it may decrease down to 30%.

In some cases, it can be more efficient and economical to use a combination of heating methods such as convective-conductive and convective-radiative drying rather than using a single drying method [14]. As a single drying method, convective drying is generally preferred in many industrial applications.

1.2.3 Drying of Powders

Particle technology has an indispensable place in various industrial applications. Almost all particulate products are subjected to drying at the end of their production process. Especially before packaging, they have to be dried to desired moisture content and then cooled. Table 1.1 gives the list of conventional dryer types operating with powders and their typical industrial characteristics.

Table 1.1 Comparison of dryer types operating with powders [15]

Criterion	Rotary Dryer	Flash Dryer	Conveyor Dryer	Fluidized Bed Dryer
Particle Size	Large range	Fine Particles	500 μm-10mm	50-2000 μm
Particle Size Distribution	Flexible	Limited	Flexible	Limited
Typical Residence Time	10-60 min	0-10 s	1-6 h	10-60 min
Flooring Area	Large	Large Length	Large	Small
Turndown ratio	Large	Small	Small	Small
Attrition	High	High	Low	High
Power Consumption	High	Low	Low	Medium
Maintenance	High	Medium	Medium	Medium
Energy Efficiency	Medium	Medium	High	High
Ease of Control	Low	Medium	High	High
Capacity	High	Medium	Medium	Medium

Flash dryers perform the fastest drying operation but very high inlet gas temperatures (typically above 600 °C) are required. Moreover, they can only handle very fine particles and typical energy consumption is in the range of 4500-9000 kJ/kg H_2O evaporated. Rotary dryers provide high thermal efficiency and handle heat sensitive materials especially by cocurrent flow mode. Their typical energy consumption is in the range of 4600-9200 kJ/kg H_2O evaporated in industrial applications. Conveyor dryers can be used for any kind of materials and their design is very simple. On the other hand, they may have some operational disadvantages such as longtime drying, non-uniform product quality and high energy consumption [14].

Fluidized bed drying is the most advantageous technique known for handling particulate solids. They provide high drying rate, easy process control, high energy efficiency and low maintenance cost. Typical energy consumption is in the range of 4000-6000 kJ/kg H_2O evaporated and it is the lowest one compared to the other competitors.

A typical fluidized bed dryer is commonly operated at gas velocities up to four times of the minimum fluidization velocity. High initial moisture content of wet materials requires higher velocities of gas than the same operations with dry particles. Water forms bridges

between particles and it results in an increase in cohesiveness. Thus, wet particles may remain stationary at lower levels of the bed at the initial stage of drying [14]. For effective drying in a fluidized bed, hydrodynamics of the system should be investigated comprehensively.

1.3 Fluidization Technology

1.3.1 Fundamentals of Fluidization

Fluidization technology is extensively used for particle handling in many industrial applications owing to its favorable fluid-solid contact efficiency and higher rates of mass and heat transfer. The first attempt was Winkler process to gasify lignite coal in a fluidized bed in 1926. Then, in 1942, fluidization made a good start at industry with catalytic cracking application [16]. It is now being used in mineral processing, coal and biomass gasification, combustion, environmental protection, healthcare products, pharmaceuticals, dyestuffs and pigments, biotechnology, ceramics, cement, chemicals and other particulate solids handling industries.

Fluidization converts a bed of solid particles into fluidlike state through contact with a gas or liquid. Gas-solid fluidization can be applied in different states according to the process. The fluidization state of particles depends on mainly properties of the gas and solid particles. Figure 1.3 illustrates the different regimes of fluidization resulting from different velocity from packed-bed to pneumatic state for constant particle properties and equipment.

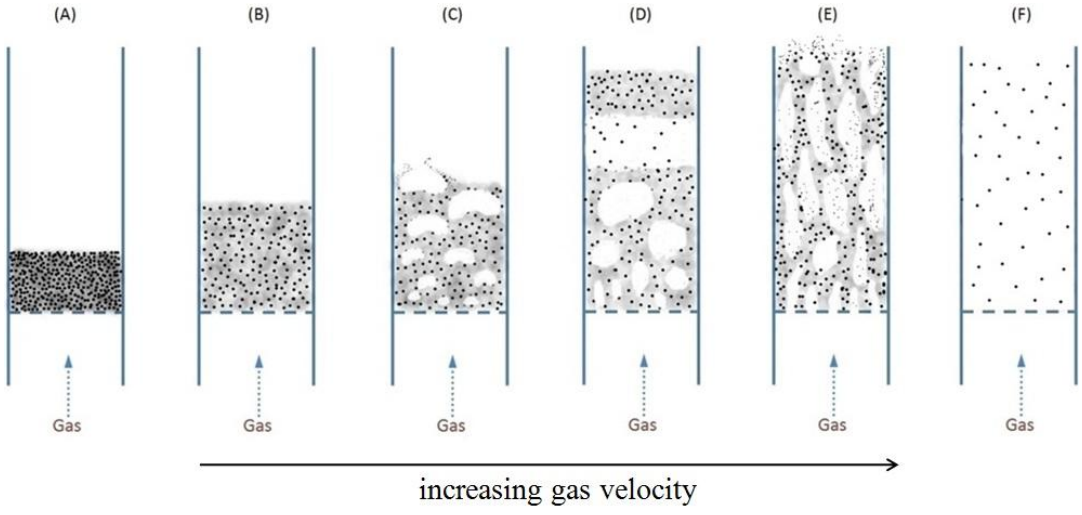

Figure 1.3 Different regimes of fluidization: (A) Fixed Bed (B) Minimum Fluidization (C) Bubbling Fluidization (D) Slugging (E) Turbulent Fluidization (F) Pneumatic Transport (Based on [16])

Fixed bed is the regime of a bed of particles packed in a vessel showing no visual change except for some vibrations due to the flow of a fluid through it. The fixed bed expands and the fluid can find more spaces to move upward among the solids with an increase in the fluid flow rate, hence a certain level of the bed surface is reached and pressure drop of the bed does not increase anymore by increasing the flow rate. The starting point of this motion of the bed is called incipient or minimum fluidization with a corresponding minimum fluidization velocity (U_{mf}). When bubbles are formed in the bed by further increasing the flow rate, its new name is bubbling bed with a corresponding minimum bubbling velocity (U_{mb}). The bubbles get bigger and bigger with greater flow rates and when bubble sizes reach a value over 60% of the bed diameter, the regime becomes slugging. If the particles are fluidized at a higher fluid velocity exceeding the terminal velocity of the particles, the bed moves in turbulences, various shapes and sizes of bubbles, and irregular spaces among solid clusters. These types of beds are called turbulent beds. After further increases of fluid flow rate, the particles get entrained from the bed in which exhibiting a complete lean phase fluidized bed and the operation becomes pneumatic transport.

1.3.2 Geldart's Classification of Particles

To understand and visualize clearly the expansion and fluidization behaviors of the particles at ambient conditions, Geldart [17] made a very useful classification. He classified the particles into four groups as A, B, C and D (Figure 1.4). He characterized them by density difference ($\rho_p - \rho_f$) and mean particle size (d_p).

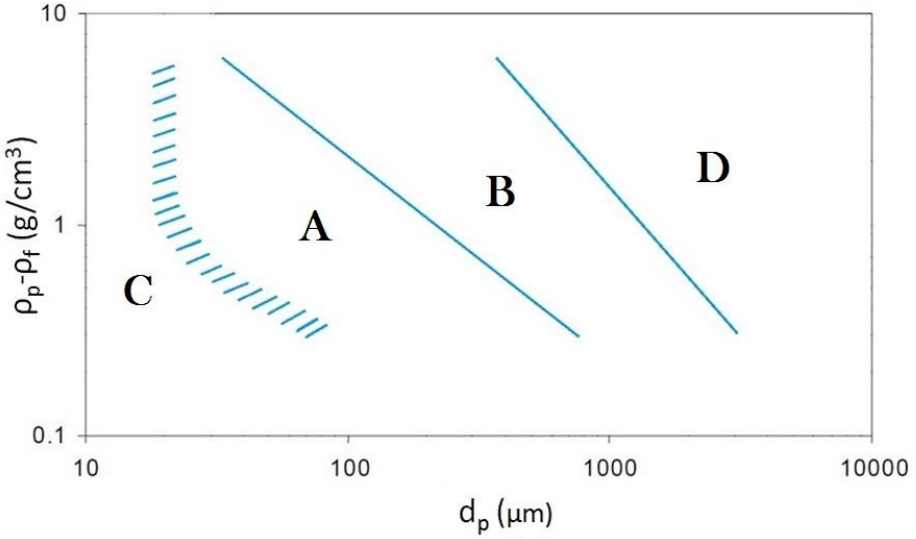

Figure 1.4 Geldart's classification of particles

Group A (Aeratable): Typical examples of this type are cracking catalysts (FCC). For this group, the characteristic d_p value varies between 30-100 μm in most cases. They are fine and aeratable particles, hence they fluidize nicely. There is a noteworthy range between two critical gas velocities of minimum fluidization and minimum bubbling. When the gas flow is cut off, the bed collapses slowly.

Group B (Sand-like): Sand particles are good examples for this group. They can be called as intermediate size particles [18]. They cannot be fluidized as homogenously as Group A particles and they start to bubble when U_{mf} is reached. Thus, U_{mf} is very close to U_{mb} for this type of particles. A bed of Group B collapses quickly when the gas flow is cut off.

Group D (Spoutable): They are the coarsest particles which can be fluidized poorly. They can be spouted preferably and yield a better mixing quality when compared with fluidization. For most cases, d_p is greater than 1 mm.

Group C (Cohesive): They are finer than Group A particles with typical d_p values less than 20 μm and density differences larger than 1 g/cm^3. Flour is typical of these particles. When superficial gas velocity exceeds U_{mf}, gas tries to escape the bed by forming vertical channels rather than fluidize. Interparticle forces determine the behavior of the powders in this class. One has to understand these interparticle forces before designing and operating a fluidization process of such powders.

1.3.3 Interparticle Forces Affecting Powder Fluidization

Comprehension of interparticle forces between powders can be done best after defining what powders really are. According to Rietema [19], it is very complicated to define powders. Powders are not a solid, liquid or gas, even though they can withstand some mechanical stress, flow under certain cases and be compressed to a certain level. They can be treated sometimes as a whole, but not always. Especially in fluidization, the gas phase and the powders should be considered together to be able to characterize their behavior. The fluidization behavior of powders strongly depends on the interaction between the gas phase and the solid phase. Powders can be classified according to their flowability characteristics in most cases. However, it is wrong to classify them regardless of considering the other possible conditions (different gas properties, temperature, pressure etc.).

In addition to Geldart's classification, some other attempts have been made to extend this classification to include operating conditions other than ambient conditions. Yang [20] proposed a modification of Geldart's classification for different fluid densities and viscosities and showed that applying different fluid properties can lead to Group B particles behave like Group A particles. Liu et al [21] reported that even Group D particles can be fluidized similar to Group A particles at high pressures. Therefore, based on

Geldart's classification, it can be concluded that it is more accurate to use Group A, B, C and D 'behavior' instead of using only the terms of group or class.

According to Geldart [22], Group A powders can be called 'slightly cohesive' since interparticle forces are small compared with the hydrodynamic forces when they are fluidized. Inversely, in Group C, the interparticle forces are appreciably higher than the hydrodynamic forces, hence they are hardly-fluidize, sticky and prone to channeling materials. On account of being an identifying parameter, ratio of tap to aerated bulk density indicates a critical range for ρ_{tb}/ρ_{ab}. Group C powders and Group A powders have ratios bigger than 1.4 and smaller than 1.25, respectively. Additionally, those in the range between 1.25-1.4 may exhibit the behaviors of both groups.

Grace [18] suggested boundaries between Geldart Groups such as A-C, A-B and B-D. He stated that the powders at the boundary between Groups C and A (Figure 1.4) are affected strongly by interparticle forces. Interparticle forces due to the wetness of particle surfaces (capillary forces), electrostatic charges and the Van der Waals forces are known to cause the adhesion of a particle to a wall or to another particle.

1.3.3.1 Van der Waals Forces

Van der Waals forces (or interactions) are named after Dutch scientist Johannes Diderik van der Waals who first pointed out the attractions between gas molecules resulting deviations from the ideal gas law at high pressures. His hypothesis was quantified by Fritz Wolfgang London's studies on intermolecular forces. London-van der Waals forces include attractions between atoms, molecules, surfaces, as well as other molecular forces. Possessing a temporary dipolar character due to changes in electronic configurations, molecules interact with each other at small separation distances (0.2-1 nm) [23]. The attractive interaction is inversely proportional to the sixth power of the particle radius [24]. In a fluidized bed, fluidization of the powders showing Group C behavior is dominantly governed by this force with the order of magnitude larger than gravitational and hydrodynamic forces [23]. The Van der Waals force between two spheres is expressed by

$$F_v = \frac{2\,S\,r}{12\,z^2} \tag{1.1}$$

where S is Hamaker constant (J), a material property; r is radius (m) and z is separation distance between spheres (m).

As expressed in eqn. (1.2), it is possible to determine the Hamaker constant of two different materials in interaction.

$$S_{12} = \sqrt{S_{11}S_{22}} \tag{1.2}$$

If another material takes place between the other two, the Hamaker constant for three different material becomes

$$S_{132} = \left(\sqrt{S_{11}} - \sqrt{S_{33}}\right)\left(\sqrt{S_{22}} - \sqrt{S_{33}}\right) \tag{1.3}$$

As can be seen from eqn. (1.3), Van der Waals force can be negative with a value of S_{33} between S_{11} and S_{22}. Thus, a repulsion force may occur instead of a cohesive force [25].

In real systems, shapes of particles are different from sphere and geometrical factors can change the Van der Waals attractions due to various contact area and separation distance values. In addition, physically adsorbed gases increases the cohesion effects within a bed of powders [26]. Adsorption leads to alterations in separation distance and Hamaker constants.

1.3.3.2 Electrostatic Forces

Due to formation of potential difference or electrostatic charge by friction, particles flowing in a gas medium are affected by electrostatic forces. By assuming that the particles are uniformly charged and the charging is concentrated at the centers, two contacting spherical particles are under the effect of cohesive force as shown below

$$F_E = \frac{\pi\sigma_1\sigma_2}{\alpha_0} 4r^2 \tag{1.4}$$

where σ_1 and σ_2 are charge densities (C/m^2) of the two particles, α_0 is dielectric constant (F/m) in vacuum [25].

Bailey [27] concluded in his studies that powders are variably charged by electrostatic effects by friction. Charged powders can stick on the metallic walls of a fluidized bed column and alter the fluidization quality.

1.3.3.3 Capillary Forces

Capillary condensation of the fluid may occur between the particles in close contact, and hence a contribution of capillary force takes place in addition to Van der Waals interaction at humidity values larger than 65% [23]. The magnitude of capillary force is not a function of the size of liquid bridge (Figure 1.5) but only of parameters such as the liquid surface tension δ, its contact angle θ on the solid surface, and the radius r of the smooth curved surfaces [28],

$$F_l = 2\pi\delta r cos\theta \tag{1.5}$$

The contact angle θ can be assumed to be zero in the case of water. The equation is called the Laplace-Young equation [25].

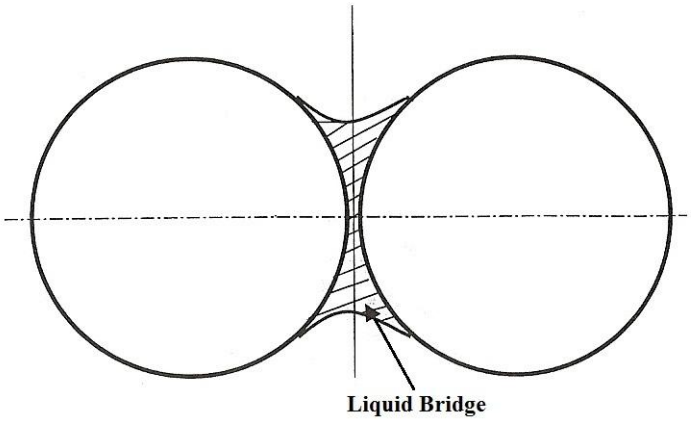

Figure 1.5 Liquid bridge between two spherical particles

For two smooth, spherical particles, totally wetting the particle surfaces, capillary force becomes

$$F_l = 2\pi\delta r \tag{1.6}$$

Geldart and Wong [29] observed that different values of relative humidity of air up to about 30% have small effect on fluidization. Expansion decreases with relative humidity when the hydrodynamic drag forces are small (low velocities) and increases with higher velocities of air giving greater mechanical strength at above 30% *RH*. In the second part of their study [30], they reported that the bed of Group A particles collapses more rapidly when high (> 30%) relative humidity values are applied.

1.3.4 Effects of Cohesive Forces on Fine Particles

Different from the other Geldart Groups [17], Group C particles cannot be fluidized in conventional fluidized beds. They are very fine and sticky materials because of cohesive interparticle forces. They channel or lift as a plug rather than fluidize when fluid flows through them [18]. Plugging, channeling and agglomeration can occur during fine particle fluidization. The interparticle forces of Group C particles have to be broken by applying some modifications to conventional fluidized bed dryers. Otherwise, undesired operational limitations become inevitable. Multistage, hybrid, pulsating, mechanically vibrated or agitated, jetting, recirculating fluidized bed dryers, spouted and spout-fluid bed dryers can be given as successful modifications in industry. Modified fluidized bed dryers can operate with extended range of particle size (10 μm -10 mm) and wider particle size distributions. They can reduce attrition, energy consumption and enhance product quality [14].

1.4 Drying Process in Fluidized Bed Dryers

Fluidized bed drying process of solid materials consists of simultaneous heat and mass transfer. In fluidized bed dryers without immersed heaters for additional conductive heating, convective heat supplied from drying medium evaporates the moisture as can be seen in Figure 1.6.

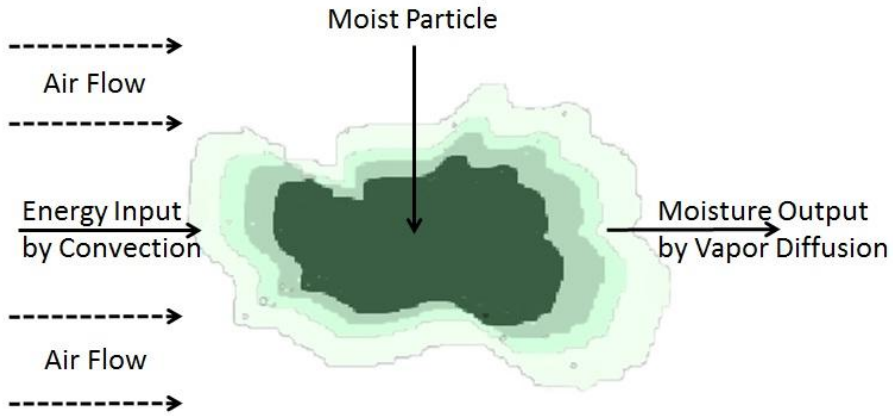

Figure 1.6 Transfer mechanisms in a fluidized bed dryer

The drying behavior of solids can be characterized by measuring the loss of moisture content (X) as a function of time [14]. As can be seen in Figure 1.6, the plot of variation of moisture content with time and the plot of drying rate expressed as the derivative $-dX/dt$ versus time are the characteristics of drying for a given material and drying conditions. When a wet solid is subjected to convective drying, heat transfer from the surrounding air evaporates the moisture through a very thin film formed by unbound moisture on the solid surface. Simultaneously, bound moisture is transferred to the surface with the same rate as the evaporation takes place. This process continues until the end of constant drying rate (N_c) period shown in Figure 1.7 with the indicator 1. Due to the nature of the fluidization technique, in constant drying rate period, characteristics of a drying operation are majorly identified by the flow rate, temperature and humidity of drying air. Due to the fact that the rate of moisture diffusion from internal pores of the solid cannot compensate the evaporation rate, a significant decrease in film thickness occurs at the surface. On further drying, the moisture content of the bed material reaches a critical value, X_c, which results in some dry spots upon the surface. These spots gradually occupy the rest of the exposed surface and the original surface film entirely evaporates at the end of region 2, namely the first stage of falling rate period. From the beginning of region 3, the second stage of the falling rate period, drying is totally controlled by diffusion of moisture within the solid

resulted from concentration gradients between the inner parts and the surface. Then, the diffusion rate slowly decreases through region 3 and drying operation stops when the moisture content of the solid reaches the equilibrium value X^* [13,14,31].

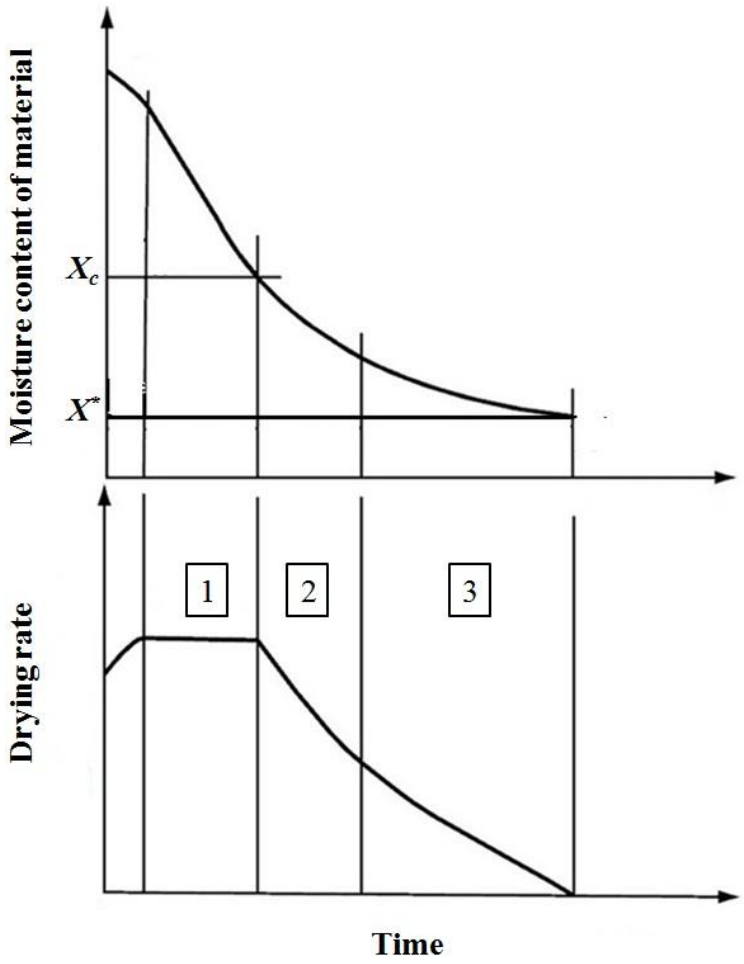

Figure 1.7 Characteristic curves of convective drying (modified from [14])

1.5 Vibrated Fluidized Bed (VFB) Drying

Fluidized bed dryers can be successfully and efficiently employed for drying of wet particulate materials as long as the bed of such materials can be kept in a fluidized state. Conventional fluidized beds can have some restrictions for various industrial applications. The reasons of these possible restrictions are wide residence time distribution, fluid bypass and reduction in fluid-solid contact due to low-quality fluidization of cohesive powders, attrition of the friable particles, elutriation and entrainment of the fines. Therefore, some

modifications on operational characteristics and design of the bed geometry can be made to overcome these deficiencies.

The poor-quality fluidization of the cohesive particles during a drying process can be avoided by external means such as rotation, centrifugation, vibration, agitation [32,33] and addition of easy-to-fluidize large particles or sub-micron particles [34,35]. Among all the applicable modifications, mechanical vibration technique in fluidization has the biggest commercial success. The combination of vibration and fluidization can provide the following advantages over conventional fluidized beds [14,36–39]:

- A smooth fluidization of hard-to-fluidize particles is possible to achieve by combining vibration and the flow of fluid.
- Attrition due to solid-solid and solid-wall collisions is minimized appreciably.
- Minimum fluidization velocity decreases considerably, thus lower operating gas velocities are used in applications successfully. This helps to avoid entrainment of fines from the bed.
- It becomes easy to handle with friable, abrasive and heat sensitive materials; hence application fields of fluidized beds can be extended.
- Polydispersity of the materials is not an operational drawback for vibrated fluidized beds, since low gas velocities can fluidize fine particles while coarser ones are in mobile state. Then, effective heat and mass transfer can be obtained within the fluidized bed.
- Adjustable amplitude and frequency parameters offer an easier control of residence time distributions of polydisperse particles in various applications.
- High value products are obtained by maximizing homogeneity.
- Aggregate size is reduced and fluidization quality is improved when nanoparticles are fluidized by means of external mechanical vibration.

In the literature, the majority of the studies on vibrated fluidized beds are about investigation of hydrodynamics of the system. These studies are summarized in Table 2.1. However, to the author's knowledge, there is no study on drying of Group C particles in a vibrated fluidized bed dryer. Therefore, the objective of this thesis study is to characterize the hydrodynamics and drying performance of a vibrated fluidized bed operating with micronized clinoptilolite particles in order to determine the suitable operating conditions for drying application. To achieve this objective, in the first part of this study, the effective vibration conditions were determined for a high-quality fluidization in a cold fluidized bed system. In light of the outcomes of the first part, drying experiments were conducted by using the most effective vibration conditions.

CHAPTER 2

LITERATURE SURVEY

2.1 Basic Concepts

In 1986, Geldart [40] said ‘‘The arrival time of a space probe travelling to Saturn can be predicted more accurately than the behavior of a fluidized bed chemical reactor!’’. Even after twenty seven years, deficiencies about understanding fluidization and the parameters affecting it still exist. Therefore, researchers still work on predicting hydrodynamic behaviors of fluidized beds. It can be easily expected that a modified fluidized bed is much more complicated than a conventional one.

The majority of the research studies on vibrated fluidized beds were made by Russians until 1980s. Only about 10% of the retrieved literature citations were in English in 1978 [37]. Over the past 30 years, a considerable amount of research has been conducted in the subject. However, the complexity of the vibrated fluidization mechanism requires more research studies in order to make more accurate predictions.

Vibration generally improves fluidization quality. Bed voidage distribution and homogeneity is better in a vibrated bed compared to an unvibrated bed. The effectiveness of vibration is more remarkable for fine, cohesive powders than larger powders (Group A, B). Vibration energy diminishes in the upper zones of a deep bed, thus vibrated fluidized bed operations must be made in relatively shallow beds.

Pressure drop (ΔP), minimum fluidization velocity (U_{mf}) and bed voidage (ε) parameters are nonlinear functions of dimensionless vibration strength Λ, defined as

$$\Lambda = \frac{a\omega^2}{g} \tag{2.1}$$

where a is amplitude, g is gravitational acceleration, f is frequency and ω is angular frequency ($2\pi f$) of vibration.

Earlier studies on vibrated fluidized beds [41–43] have shown that at vibration strength values less than 1, powders slide smoothly in a circulatory motion within the bed and interparticle friction is insufficiently reduced resulting in a poor contribution to

fluidization. If vibration strength is increased to 1, bed of particles starts to fluidize under the coordinate effect of both fluidizing gas and mechanical vibration since the gravitational acceleration is balanced by the vibrational acceleration. If greater vibration strength values are applied, the bed material disconnects from the distributor and particles bound up and down within the bed due to more pronounced effect of mechanical vibration.

2.2 Hydrodynamics of Vibrated Fluidized Beds

Table 2.1 summarizes the major studies on hydrodynamics of vibrated fluidized beds. In these studies, effects of vibration parameters on fluidization characteristics were investigated. The findings of these studies are summarized under the following three sub-sections:

1) Effect of vibration on pressure drop across the bed
2) Effect of vibration on minimum fluidization velocity
3) Effect of vibration on bed expansion and bed voidage

Table 2.1 Major experimental studies on hydrodynamics of vibrated fluidized beds

Researchers	Material		OPERATING PARAMETERS				
	Type	**Particle Size (μm)**	**Bed Dimensions (m)**	**Amplitude (mm)**	**Frequency (Hz)**	**Vibration Strength (Λ)**	**Static Bed Height (mm)**
Bratu and Jinescu [41]	Marble Silica gel Polystyrene	175-450 175-450 250-500	0.05	0-3	0-35	-	33-70
Gupta and Mujumdar [42]	Molecular sieve Silica gel Mustard seed Polyethylene A Polyethylene B	2200-3900 910-3900 2200 3110 3830	0.2x0.2	0-4.2	0-105	-	12.5-100
Ringer and Mujumdar [43]	Molecular sieve Polyethylene Glass beads	2500 3500 700	0.2x0.2	2-4.25	0-16	0-4.4	25-126
Malhotra et al. [44]	Glass ballotini	353-667	0.202x0.05	4.25	0-16	0-4	95-120

Table 2.1 Major experimental studies on hydrodynamics of vibrated fluidized beds (Cont'd)

Researchers	Material		OPERATING PARAMETERS				
	Type	**Particle Size (μm)**	**Bed Dimensions (m)**	**Amplitude (mm)**	**Frequency (Hz)**	**Vibration Strength (Λ)**	**Static Bed Height (mm)**
Erdesz and Mujumdar [45]	Sand Polystyrene Salt Sugar	150-500 2750 500 500	0.108	1.85	-	0-12.93	60-140
Satija and Zucker [46]	Granules	720	3.05x0.305	3.18-6.35	-	-	-
Marring et al. [47]	Glass ballotini Potato starch	65.8 34.6	0.288	-	30-90	0-9	500
Kuipers et al. [35]	Potato starch	52.2	0.288	-	10-90	1-8	740
Noda et al. [48]	Glass beads	6	0.065	-	-	0-12	-
Wank et al. [49]	Boron nitride	5-11	0.04	-	20-60	2-6	76.2

Table 2.1 Major experimental studies on hydrodynamics of vibrated fluidized beds (Cont'd)

Researchers	Material		OPERATING PARAMETERS				
	Type	Particle Size (μm)	Bed Dimensions (m)	Amplitude (mm)	Frequency (Hz)	Vibration Strength (Λ)	Static Bed Height (mm)
Tasirin and Anuar [50]	Flour	15-34	0.15	-	50	13-18	200
Mawatari et al. [51]	Glass beads	6-100	0.065	0.5-1.5	30-50	0-15	65
Mawatari et al. [52]	Glass beads	6-100	0.065	0.5-1.5	30-54	-	65
Mawatari et al. [53]	Glass beads	6-100	0.065	0.5-1.5	30-45	1.81-12.24	65
Silva-Morris and Rocha [54]	Adipic acid	75-600	0.1	0-20	0-37	0-3.6	(300 g)
Nam et al. [55]	Silica paritcles	0.012	0.0625	-	30-200	0-3	-
Daleffe and Freire [56]	Ballotini glass spheres	1100-1850	0.115x0.2	3	-	0-1.5	80

Table 2.1 Major experimental studies on hydrodynamics of vibrated fluidized beds (Cont'd)

Researchers	Material		OPERATING PARAMETERS				
	Type	Particle Size (µm)	Bed Dimensions (m)	Amplitude (mm)	Frequency (Hz)	Vibration Strength (Λ)	Static Bed Height (mm)
Jin et al. [57]	Millet Resin Glass beads Sand 1 Sand 2 FCC Bi-Mu-P	1640 940 720 300 160 64 33	0.148	0-1	0-45	0-8.24	100-400
Alavi and Caussat [34]	Yttrium oxide	1.2	0.05	0.5-10	19-25	-	0-200
Mawatari et al. [58]	Glass beads	6	0.065	0-2.3	40	-	65
Xu and Zhu [59]	Al_2O_3 TiO_2 $CaCO_3$ Glass beads	4.8 5.2 5.5 6.1-216	0.1	0-3	0-50	-	100

Table 2.1 Major experimental studies on hydrodynamics of vibrated fluidized beds (Cont'd)

Researchers	Material		OPERATING PARAMETERS				
	Type	**Particle Size (µm)**	**Bed Dimensions (m)**	**Amplitude (mm)**	**Frequency (Hz)**	**Vibration Strength (Λ)**	**Static Bed Height (mm)**
Jin et al. [60]	Millet Resin Glass beads Sand	1640 940 720 300	0.148	0-1	0-45	0-8.24	100-400
Brod et al. [61]	Eggshell	729	-	0.15-1.51	60	2.1-21.8	-
Barletta et al. [62]	FCC powder	77	0.085	0-12.7	0-100	-	(800 g)
Daleffe et al. [63]	Ballotini glass spheres	1290-3670	0.114	0-9	0-12.87	0-2	100
Xu and Zhu [64]	Glass ballotini FCC powders	6-216 65	0.1	0-3	0-50	-	100
Yang et al. [65]	SiO_2 TiO_2 ZnO	0.03 0.01 0.02	0.04	0-3	0-45	-	70

Table 2.1 Major experimental studies on hydrodynamics of vibrated fluidized beds (Cont'd)

Researchers	Material		OPERATING PARAMETERS				
	Type	**Particle Size (µm)**	**Bed Dimensions (m)**	**Amplitude (mm)**	**Frequency (Hz)**	**Vibration Strength (Λ)**	**Static Bed Height (mm)**
Kaliyaperumal et al. [66]	SiO_2	0.016	0.1	0.1-0.45	5-40	-	-
	Al_2O_3	0.016					
	TiO_2	0.53					
	ZrSi	0.74					
	$BaSO_4$	1.82					
Lima and Ferreira [67]	Fresh leaves	6500-77100	0.11x0.2	-	-	0.5-1	35-45
Nunes et al. [68]	Sodium Bicarbonate	75	0.1	0-20	0-60	0.2-2.9	(450 g)
Zhang et al. [69]	Fly ash	44-105	0.1x0.15	0-0.381	60	-	12
Barletta and Poletto [70]	Silica	7.6	0.085	-	15-150	2, 10	(300 g)
	Potato Starch	21					(225 g)
Sadeghi and Khoshtaghaza [71]	Black tea	840	-	1, 3	4, 10	0-1.184	80
Zhu et al. [72]	Glass beads	1800-3200	0.24x0.08	-	-	1-3	80-320

2.2.1 Effect of Vibration on Pressure Drop Across the Bed

In fluidized bed studies, pressure drop versus superficial gas velocity ($\Delta P - U_0$) diagrams are very useful to determine the quality of fluidization, especially when visual observations are not possible. Figure 2.1 illustrates an ideal pressure drop curve commonly obtained with a bed of uniformly sized particles. As can be seen, for the relatively low gas velocities in a fixed bed, the pressure drop is approximately proportional to gas velocity, and usually reaches a maximum, ΔP_{max}, slightly higher than the static pressure of the bed. Static pressure drop of the bed, ΔP_{mf}, is equal to weight of the bed per unit cross sectional area in the condition of high-quality fluidization. When gas velocity is decreased, the fluidized particles settle down to form a loose fixed bed without exhibiting a maximum pressure drop. If the gas flow is eventually turned off, the bed turns back to its stable initial state [16]. In the literature, the difference between the curves obtained by increasing and decreasing gas velocities is designated as hysteresis. Due to this hysteresis effect, it is usually preferred to use pressure drop versus decreasing gas velocity curves for the hydrodynamic analysis. On the other hand, in vibrated fluidized beds, maximum pressure drop disappears along with the effect of vertical vibration.

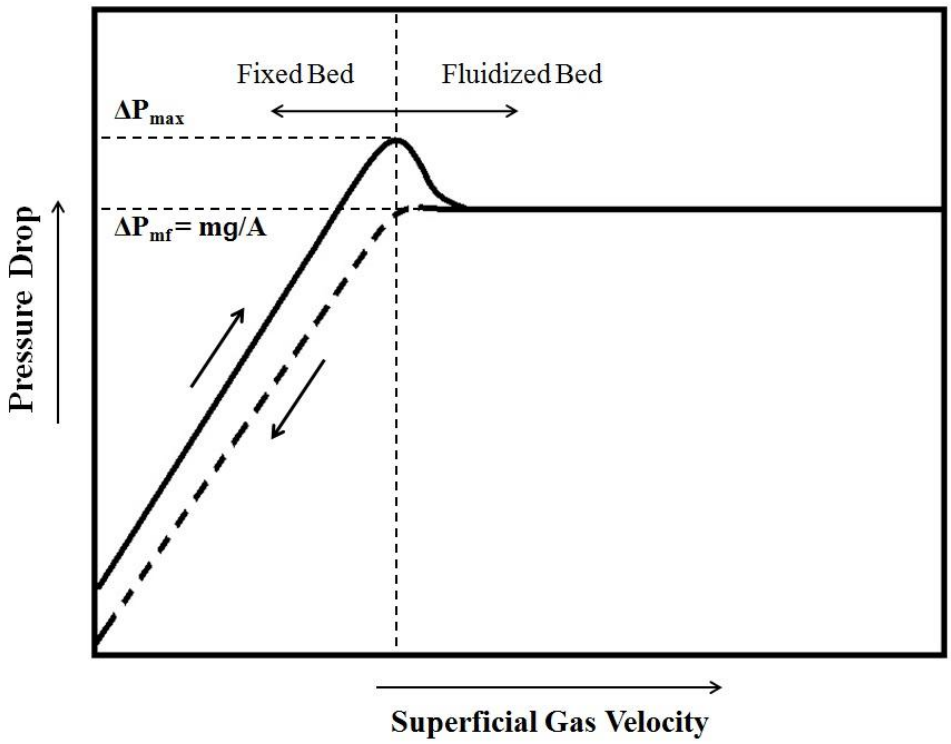

Figure 2.1 An ideal pressure drop curve of fluidization

Marring et al. [47] used a dimensionless parameter, fluidization index (FI), instead of pressure drop to analyze the behavior of cohesive powders expressed by

$$FI = \frac{\Delta P\, A}{mg} \tag{2.2}$$

where A is the area of the horizontal cross section of the bed. The fluidization index, an indication of fluidization quality, is the ratio of the pressure drop over the bed to the weight of the bed per unit cross sectional area. Figure 2.2 shows the possible variations of fluidization index curves which can be obtained in real cases of fluidization. When the fluidization is good, pressure drop over the fluidized bed is approximately equal to the weight of bed per unit cross sectional area, where fluidization index is equal to 1, namely unity (curve (a)). A lower fluidization index than unity can be observed if poor fluidization due to cohesive forces resulting in channels and rat holes (curve (b)). On the other hand, fluidization index can be higher than unity if a layer of the bed sticks on the distributor or due to shear stress between the bed and the wall (curve (c)).

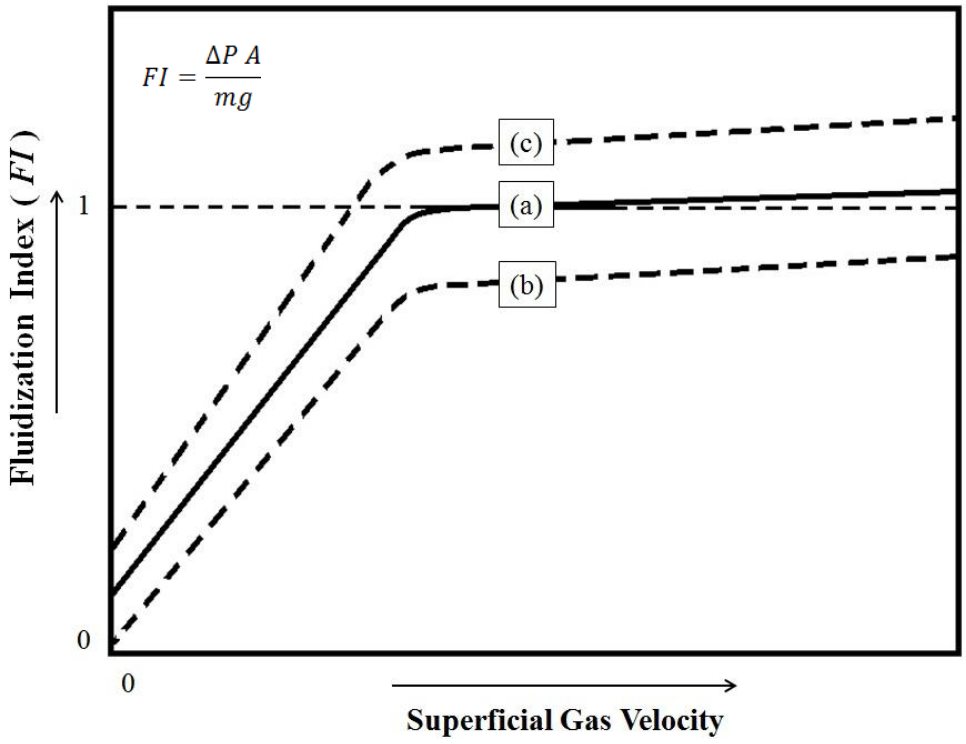

Figure 2.2 Variations of fluidization index curves in real cases of vibrated fluidization

Being the first comprehensive study, Bratu and Jinescu [41] observed variations of $\Delta P - U_0$ curves of the beds of Group A and Group B particles under various vibration conditions. Throughout approximately a hundred of diagrams, they made very important and descriptive conclusions by representing the results in logarithmic coordinates (Figure 2.3).

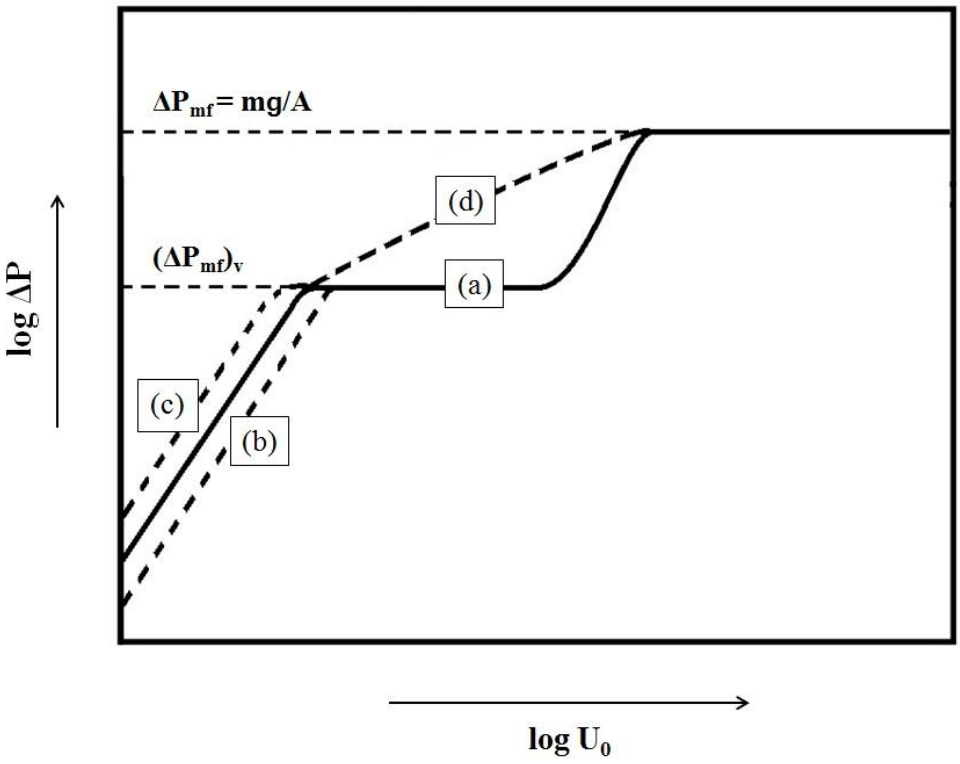

Figure 2.3 ΔP-U_0 diagram of a vibrated fluidized bed (Modified from [41])

In Figure 2.3, the bed remains in fixed bed state under vibration effect until reaching the pressure drop at vibration assisted fluidization, $(\Delta P_{mf})_v$. Following path (a), the range where this pressure drop value changes stepwise with respect to increasing gas velocity is a function of vibration strength. This range may disappear when vibration strength is high enough, and therefore path (d) is followed. In addition, deviations from solid fixed bed line occur when different vibration strength values are applied. Negative deviations, e.g. path (b), can be observed with smaller vibration strengths while positive deviations, e.g. path (c), can be observed with higher vibration strengths. At and after ΔP_{mf} point, pressure drop is equal to the one at incipient fluidization under unvibrated condition. In other words, the corresponding gas velocity value at this point is equal to U_{mf} in the absence of vibration.

In the light of their findings on pressure drop curves, Bratu and Jinescu [41] came up with a correlation to predict the pressure drop at minimum fluidization under vibration condition

$$(\Delta P_{mf})_v = \Delta P_{mf}(\frac{a\omega^2}{g})^{-b} \tag{2.3}$$

where the exponent b can change as a function of particle size and density (d_p , ρ_p).

Another extensive study on hydrodynamics of vibrated fluidized beds was conducted by Gupta and Mujumdar [42]. In their study, the effects of amplitude and frequency on pressure drop, a minimum mixing velocity defined instead of minimum fluidization velocity and overall hydrodynamic characteristics of the bed were discussed in details. They classified the shape of $\Delta P - U_0$ curves into three separate types as Type A, Type B and Type C as shown in Figure 2.4. This approach is very similar to the one which Bratu and Jinescu [41] made before. The only discernable difference is the addition of Type A curve when small vibration strengths are applied. Expectedly, its shape is very close to the typical curve obtained in conventional fluidized beds with the absence of ΔP_{max}. Type B and Type C curves coincide with the paths of (d) and (a) in Figure 2.3, respectively.

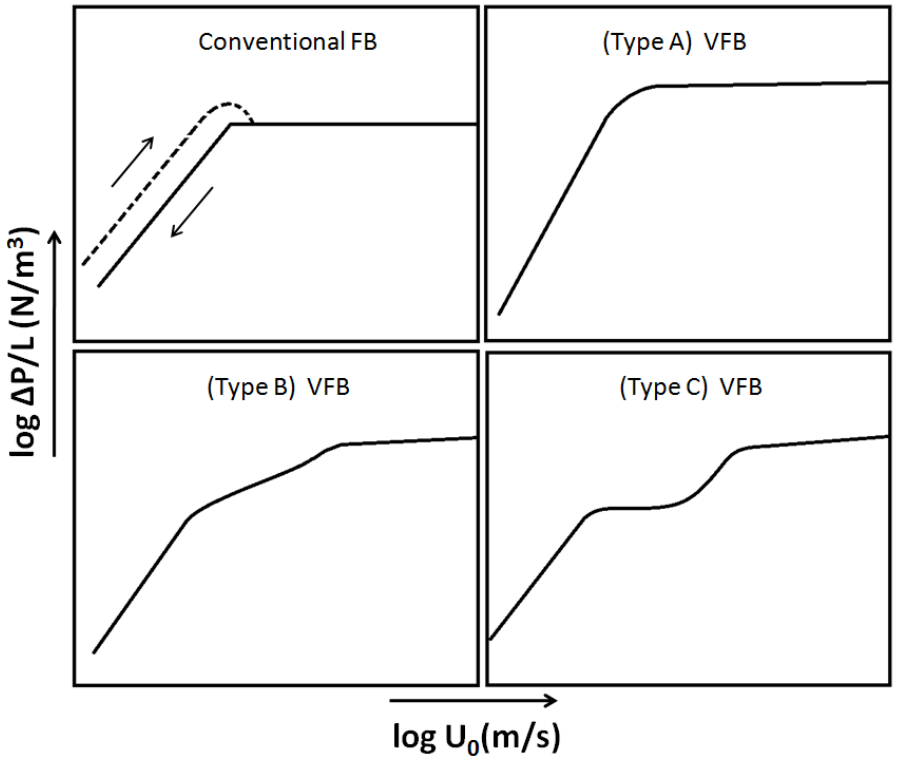

Figure 2.4 Types of pressure drop-velocity curves in fluidized beds (FB) and vibrated fluidized beds (VFB) (Modified from [42])

According to Gupta and Mujumdar [42], on the way from Type A to Type C, vibration plays a gradually increasing role on dynamics of the bed. They proposed a correlation for vibrated fluidized bed pressure drop as shown below;

$$\frac{(\Delta P_{mf})_v}{\Delta P_{mf}} = 1 - 0.0935 \left(\frac{d_p}{H}\right)^{0.946} \left(\frac{a\omega^2}{g}\right)^{0.606} \phi_s^{1.637} \quad (2.4)$$

where H is bed height (m), and ϕ_s is sphericity (shape factor). Following Gupta and Mujumdar, Malhotra et al. [44] investigated the pressure drop behavior of dry and sticky (wetted with glycerin) glass ballotini particles with diameters of 353 μm and 667 μm in a rectangular bed. They concluded that sticky particles behave differently from dry particles even in vibrated case. Above a certain value of glycerin content, it was impossible to obtain a typical pressure drop curve of fluidization without the aid of intense vibration strength. As a similar study, Daleffe and Freire [56] investigated characteristic fluid-dynamic curves of $\Delta P - U_0$ of ballotini glass spheres with diameters of 1.1, 1.55 and 1.85 mm. The liquid used was glycerin. They observed low standard deviations of the curves when the bed is in fixed bed region. Then, standard deviations increased appreciably with incipient fluidization [56,63].

Marring et al. [47] observed that higher cohesiveness of potato starch caused a decrease in the slope of $FI - U_0$ curve. Additionally, fluidization of potato starch could not be achieved without vibration. An increase above unity of FI was seen due to shear stress between the bed and the walls.

Noda et al. [48] investigated the fluidization behavior of glass beads (6 μ) in a vibrated fluidized bed at atmospheric and reduced pressure. Stable fluidization was only obtained under vibration condition. $\Delta P - U_0$ curves were found to be very similar to the characteristic curves of a conventional fluidized bed when vibration was applied.

Erdesz and Mujumdar [45] observed that increasing vibration strength from 0 to about 13 leads to a decrease in pressure drop for particle sizes of 150-2750 μm. Similarly, Silva and Morris [54] obtained results indicating that pressure drop reduces as a result of the increase in vibration frequency and amplitude (d_p=75-600, Λ=0-3.6). Inversely, Tasirin and Anuar [50] reported that pressure drop increased when vibration strength is increased between 13 and 18 in vibrated aeration of flour powders with particles sizes in the range of 15-34 μm. Xu and Zhu [59] reported that higher bed pressure drops were found with mechanical vibration for all powders (4.8-216 μm) examined. On the other hand, Mawatari et al. [51,53] could not find a significant change in pressure drop with increasing vibration strength (d_p=6-100, Λ=1.81-12.24).

Expectedly, in several studies [48,51,53,55,58,59] on vibrated fluidization of cohesive powders including nano-sized and submicron particles, a typical pressure drop curve of fluidization could not be obtained without vibration. The differentiation between fixed bed and fluidized bed was clearly seen only with vibration.

Considering all of the studies mentioned above, it can be easily seen that there is no concurrence on the vibration dependence of pressure drop across the bed. Different operational parameters and material properties result in various trends of $\Delta P - U_0$ curves. On the other hand, for most cases, it can be concluded that vibration reduces pressure drop across the bed of large particles whilst pressure drop across the bed of cohesive particles tend to increase or remain unchanged compared to ΔP_{mf} (total weight of the bed over cross section).

2.2.2 Effect of Vibration on Minimum Fluidization Velocity

In polydisperse particle systems, U_{mf} is defined by convention as the intersection of the fixed bed line with fluidized bed line in pressure drop versus superficial gas velocity curves [16]. At incipient fluidization, combination of Ergun equation and the force balance over the bed is given by

$$\frac{1.75}{\varepsilon_{mf}^3 \phi_s} Re_{mf}^2 + \frac{150(1-\varepsilon_{mf})}{\varepsilon_{mf}^3 \phi_s^2} Re_{mf} = Ar \tag{2.5}$$

where Archimedes (Ar) number is defined as

$$Ar = \frac{d_p^3 \rho_g (\rho_p - \rho_g) g}{\mu^2} \tag{2.6}$$

For small particles, Re_{mf} is less than 20 and U_{mf} is expressed by [16]

$$U_{mf} = \frac{d_p^2 (\rho_p - \rho_g) g}{150\mu} \frac{\varepsilon_{mf}^3 \phi_s^2}{1-\varepsilon_{mf}} \tag{2.7}$$

A considerable amount of studies [45,47,48,50,51,53,59,66,70,71] showed that minimum fluidization velocity decreases with vibration strength. Marring et al. [47] observed a decrease in U_{mf} when vibration was applied to the bed of Group A particles. They also reported that moisture content has an increasing effect on U_{mf} in the vibrated bed of Group C particles. Noda et al. [48] found that U_{mf} for the glass beads of 6 μm at atmospheric pressure is decreased slowly with the vibration strength while the effect of vibration strength under reduced pressure (1000 Pa) on U_{mf} is less than that under atmospheric pressure. Xu and Zhu [59] found that U_{mf} decreases with vibration frequency and amplitude, and also a critical point of frequency (35 Hz) exists for their system. For the bed of glass beads (10 and 39μm), at lower frequencies than 35 Hz, U_{mf} decreases with increasing frequency, whereas the decreasing tendency is leveled off at about 30 Hz. At higher frequencies than 35 Hz, however, U_{mf} increases slightly with frequency. On the contrary to these studies, based on their experimental conditions, some authors [55,66] reported that vibration did not affect U_{mf} significantly.

Xu and Zhu [64] proposed a new correlation to predict U_{mf} for fine cohesive particles. The correlation based on Ergun equation and force balance over a fluidized bed taking Van der Waals forces into account is given by

$$Re_{mf}^2 \frac{85.71(1-\varepsilon_{mf})}{\phi_s} Re_{mf} = E_g + E_c \tag{2.8}$$

where F_g and F_c are defined as the effects of gravitational force and cohesive force, respectively, expressed by

$$E_g = 0.57\phi_s \varepsilon_{mf}^3 Ar \tag{2.9}$$

$$E_c = 4.7 \times 10^{-9} \frac{\phi_s \varepsilon_{mf}^{0.52} \rho_g d_p}{H_0 \mu^2} \tag{2.10}$$

According to Xu and Zhu [64], introduction of cohesive forces in calculation of U_{mf} for both vibrated and unvibrated beds resulted in higher accuracy compared to two commonly used correlations of Leva [73] and Wen and Yu [74].

2.2.3 Effect of Vibration on Bed Expansion and Bed Voidage

At the onset of fluidization, the fixed bed expands and the gas can find more spaces to move upward among the solids with an increase in the gas flow rate, hence a certain level of the bed surface is reached. When fluidization regime changes by further increasing the flow rate, the bed height and the bed voidage becomes larger. The bed voidage is one of the important parameters in designing and operating vibrated fluidized beds. The total bed voidage is the fraction of the overall bed volume occupied by the fluid consisting of the voids between particles:

$$\varepsilon = 1 - \frac{\rho_a}{\rho_p} \tag{2.11}$$

where ρ_a is the apparent density of the bed. At minimum fluidization condition, bed voidage can also be predicted experimentally by using the force balance below,

$$\frac{\Delta P}{H_{mf}} = (1 - \varepsilon_{mf})(\rho_p - \rho_g)g \tag{2.12}$$

Wank et al. [49] also proposed an expression of force balance by taking the vibration effect and total interparticle cohesive force into account

$$\frac{\Delta P}{H_{mf}} = (1 - \varepsilon_{mf})(\rho_p - \rho_g) + \frac{6F_c}{H_{mf}} - (1 - \varepsilon_{mf})(af^2)\rho_p \tag{2.13}$$

where F_c is interparticle cohesive force which may include van der Waals, electrostatic and capillary forces between particles within the bed. In the event of significant vibration and cohesive force effects on a fluidized bed system, eqn. (2.13) can be also used to predict ε_{mf}.

Bed voidage and its distribution inside the bed determine the fluidization quality. A number of studies on vibrated fluidized beds operating with fine particles [47,48,50,53,59] have shown that vibration give cause for decrease in bed voidage at minimum fluidization condition. According to Tasirin and Anuar [50], the decrease in ε_{mf} explains the reduction in U_{mf} also. Mawatari et al. [52] reported that the bed expansion ratio based on minimum fluidization condition (H/H_{mf}) increases with vibration at gas velocities larger than U_{mf}. In another study [51], they observed an increasing trend in bed expansion ratio (H/H_0) for various Group C particles. Jin et al. [60] found that the axial and radial distribution of voidage becomes more homogenous with vibration. Their results also showed that the effect of vibration on bed expansion reduces with bed height due to larger resistance to the vibration energy transfer. Similar results have also been obtained in different studies [57,65,66].

Xu and Zhu [64] came up with a correlation by suggesting the particle size has a significant effect on the bed voidage. The bed voidage at the onset of fluidization is inversely proportional with particle size and expressed as a function of d_p.

$$\varepsilon_{mf} = 0.77(d_p \times 10^6)^{-0.124} \tag{2.14}$$

Additionally, they remarked that vibration parameters should be taken into account in eqn. (2.8) and eqn. (2.14) due to appreciable effects of mechanical vibration on U_{mf} and ε_{mf}.

2.3 Drying Characteristics of Vibrated Fluidized Beds

As summarized in section 2.2, there are many hydrodynamic studies showing that vibrated fluidized beds can be used successfully with cohesive particles. However, to the author's knowledge, there is no study on drying of Group C particles in vibrated fluidized beds. As can be seen in Table 2.2, the studies reported in the literature shows that the majority of the vibrated fluidized bed drying research was made with Group B and Group D particles. In these studies, effects of operating conditions on drying characteristic were investigated. The findings of these studies are summarized in the following sub-sections:

1) Effect of vibration parameters
2) Effect of gas inlet temperature and superficial gas velocity
3) Effect of static bed height
4) Effect of initial surface moisture content

Table 2.2 Major experimental studies on vibrated fluidized bed drying

Researchers	Material		OPERATING PARAMETERS					
	Type	**Particle Size (mm)**	**Air Inlet Temperature (°C)**	**Bed Dimensions (m)**	**Amplitude (mm)**	**Frequency (Hz)**	**Vibration Strength (Λ)**	**Static Bed Height (mm)**
Gupta [37]	Molecular sieve	2.2-3.9	30-47	0.2x0.2	0-4.25	0-75	-	25
	Silica gel	0.55-2.2	48-51		0-4.15	0-100		12.5-50
Suzuki et al. [75]	Resin particles	0.42-0.59	42	0.11	-	-	0.17-0.45	40-80
Suzuki et al. [76]	Glass beads	0.11-0.35	50-60	0.11	-	-	0-1.21	40
Hasatani et al. [77]	Brick particles	0.62, 1.19	40-60	0.5x0.15	-	58.7	1.6-4.4	-
Nilsson and Wimmerstedt [78]	Sand	0.28	60-135	- (Pilot scale)	2	-	-	50, 100
	Penta erythritol	0.38	132					50
	Sodium formate	0.32	60, 130					50
	Apetite	3.6	127, 160					100

Table 2.2 Major experimental studies on vibrated fluidized bed drying (Cont'd)

Researchers		Material		OPERATING PARAMETERS					
		Type	**Particle Size (mm)**	**Air Inlet Temperature (°C)**	**Bed Dimensions (m)**	**Amplitude (mm)**	**Frequency (Hz)**	**Vibration Strength (Λ)**	**Static Bed Height (mm)**
Dong et al. [79]		Corn Silica gel Citric acid	0.1-3	70-100	0.18	1-3	0-21	-	20-60
Pan et al. [80]		Citric acid Refined salt	0.25-1.2 0.2-1.1	20-60 20-80	0.18	1-3	0-17	0-3.5	20-60 40-70
Pan et al. [82]	Batch	Sea sand	0.07-0.8	85	0.24	0-3	0-20	-	60
	Cont.	Wheat bran			2x0.2	0-3	0-20		
Ramesh and Rao [81]		Rice	-	160-240	0.5x0.15	-	-	-	-
Pan et al. [83]	Lab scale	Moyu pieces	10x10x3	100-120	0.24	0-3	0-20	-	-
	Pilot scale		≤30x30x3		2x0.2	0-3	16	0-3	-

Table 2.2 Major experimental studies on vibrated fluidized bed drying (Cont'd)

Researchers	Material		OPERATING PARAMETERS					
	Type	**Particle Size (mm)**	**Air Inlet Temperature (°C)**	**Bed Dimensions (m)**	**Amplitude (mm)**	**Frequency (Hz)**	**Vibration Strength (Λ)**	**Static Bed Height (mm)**
Pan et al. [84]	Carrot	12x12x3 12x12x6 12x12x9	95-130	0.24	3	16	-	40-80
Pan et al. [85]	Carrot	12x12x6	130	0.24	3	16	-	100
Moreno et al. [86]	Sawdust	0.89-3.56	70-130	0.3x0.3	2.5-5	7-12.5	-	100-350
Soponronarit et al. [87]	Paddy	-	125-140	0.6x2.1x1.2	5	7.3	1	115
Pan et al. [88]	Inert particles	4.43, 4.76	80-140	0.143	3	16	-	60-100
Cruz et al. [89]	Milk powder	0.15-0.2	70-80	0.25	0.75-2.25	60	-	20
Alvarez et al. [90]	Turnip seeds	1.98	70	0.12	1.65-1.95	11.4-24.8	1-4	(500g)

Table 2.2 Major experimental studies on vibrated fluidized bed drying (Cont'd)

Researchers	Material		OPERATING PARAMETERS					
	Type	Particle Size (mm)	Air Inlet Temperature (°C)	Bed Dimensions (m)	Amplitude (mm)	Frequency (Hz)	Vibration Strength (Λ)	Static Bed Height (mm)
Silva-Moris and Rocha [91]	Adipic acid	0.311	60-100	0.1	10	3.33	0.5	60
Meili et al. [92]	Ballotini	2.19	80, 100	0.114	3, 15	8.14, 18.24	0, 4	90
Stakic and Urosevic [93]	Poppy seeds	0.75	50-90	0.15	1-5	9.65-19.65	-	15-30
Sadeghi and Koshtaghaza [71]	Black tea	0.84	100-130	-	1, 3	4, 10	0-1.184	80

2.3.1 Effect of Vibration Parameters

During vibrated fluidized bed drying of molecular sieve granules, Gupta [37] observed no appreciable change in the shape of the drying rate curves take place as a result of vibration. Considering the range examined, he reported that the similarity between vibrated and unvibrated case is due to the vibration independence of drying mechanism in the falling rate period. He also investigated the effects of vibration frequency and amplitude on drying characteristics. According to his findings, drying rate was found to decrease and then increase with frequency at lower and higher values of vibration strength than 1, respectively. On the other hand, no clear trends were observed in the drying rate with vibration amplitude. Similar results were also reported by Dong et al. [79]. Suzuki et al. [75,76] provided two comprehensive examinations of the basic characteristics of a vibrated fluidized bed dryer. According to their results, the uniformity of moisture content in the bed becomes remarkable under appropriate vibration conditions. Vibration enhances particle circulation rate and drying rate. However, the effect of vibration decreases as particle size increases. In several studies [78,79,93], it was also reported that vibration enhances mixing of particles and results in better fluidization. Furthermore, the drying time can be reduced when the vibration strength is increased [71,77].

Another advantage of mechanical vibration is the decrease in required air velocities [71,76,86,91] for drying operations. For this reason, it reduces electrical energy consumption of dryer compared to fluidization technique without vibration [71,87].

Alvarez et al. [90] investigated the effects of vibration amplitude and frequency on drying kinetics. The drying time was found to decrease with high frequencies working with small amplitudes and air velocity. On the other hand, at large amplitudes and air velocities, frequency also caused a decrease in drying time. Similarly, vibration amplitude enhanced drying rate.

2.3.2 Effect of Gas Inlet Temperature and Superficial Gas Velocity

As expected, drying rate increases with air velocity and air inlet temperature [71,75,77,79,80,86,88,89,91,93]. Suzuki et al. [76] reported that particle circulation rate increases with air velocity. Pan et al. [80] studied drying of sticky and agglomerating materials. The results showed that the increase in superficial air velocity leads to better fluidization which results in a rapid increase in the drying rate. Cruz et al. [89] found air inlet temperature to enhance drying rate significantly and affect product quality. They also reported that air velocity affects powder properties by carrying out more fines.

Moreno et al. [86] proposed that the reduction of required air velocities for vibrated case can be up to 50% in relation to U_{mf} and operating air velocities improve drying kinetics. Besides, operation temperature was found to be the most influential parameter upon residence time in the dryer.

2.3.3 Effect of Static Bed Height

Suzuki et al. [75] suggested that the effect of vibration on the particle circulation rate decreases as the bed height increases. To obtain the desired particle circulation rate and homogeneity of moisture content in the bed, an optimum vibration strength value has to be determined by taking the specific material used and the bed height into consideration. Pan et al. [80] concluded that constant drying rate decreases almost linearly with bed height at a given vibration strength and air velocity. A decreasing trend of drying rate with bed height was also reported in another study of Pan et al. [84]. Moreno et al. [86] found that bed height influences drying time but drying behavior does not change appreciably with bed height.

2.3.4 Effect of Initial Surface Moisture Content

Moreno et al. [86] observed that drying rates do not vary with different initial moisture contents during constant rate period drying. Silva-Morris and Rocha [91] reported that the highest quality of fluidization while drying is obtained with the lowest value of moisture content. However, the differences were not found to be significant. Surely, these insignificant changes in fluidization quality and hence drying kinetics are due to inconsiderable effect of capillary forces.

CHAPTER 3

EXPERIMENTAL

3.1 Experimental Set-Up

Within the scope of this work, the greatest efforts were made to design and construct two fully equipped vibrated fluidized bed systems for the analyses related to hydrodynamic and drying experiments, respectively. The fluidized bed column of the first system was made of plexiglass (polymethylmethacrylate) to permit visual observations of the fluidization behavior during hydrodynamic tests. However, the use of a plexiglass column for the drying tests was found to be impossible due to the maximum service temperature value (80-90 °C) of the material. Therefore, the fluidized bed dryer was made of nickel-chrome stainless steel material. Both systems have the same dimensions and were mounted on the same vibration system during the experiments.

3.1.1 Vibration System

Figure 3.1 shows the three dimensional sketch of mechanical vibrating system that the fluidized beds were mounted on. The vibration base consisting of a vibro-motor was screwed on four identical springs which can be tightened or released by means of two nuts on each of the mounting rods. The vibro-motor is an external electric vibrating motor having twelve semi-circle shaped unbalanced weights positioned reciprocally. With the centrifugal force applied by the rotational movement of the unbalanced weights, a vertical motion of vibration was obtained. Additionally, an adjustable holder was constructed and placed at the top of the fluidized bed columns to prevent the possible horizontal movements. The vibration amplitude was controlled by changing the position of the nuts and the number of unbalanced weights on the vibro-motor (Kem-P Electric Motors Ltd. Co.) with a capacity of centrifugal force of 22 kg at 50 Hz. The amplitude of vibration was measured by a microelectromechanical (Analog Devices, Inc. ADXL001) accelerometer and the frequency was adjusted with an inverter.

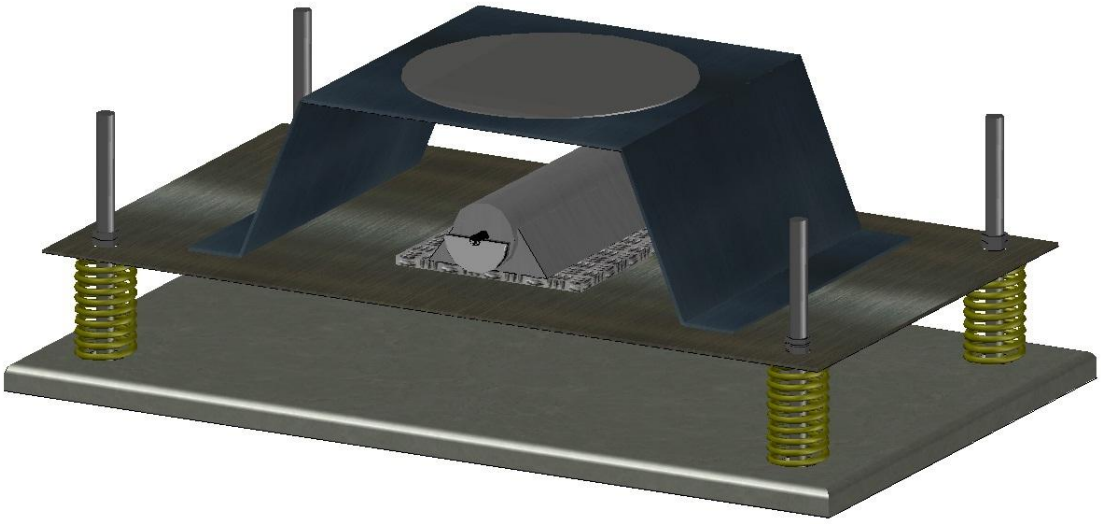

Figure 3.1 Mechanical vibration system

3.1.2 Experimental Set-Up and Method for Hydrodynamic Tests

A detailed three dimensional sketch of the fluidized bed system and a schematic of the experimental set-up used in the hydrodynamic studies are shown in Figure 3.2 and Figure 3.3, respectively.

Figure 3.2 Fluidized bed apparatus used in hydrodynamic experiments

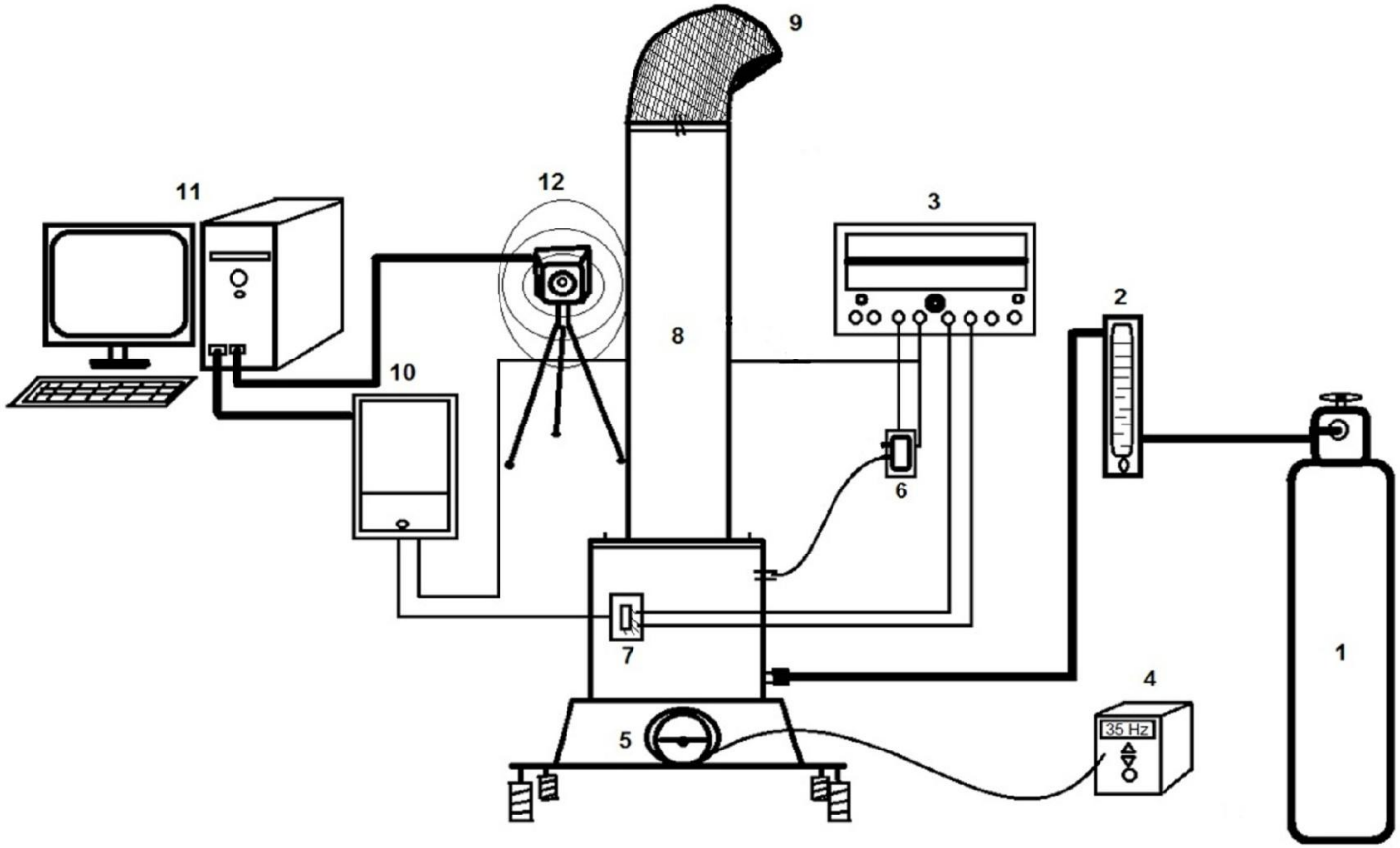

Figure 3.3 Experimental set-up: 1) N_2 Tube 2) Rotameter 3) DC Supply 4) Inverter 5) Vibro-motor 6) Pressure Transducer 7) Accelerometer 8) Fluidized Bed 9) Bag Filter 10) Data Acquisition Card 11) Computer 12) Digital Camera

The fluidized bed apparatus consists of a delrin (polyoxymethylene) plenum and a plexiglass column with an inner diameter of 80 mm and height of 1000 mm. Pure nitrogen was used as the fluidizing gas. The gas was distributed into the bed by using a 1 μm filter grade sintered porous stainless steel disc of 3 mm thickness given in Figure 3.4 (GKN Sinter Metals Inc.). The nitrogen flow through the bed was controlled by a flowmeter (Cole Parmer Inst. Co. EW-03227-24) with a range from 0 to 3868 cm^3/min. Pressure drop measurements were made by using a differential pressure transducer (Omega Eng. Inc. PX142-002D5V) connected to plenum just below the gas distributor. Pressure drop of the bed was obtained by subtracting the pressure drop of the gas distributor from the total pressure drop across the bed. Bed height was measured with a paper ruler taped to the front side of the plexiglass column. Visual observations of the fluidization behavior were also recorded by a digital camera (IDS GmbH. uEye-UI-2210-M) with the ½" VGA monochrome and color CCD sensor delivering a resolution of 640 x 480 pixels.

Figure 3.4 Sintered porous metal gas distributor

To determine the effective vibration conditions to obtain high fluidization quality during a drying process, the effects of mechanical vibration and moisture content of the bed material on fluidization index, minimum fluidization velocity, bed voidage and bed expansion ratio were first examined in this cold fluidized bed system.

Each experimental run was started by adjusting the vibration parameters and loading the previously prepared batch of 300 g clinoptilolite material. The reason of using the same weight of the bed material in each experiment is that there was a change in initial bed height values under different vibration conditions. The effect of vibration frequencies on fluidization index, minimum fluidization velocity, bed voidage and bed expansion ratio

were examined for two different moisture contents (X= 9%, 15% w.b.). The moisture contents of the materials were measured by a moisture analyzer (OHAUS Corp. MB45) at 200 °C. In the present study, the vibration strength was kept constant at 1.8 and 1.5 values due to the limitations of the vibration system. Different vibration frequencies (20, 30 and 40 Hz) were applied at each vibration strengths. Operational conditions used in hydrodynamic tests are listed in Table 3.1.

Table 3.1 Operational conditions used in hydrodynamic tests

Ambient temperature (°C)	22±1
Ambient relative humidity (%)	40±2
Fluidizing gas	Pure nitrogen
Weight of the bed material (g)	300
Moisture content of the bed material (% w.b.)	9, 15
Vibration strength	1.5, 1.8
Vibration frequency (Hz)	20, 30, 40

Sampling of pressure signals was made by using a data acquisition system (National Instruments Corp.) with LabVIEW program. 3000 data were collected with a sampling frequency of 1000 Hz for each measurement. Measurements were repeated three times for each measurement point and the average values were used. In addition, three sets of experiments were conducted to check the reproducibility of the results and the average values are reported in this thesis.

Data acquisition and analog-digital conversion of the signals were carried out by using a data acquisition card (NI PCI-6280) with a sampling rate of 500 kS/s. The block diagram and virtual interface of LabVIEW program written for collection of pressure drop data are shown in Figure 3.5 and 3.6, respectively.

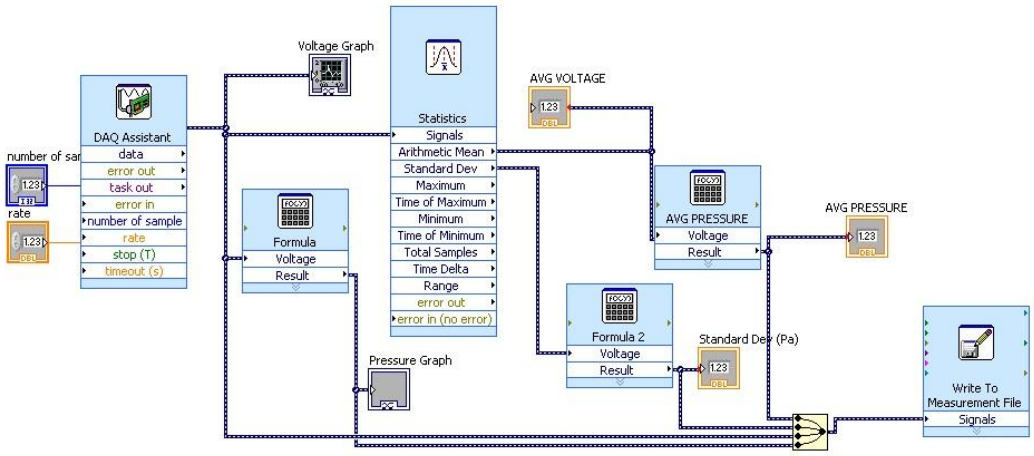

Figure 3.5 Block diagram of LabVIEW program for hydrodynamic tests

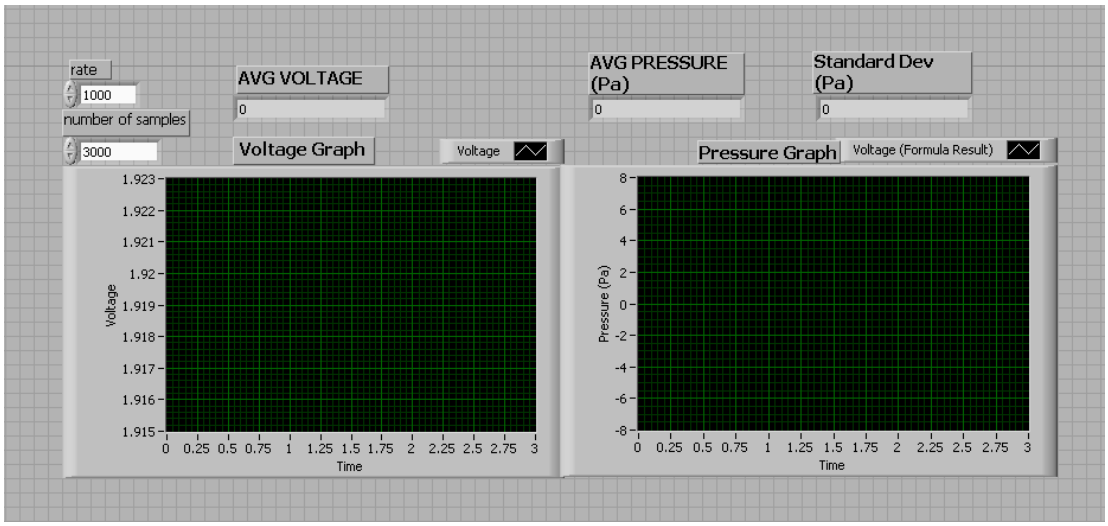

Figure 3.6 Virtual interface of LabVIEW program for hydrodynamic tests

3.1.3 Experimental Set-Up and Method for Drying Tests

The nickel-chrome stainless steel fluidized bed dryer designed for the second part of the experimental study is shown in Figure 3.7. The dryer column has an inner diameter of 80 mm and a height of 600 mm. The diameter of the column was selected to be equal to the previous unit in order to obtain the same hydrodynamic phenomena inside the system. A custom-made exhaust duct and a feeding pipe were welded at the top section of the column. The inlet diameter of exhaust duct was expanded from 23 mm to 100 mm in order to reduce the velocity of exiting moist gas by using a conical apparatus and a pipe bend. In addition, a polyamide cap equipped with a 500 mm-long plastic pipe was mounted at the

outlet of the exhaust duct. Therefore, a high-accuracy measurement of relative humidity could be made without disturbance possibly caused by ambient air.

Figure 3.7 Fluidized bed dryer

Figure 3.8 provides a view of the insulated fluidized bed dryer and other subsystems. The experimental set-up used in drying experiments is also shown schematically in Figure 3.9. Due to the lack of an air dehumidifier device, pure nitrogen was used as the drying gas.

Prior to feeding into the plenum, the drying gas was passed through an electrical pre-heater which was designed and constructed specially for this system. The heater was designed with a stainless steel tube of 100 mm outer diameter and a cross frame heating coil of 500 Watt heating capacity. The nickel-chrome heating coil was insulated by ceramic beads on a stainless steel support frame which was firmly fixed to the inside of the tube. The ends of the heating coil were enclosed in the top section of the heater for ease of electrical wiring. To minimize the heat loss, the heater and the fluidized bed dryer were insulated with 50 mm thick rockwool. In addition, a rockwool insulated duct conveyed the drying gas from the heater to the plenum of the vibrated fluidized bed dryer.

Figure 3.8 A photograph of the vibrated fluidized bed dryer system

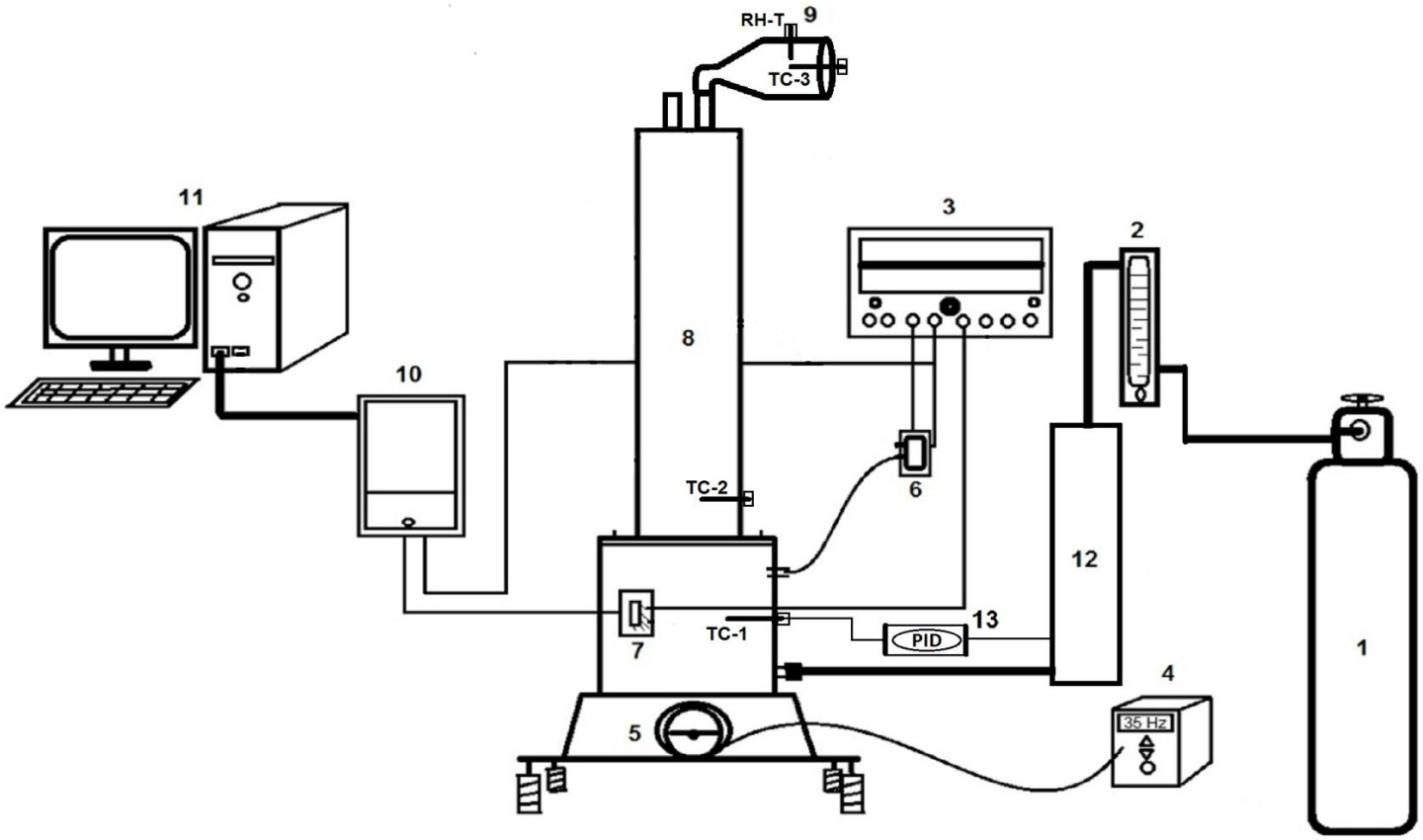

Figure 3.9 Experimental set-up: 1) N_2 Tube 2) Rotameter 3) DC Supply 4) Inverter 5) Vibro-motor 6) Pressure Transducer 7) Accelerometer 8) Fluidized Bed 9) Exhaust Duct 10) Data Acquisition Card 11) Computer 12) Heater 13) PID controller **TC**: Thermocouple, **RH-T**: Relative Humidity and Temperature Sensor

In the drying experiments, a heat resistant gauge pressure transducer (Bis Sistem Co. Ltd. Keller 0-160 mbar) was used for the high sensitivity pressure drop measurements. The flow of drying gas was controlled by a flowmeter in the range of 0-59580 cm^3/min (Cole Parmer Inst. Co. EW-03227-36). Measurements of temperature were made by using 3 J-type thermocouples (Tetcis Co. Ltd.). Considering the expanded bed height during a stable bubbling regime, bed temperature was measured with a thermocouple (TC-2) located 70 mm above the bottom of the bed. Inlet gas temperature was measured by TC-1 which was installed at the midpoint of the plenum and adjusted by using a PID controller. The relative humidity-temperature (RH-T) sensors (Michell Instruments, PCMini52) and TC-3 were located at the top of the exhaust duct of the dryer. An auxiliary cable heater and a variac were used for keeping the outlet temperature constant at the outlet in order to prevent possible condensation of vapor.

To determine the suitable operating conditions for an economical drying process of clinoptilolite, three different superficial gas velocity and inlet gas temperature values were chosen for drying experiments by taking into consideration the fact that the drying time should not exceed 2 hours and the fluidization regime should stand within the boundaries of bubbling regime. Starting from this point, a wide range of gas velocity and gas inlet temperature values were applied and the results were analyzed by means of preliminary experiments conducted earlier using the experimental set-up which was constructed for hydrodynamic study. Accordingly, superficial gas velocities of 10.5, 15.8 and 21 mm/s and gas inlet temperatures of 60, 80 and 90 °C were chosen to be applied in the drying experiments at the previously determined vibration condition.

300 g of clinoptilolite material at initial moisture content of 16% (±0.1% w.b.) was loaded into the vibrated fluidized bed. The drying tests were carried out until the moisture content is below 8%. The moisture content was measured by using a moisture analyzer (OHAUS Corp. MB45) operating at 200 °C to be consistent with the industrial need mentioned in Chapter 1. To obtain drying curves, sampling of the bed material during operation with negligible disturbance to the system is crucial. Therefore, the samples were taken within 5 seconds without making any changes in drying operation during the experiments. For this purpose, a small sampling ladle with a filling capacity of 2-2.5 g was used by plunging into the bed from the top of the column. Time intervals between two sampling operations were arranged as 10 or 15 minutes depending on specific drying time of each experiment in order not to affect the bed hydrodynamics. The operational conditions used in drying tests are summarized in Table 3.2.

Table 3.2 Operational conditions used in drying tests

Ambient temperature (°C)	22±1
Ambient relative humidity (%)	40±2
Drying gas	Pure nitrogen
Weight of the bed material (g)	300
Initial moisture content of the bed material (% w.b.)	16
Final moisture content of the bed material (% w.b.)	8
Inlet gas temperature (°C)	60, 80, 90
Superficial gas velocity (mm/s)	10.5, 15.8, 21
Vibration strength	1.8
Vibration frequency (Hz)	40

Inlet and outlet gas temperatures were kept constant throughout the experiments. An auxiliary cable heater was used at the gas outlet to avoid possible condensation of the vapor. Total pressure drop of the bed, bed temperature, relative humidity and temperature of the exhaust gas were recorded continuously at every 2 seconds. 2000 data were collected with a sampling frequency of 1000 Hz for each time interval (2 seconds) and the average values were recorded. In addition, 2 sets of experiments were conducted to check the reproducibility of the results for each experiment. A section of the block diagram and virtual interface of LabVIEW program written for simultaneous collection of measurement data are shown in Figure 3.10 and 3.11.

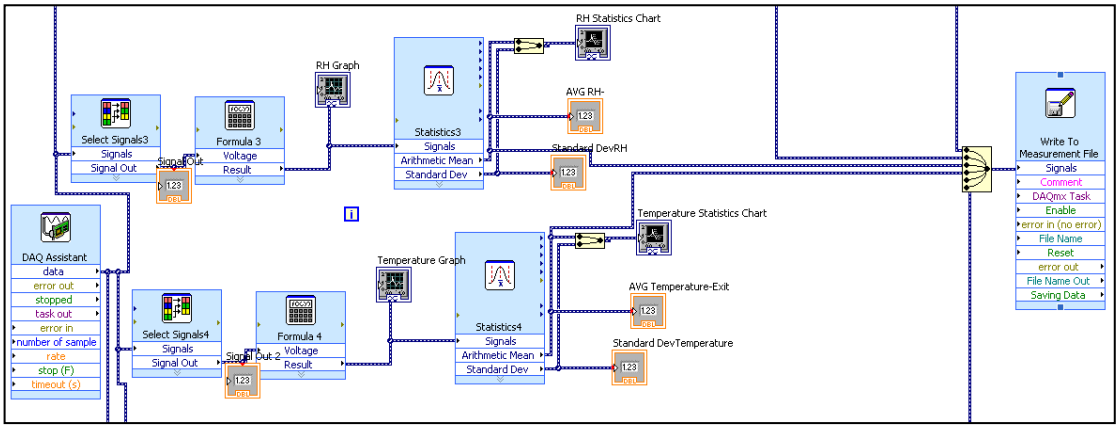

Figure 3.10 Block diagram of LabVIEW program for drying tests

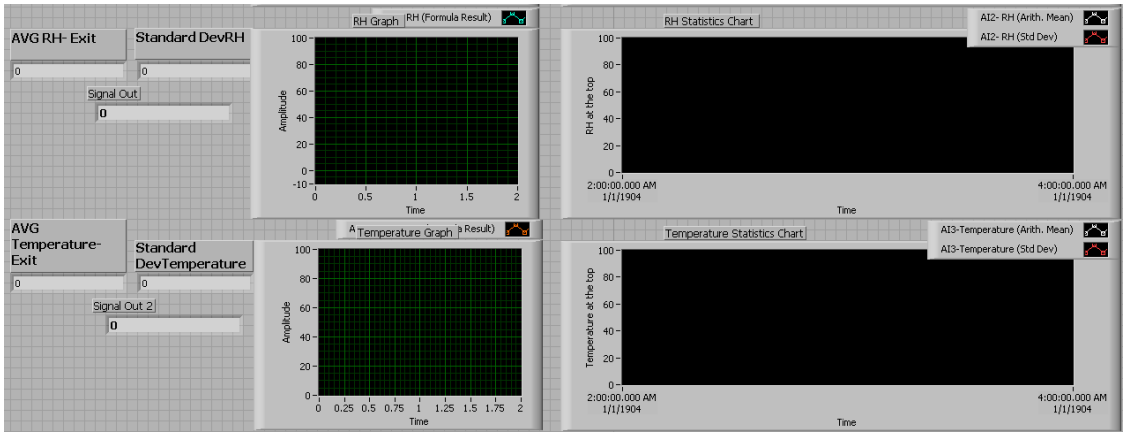

Figure 3.11 Virtual interface of LabVIEW program for drying tests

Before the installation, the measurement equipments were calibrated for reliability and accuracy of electronic components which can naturally drift over time. To quantify and improve the measurement performance of the sensors used in this study, specific calibration procedures were applied. The calibration graphs of the measurement equipments are given in Appendix A.

3.2 Properties of Clinoptilolite Particles

Animal feed additive clinoptilolite rich natural zeolite (Manisa Gördes, Western Anatolia) obtained from Rota Mining Corp. was used as bed material. The batch of raw material was sampled and the samples were characterized by X-Ray diffraction, laser diffraction (particle size analysis), helium and mercury pycnometry, scanning electron microscopy and thermogravimetric analysis.

X-Ray pattern of the clinoptilolite sample is shown in Figure 3.12. Although there are some negligible crystalline impurities, the zeolite consisted mainly of clinoptilolite. The clinoptilolite percentage was determined by reference intensity ratio (RIR) method and is given in Figure 3.13. As can be seen, the clinoptilolite purity of the bed material was found to be almost 100%. This analysis also showed that the sample is composed of negligible amounts of muscovite, montmorilonite and cristobalite.

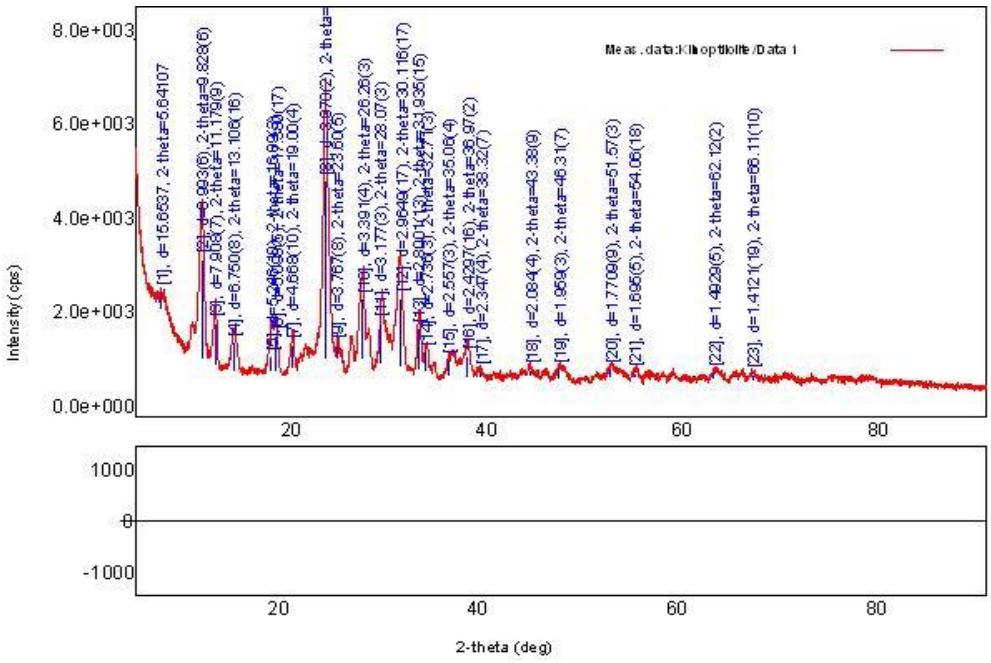

Figure 3.12 X-Ray Diffraction pattern of clinoptilolite

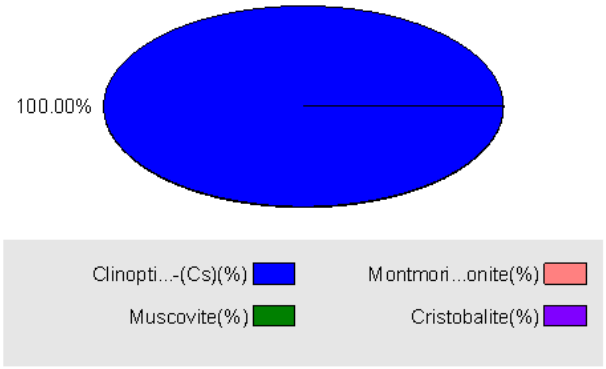

Figure 3.13 Quantitative analysis of clinoptilolite by reference intensity ratio method

The result of thermogravimetric analysis is given in Figure 3.14. During the analysis, the sample was heated from 30 °C to 980 °C with a heating rate of 10°C /min under nitrogen atmosphere. The percent weight losses indicated in Figure 3.14 can be related to loss in water content. During the heating up to 980 °C, clinoptilolite loses its unbound water up to 85 °C, and bound water is lost up to and beyond 285 °C. Therefore, for the sample under analysis, bound moisture content was found to be in the order of 11%.

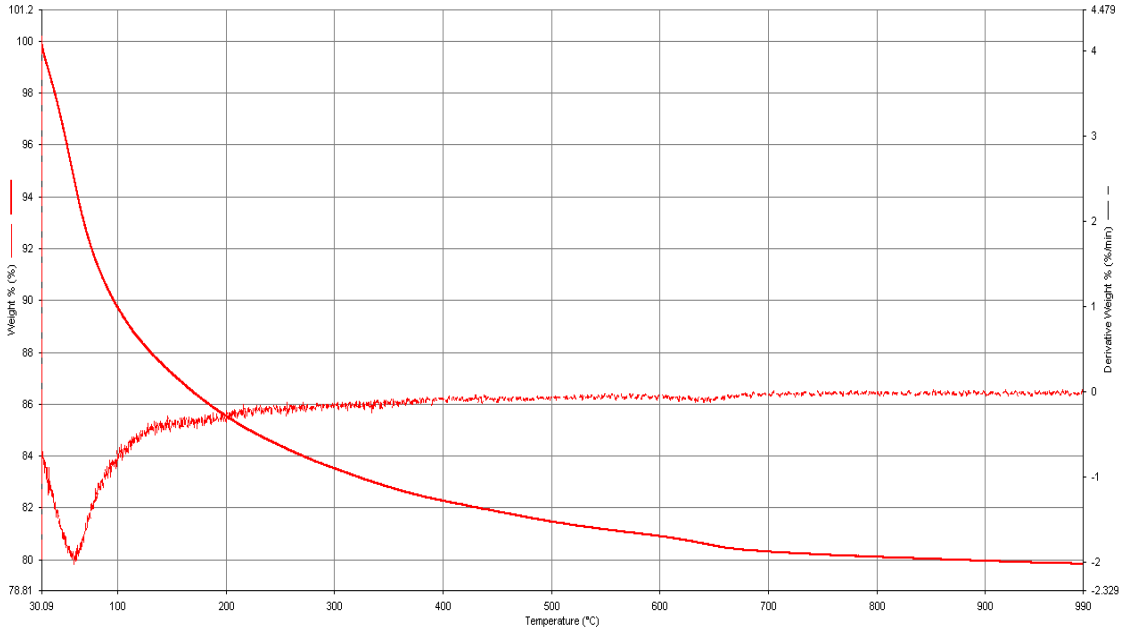

Figure 3.14 Thermogravimetric analysis of clinoptilolite

The particle size determination of clinoptilolite was performed using wet dispersion analysis in particle size analyzer (Malvern Mastersizer 2000). The result given in Figure 3.15 shows that the particle size distribution is relatively large (0.3 – 100 μm). However, polydispersity is not an operational disadvantage for vibrated fluidized beds, since low gas velocities can fluidize fine particles while coarser ones are in mobile state. The Sauter mean diameter of the clinoptilolite particles is 3 μm.

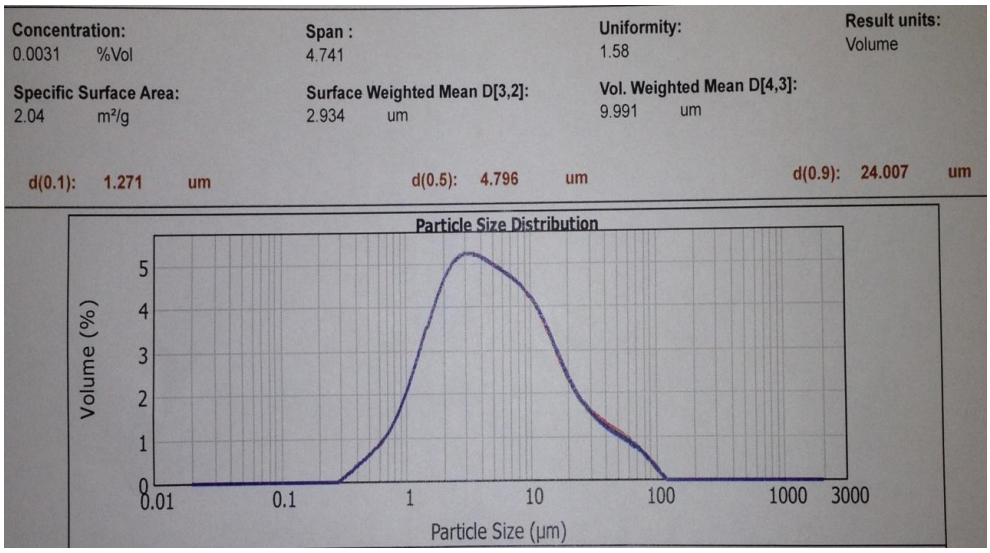

Figure 3.15 Particle size analysis of clinoptilolite

To determine density of the clinoptilolite particles, helium and mercury pycnometer methods were used. Skeletal density was measured at a helium pressure of 17 psig. To obtain bulk density and particle porosity; mercury pycnometer was operated at atmospheric pressure and 55000 psi. The skeletal, bulk and particle density results are 2140 kg/m^3, 680 kg/m^3 and 1980 kg/m^3, respectively.

An average sphericity value of clinoptilolite particles was determined by analyzing a group of randomly chosen particles on SEM micrograph (Figure 3.16). Sphericity is a measure of how spherical a particle is. It is defined as the ratio of the surface area of a sphere to the surface area of the particle with the same volume [94]. The average sphericity value of the clinoptilolite particles is 0.78.

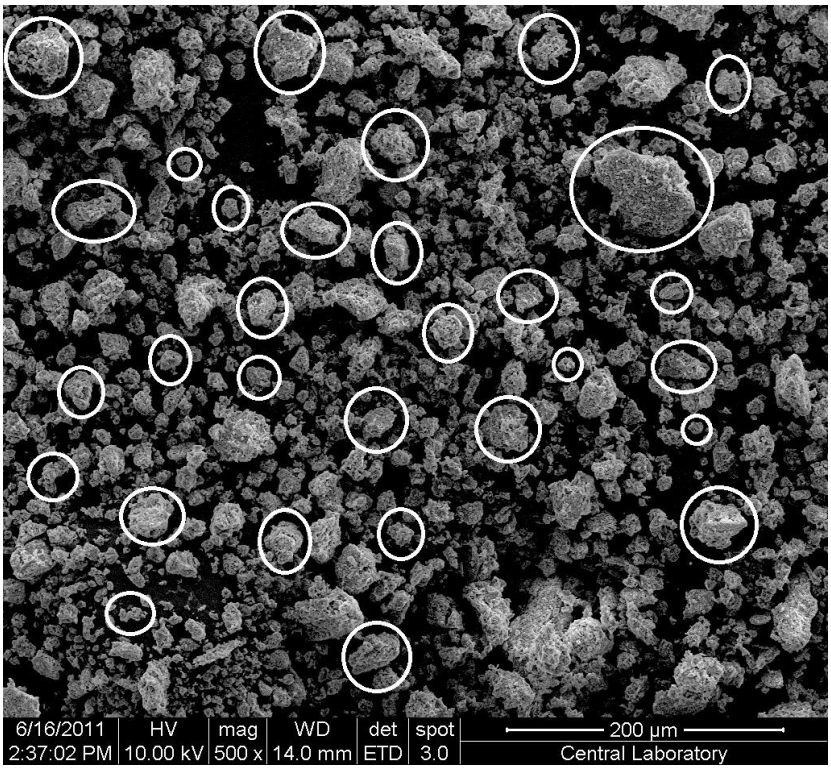

Figure 3.16 Scanning electron micrograph used for determination of sphericity

CHAPTER 4

RESULTS AND DISCUSSION

Drying is a crucial step in the processing of animal feed additive clinoptilolite since high moisture contents of the stocked products can result in molding problems, growth of microorganisms and a significant decrease in toxin binding capacities. To determine the effective operating conditions of a vibrated fluidized bed drying process of clinoptilolite, the tests were carried out in 2 separate systems. In the first part of this study, the effective and suitable vibration conditions were determined for a high-quality fluidization in a cold fluidized bed system. In light of the outcomes of the first part, drying experiments were conducted by using the most effective vibration conditions.

4.1 Hydrodynamic Tests

4.1.1 Effect of Vibration on Pressure Drop Across the Bed

In the first part of this study, preliminary experiments were conducted without vibration. During these tests, the whole bed rose upward after exceeding a certain gas velocity and then dropped down onto the gas distributor by breaking up into several parts when the gas velocity was increased gradually. Then large unstable channels, cracks and rat holes were monitored within the bed.

Figure 4.1 shows the variation of fluidization index ($\Delta PA/mg$) with respect to superficial gas velocity for both vibrated and unvibrated states of the bed. As can be seen in Figure 4.1(a), a typical fluidization curve could not be obtained in this case. With the introduction of vibration, smooth fluidization was observed. As seen in Figure 4.1(b), a typical fluidization curve was obtained and pressure drop over the bed approached the weight of the bed per cross sectional area indicating good quality fluidization.

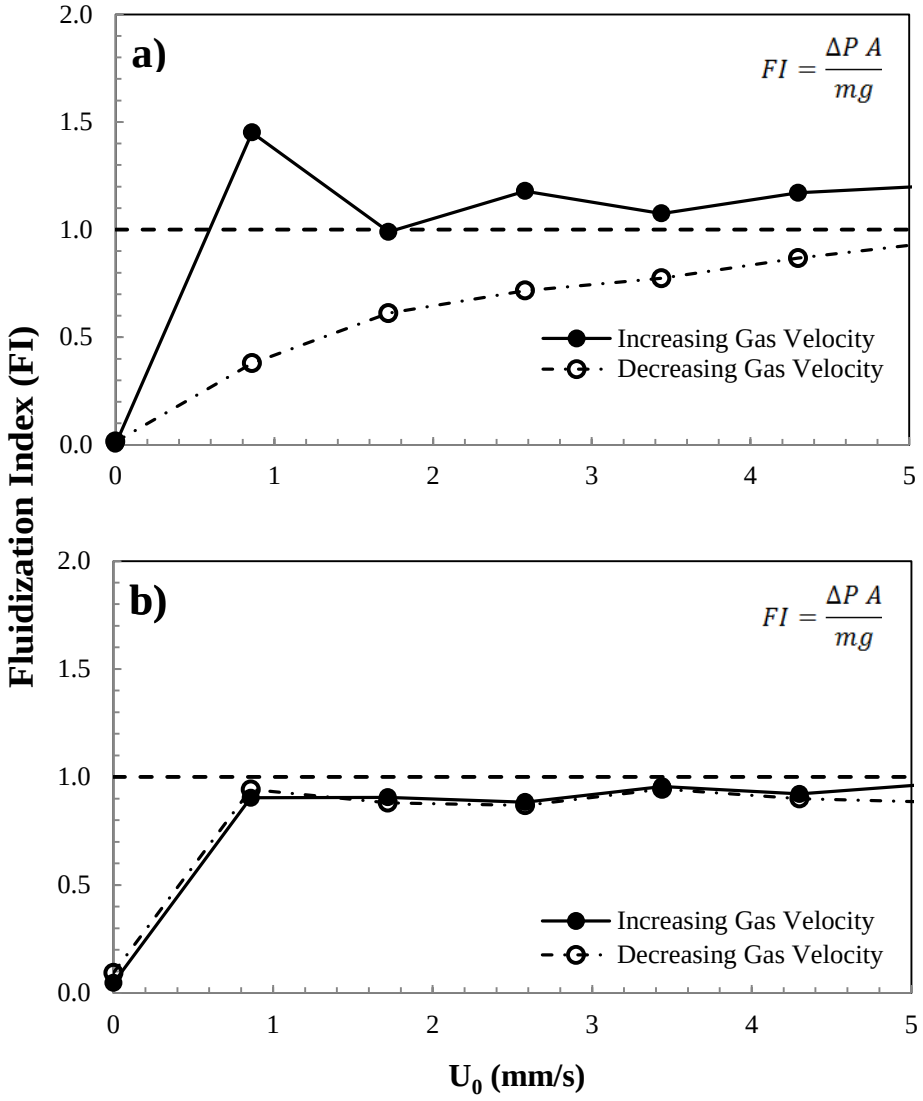

Figure 4.1 Fluidization index curves for bed material of 9 % moisture content a) No vibration b) A= 1.8, f=20 Hz

The pressure drop across the bed can be measured by either increasing or decreasing inlet gas velocities. A difference, especially in the onset of fluidization, can be observed between the two curves which are obtained by increasing and decreasing gas velocity methods. This difference is called hysteresis and is believed to be due to interparticle forces and transfer of stress to the surrounding walls. On the other hand, as can be seen in Figure 4.1(b), hysteresis can be eliminated by the detractive effect of vibration on cohesive forces and wall friction. However, if cohesive forces between particles are significant, it is also possible to observe hysteresis in vibrated fluidized beds. As can be seen in Figure 4.2, at a higher moisture content of 15 %, significant hysteresis is observed due to increase in cohesive forces with increasing moisture content. Due to this hysteresis effect, in the literature, the investigations on the hydrodynamic behavior of fluidized beds are

commonly based on the pressure drop curves obtained by decreasing the air flow rate. This approach was also adopted in this study.

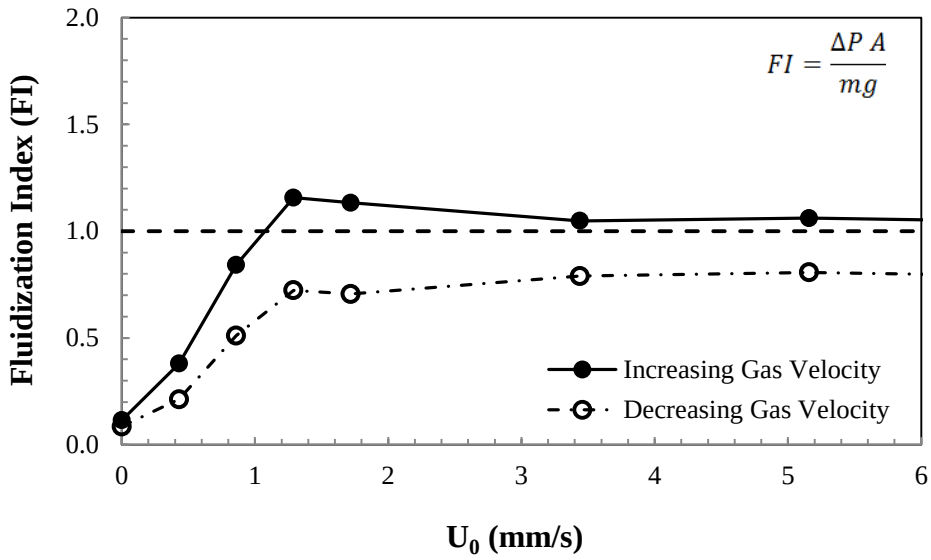

Figure 4.2 Fluidization index curves for bed material of 15 % moisture content (A=1.8, f=20 Hz)

Figure 4.3(a) and (b) show the effect of vibration strength on fluidization index curves while keeping frequency constant at 30 Hz and 40 Hz, respectively. In these tests, the bed was operated with particles having 9 % moisture content. By taking samples at the beginning and at the end of each experiment, it was monitored that the moisture content of the particles during the course of an experiment did not change. As vibration strength is increased from 1.5 to 1.8, fluidization index increases and approaches to unity pointing to higher quality of fluidization for both frequencies. In addition to these results, visual observations showed that the best fluidization quality (absence of channels and presence of smooth fluidization) was obtained with 40 Hz frequency at a vibration strength of 1.8. Therefore, in drying tests, vibration strength and frequency were decided to be set to 1.8 and 40 Hz, respectively.

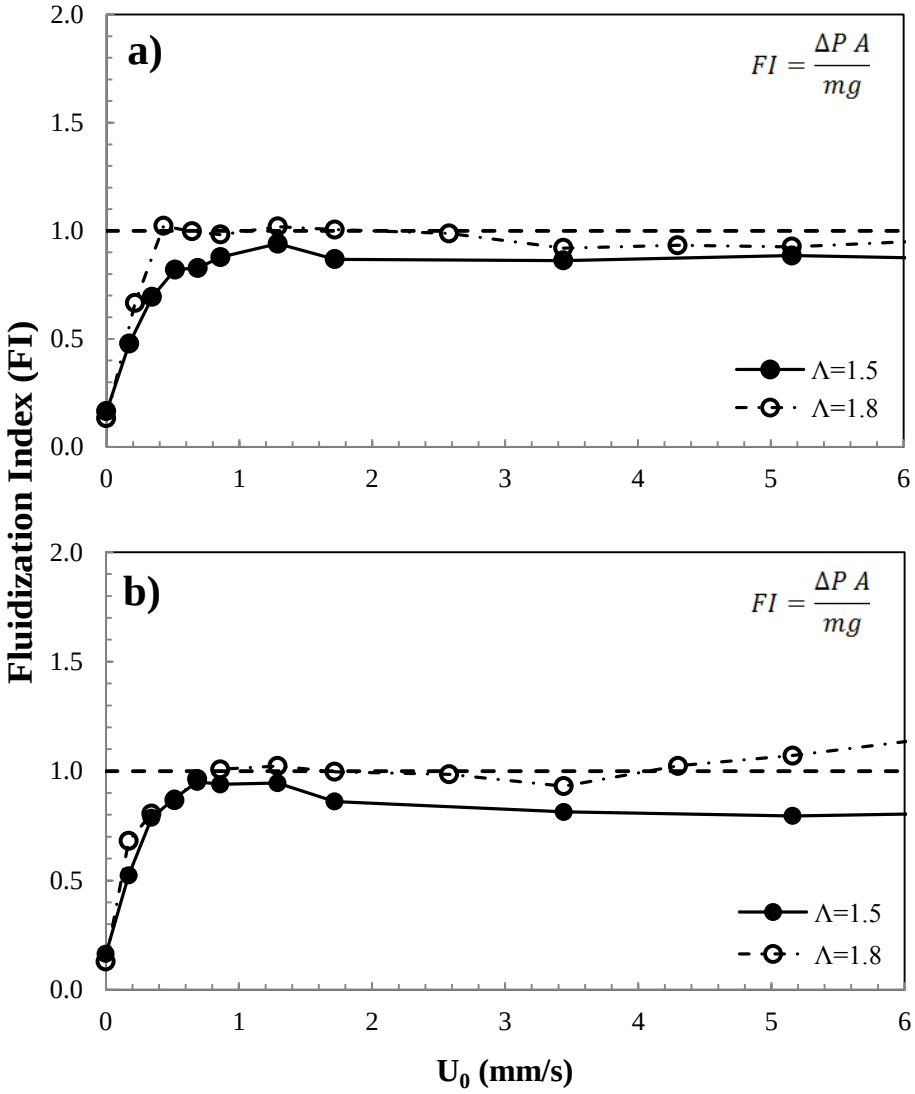

Figure 4.3 Effect of vibration strength on fluidization index curves (X= 9 %) (a)f=30 Hz, (b)f=40 Hz

Figure 4.4 shows the effect of vibration frequency on fluidization index curves for particles having 9 % moisture content at a vibration strength of 1.8. It can be easily seen that fluidization index values could reach unity at all frequencies applied. When there is no vibration, fluidization index is much lower than unity indicating poor quality fluidization due to the presence of channeling and rat holes. With the vibration, smooth fluidization was observed and fluidization index approaches unity. Similar analyses were made with particles of higher moisture content. As can be seen from Figure 4.5, fluidization index attains approximately unity at 30 and 40 Hz vibration frequencies. However, at 20 Hz of frequency, simultaneous presence of channels and bubbles was observed and fluidization index stayed below unity as a consequence of this phenomenon.

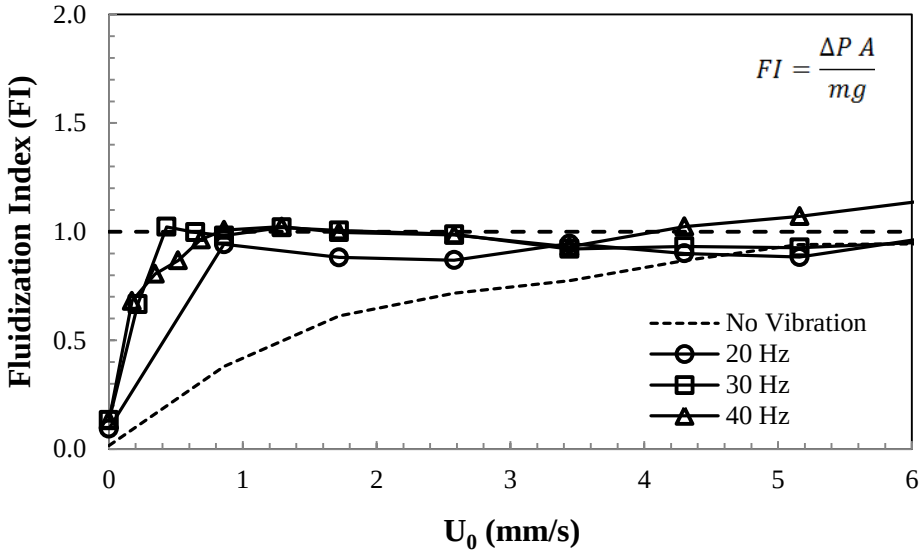

Figure 4.4 Fluidization index with different vibration conditions for decreasing gas velocity (Λ=1.8, X= 9 %)

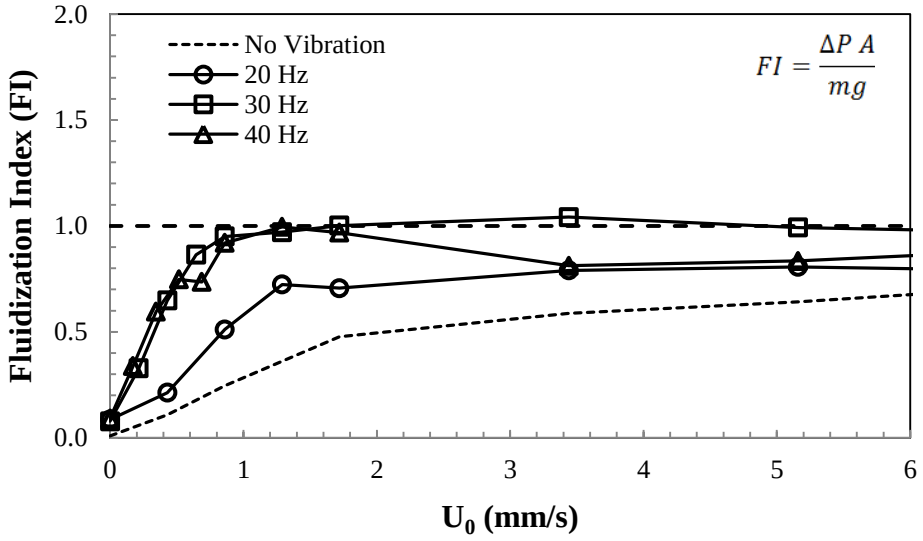

Figure 4.5 Fluidization index with different vibration conditions for decreasing gas velocity (Λ =1.8, X= 15 %)

4.1.2 Effect of Vibration Parameters on Minimum Fluidization Velocity

In the field of fluidization, minimum fluidization velocity values are commonly obtained by using the intersection points of fixed bed line and fluidized bed line (FI=1) on the fluidization index vs. decreasing superficial gas velocity curves as illustrated in Figure 4.6.

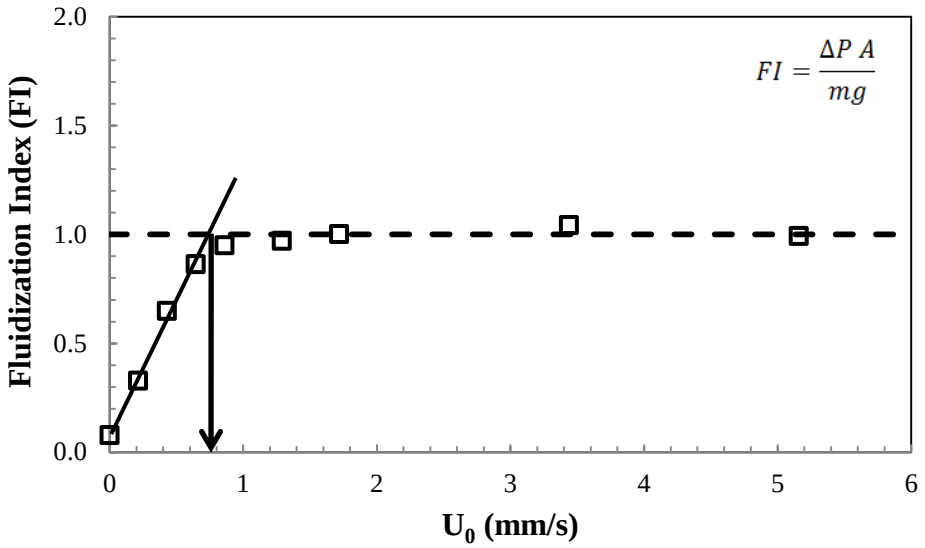

Figure 4.6 Determination of minimum fluidization velocity (A=1.8, f=30 Hz, X= 15 %)

The minimum fluidization velocity values obtained by following the same approach are summarized in Figure 4.7 and 4.8. As expected, minimum fluidization velocity decreases appreciably when vibration strength is increased at all frequencies applied. Minimum fluidization velocity also decreases significantly with vibration frequency irrespective of the moisture content of the zeolite powders. Similar to the findings of Marring et al. [47] who performed experiments in a vibrated fluidized bed using potato starch (d_p=34.6 μm, ρ_p=1500 kg/m^3), minimum fluidization velocity increased with an increase in the moisture content due to increase in cohesive forces.

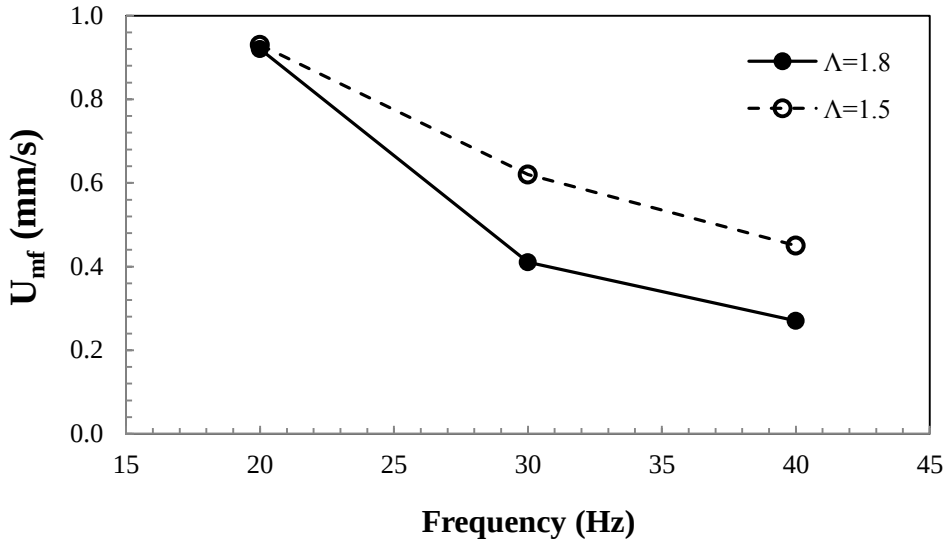

Figure 4.7 Effects of vibration conditions on minimum fluidization velocity (X= 9 %)

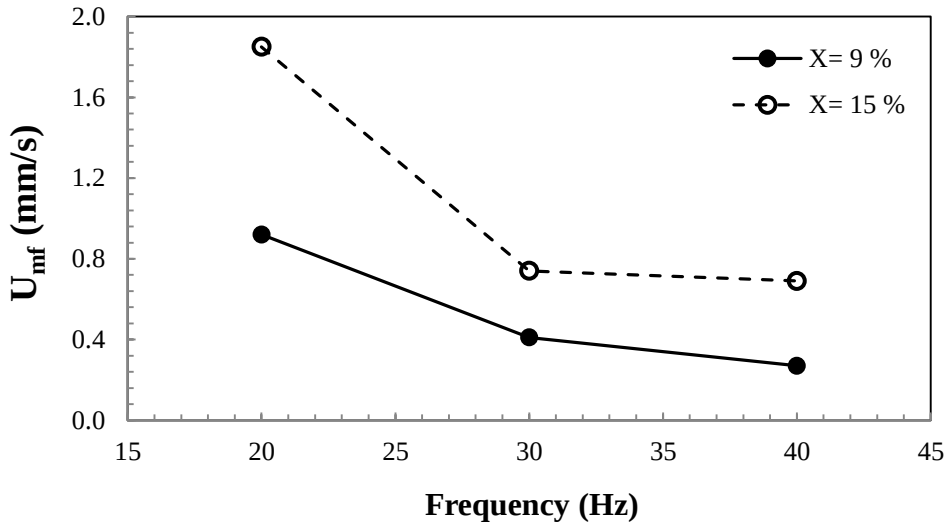

Figure 4.8 Effects of frequency and moisture content on minimum fluidization velocity (Λ=1.8)

4.1.3 Effect of Vibration Parameters on Bed Expansion Ratio

Initial bed height (H_0) and expanded bed height (H) were measured during each experiment with a paper ruler taped to the plexiglass column. The effects of vibration conditions and moisture content on bed expansion ratio (H/H_0) values are illustrated in Figure 4.9, 4.10 and 4.11. As can be seen in Figure 4.9, bed expansion ratio increases with

increasing vibration frequency at constant vibration strengths. As illustrated in Figure 4.10, it also increases when vibration strength is increased at a constant vibration frequency at high gas velocities. It can be easily seen in Figure 4.11 that, at a given superficial gas velocity, bed expansion decreases with moisture content. This means, particles with higher moisture content result in lower fluidization quality with lower expansion ratio compared to particles with lower moisture content at the same operating conditions.

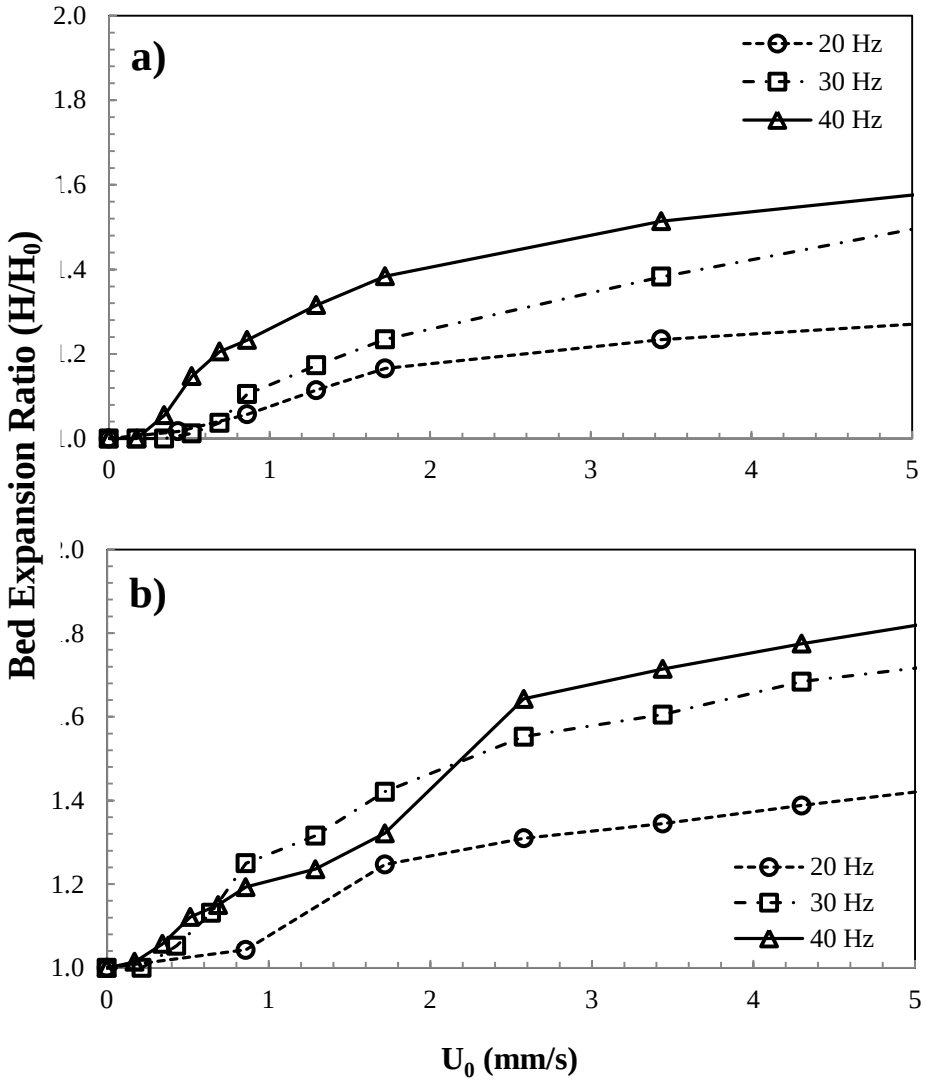

Figure 4.9 Effect of vibration frequency on bed expansion ratio (X= 9 %) (a) Λ=1.5, (b) Λ=1.8

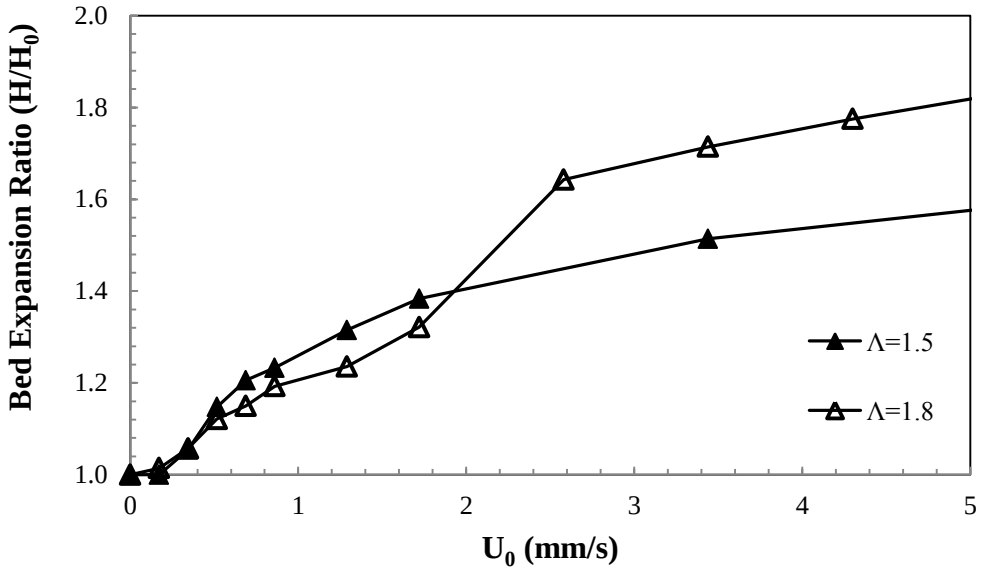

Figure 4.10 Effects of vibration strength on bed expansion ratio (f=40 Hz, X= 9 %)

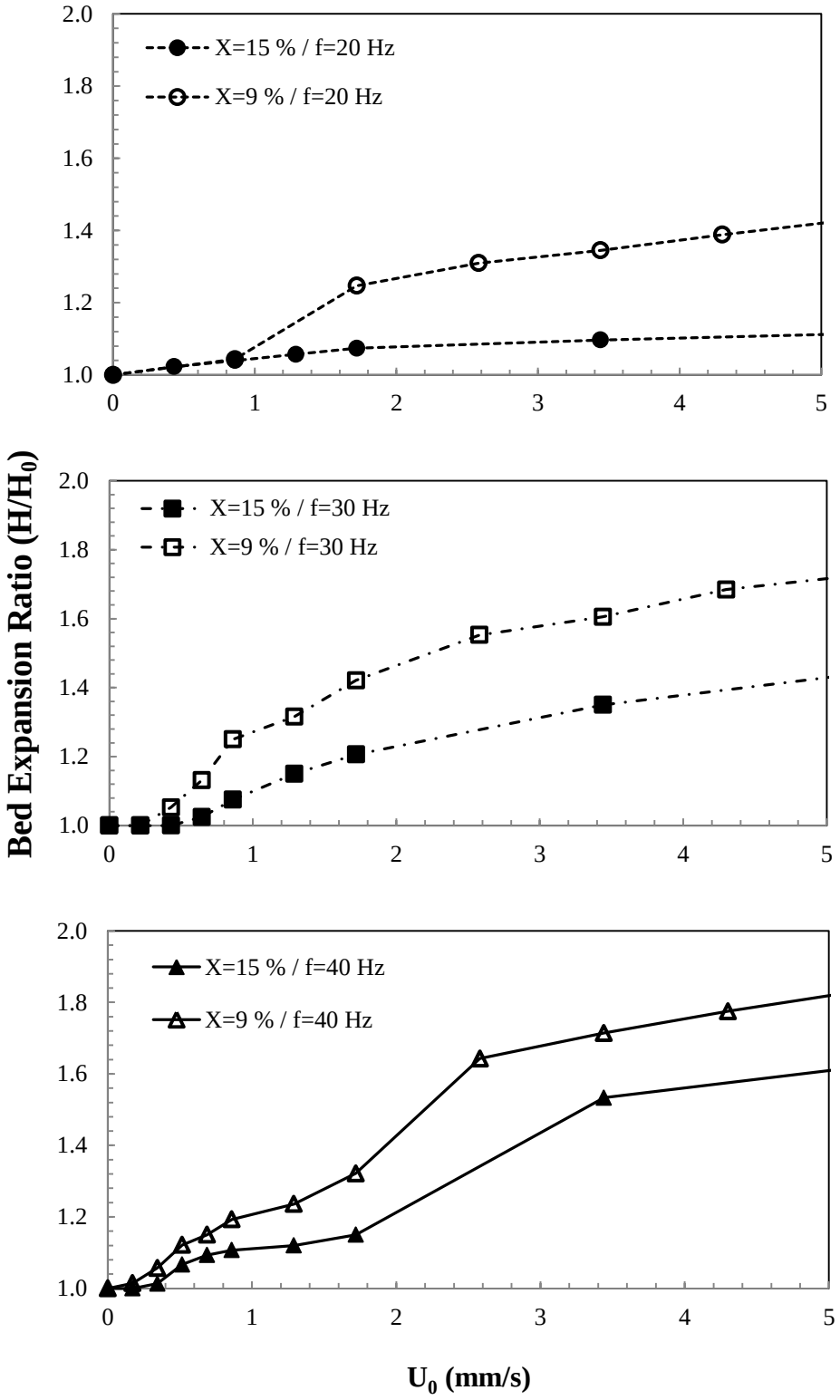

Figure 4.11 Effects of frequency and moisture content on bed expansion ratio (A=1.8)

In this study, bed height recorded at minimum fluidization condition was also used to calculate bed voidage using eqn. (2.12). Figure 4.12 illustrates the effect of vibration parameters on bed voidage at minimum fluidization. As can be seen, bed voidage decreases as vibration strength increases. This trend was also reported as an indication of reduction in minimum fluidization velocity by Noda et al. [48] and Tasirin and Anuar [50].

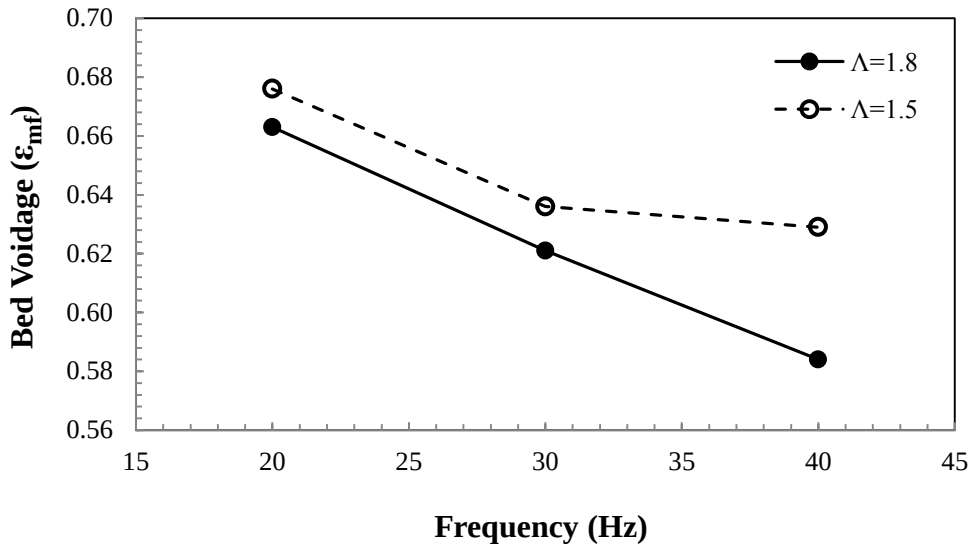

Figure 4.12 Effects of vibration parameters on bed voidage at minimum fluidization

As illustrated in Figure 4.13, bed voidage at minimum fluidization condition increases appreciably with increasing moisture content mainly attributed to the increase in cohesive forces between particles [47]. On the other hand, when frequency is increased, bed voidage decreases appreciably.

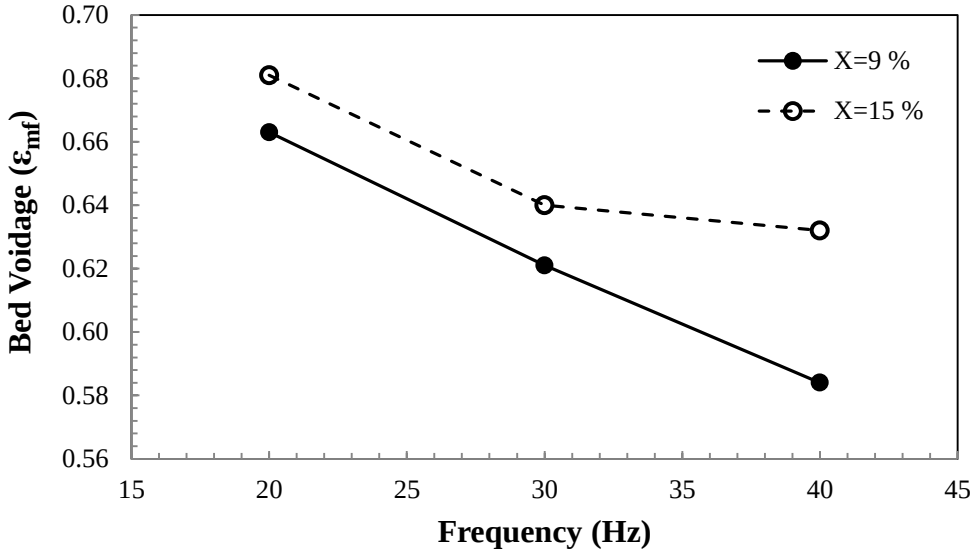

Figure 4.13 Effects of frequency and moisture content on bed voidage at minimum fluidization

4.1.4 Agglomerate Size

In vibrated fluidized beds, a successful gas fluidization of Group C particles can be achieved by reducing the effects of cohesive forces between particles (see section 1.3.3). On the other hand, in a vibrated fluidization process of such particles, fluidization behavior is always found to be agglomerate particulate fluidization. In several studies of vibrated fluidization of Group C particles, various image analysis and calculation techniques were carried out for agglomerate size determination [49,50,53,55,59,65,66,70]. As the experimental measurement of agglomerate diameter (d_a) is very difficult, it was decided to evaluate the diameters of possibly formed agglomerates within the bed by calculated results. To determine the agglomerate diameter of 6 μm glass beads under vibrated fluidization, Mawatari et al. [53] changed the particle diameter in Ergun equation (eqn. 2.5) with the agglomerate diameter to make their calculated minimum fluidization velocities agree with the experimental ones by assuming the void fraction of agglomerates is equal to bed voidage at minimum fluidization condition. Following a similar approach, mean agglomerate size values were calculated by using eqn. (2.7) using experimentally determined minimum fluidization velocity values. Agglomerate diameter was substituted by particle diameter in eqn. (2.7) in order to obtain mean agglomerate size under minimum fluidization condition which was determined for each experiment. Figure 4.14 shows that moisture content increased agglomerate size due to higher cohesiveness of the particles while Figure 4.15 shows the reducing effect of vibration strength and frequency on agglomerate size. In studies using fine particles, generally, agglomerate sizes are at least about ten times larger than single particles. Small agglomerate sizes seen in this study show that agglomerates were formed by coalescence of few particles. The reason can be due to high adsorbing capacity of zeolite particles. In addition, it should be noted that

polydispersity of the particles can be considered another reason of higher experimental minimum fluidization velocity results compared to ones predicted by using Sauter mean particle diameter in eqn. (2.7).

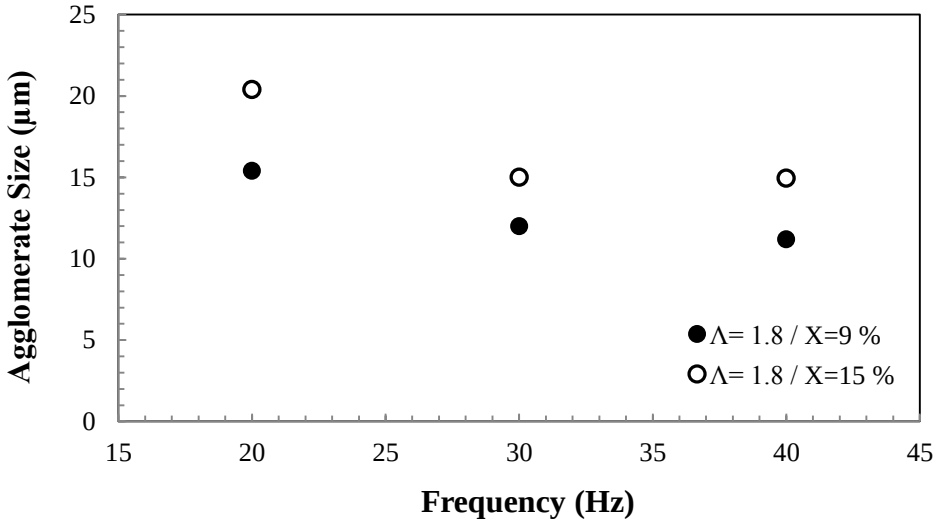

Figure 4.14 Effect of moisture content on agglomerate size

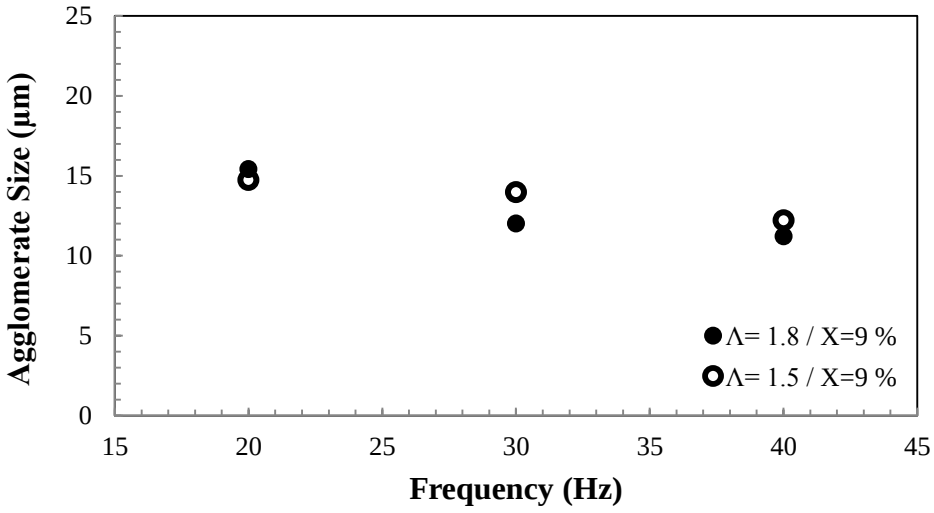

Figure 4.15 Effect of vibration conditions on agglomerate size

4.2 Drying Tests

Upon completion of the investigation of hydrodynamic behavior of the system, it was concluded that homogenous bubbling fluidization of the whole bed is obtained when the bed is vibrated with 40 Hz frequency at a vibration strength of 1.8. To determine the suitable operating conditions for economical drying of zeolite, tests were conducted at different superficial gas velocities (U_0=10.5, 15.8, 21 mm/s) and inlet gas temperatures (T_{in}=60°C, 80°C, 90°C). During the tests total pressure drop, bed temperature, exhaust gas temperature, relative humidity of exhaust gas were measured continuously. In addition, particles were sampled out from the bed every 10 or 15 minutes and their moisture content was measured.

4.2.1 Reproducibility

Two sets of experiments were conducted for each operating condition throughout this study. Reproducibility of the pressure drop, bed temperature, relative humidity of exhaust gas and the moisture content of the bed material measurements were checked. An example of the comparison made between two measurement results is given in Figure 4.16 and 4.17. Similar results obtained during rest of the experiments are given in Appendix C. As can be seen in these figures, all the measurements carried out in drying tests are reproducible. Nevertheless, the averages of two sets were reported in the remaining part of this thesis.

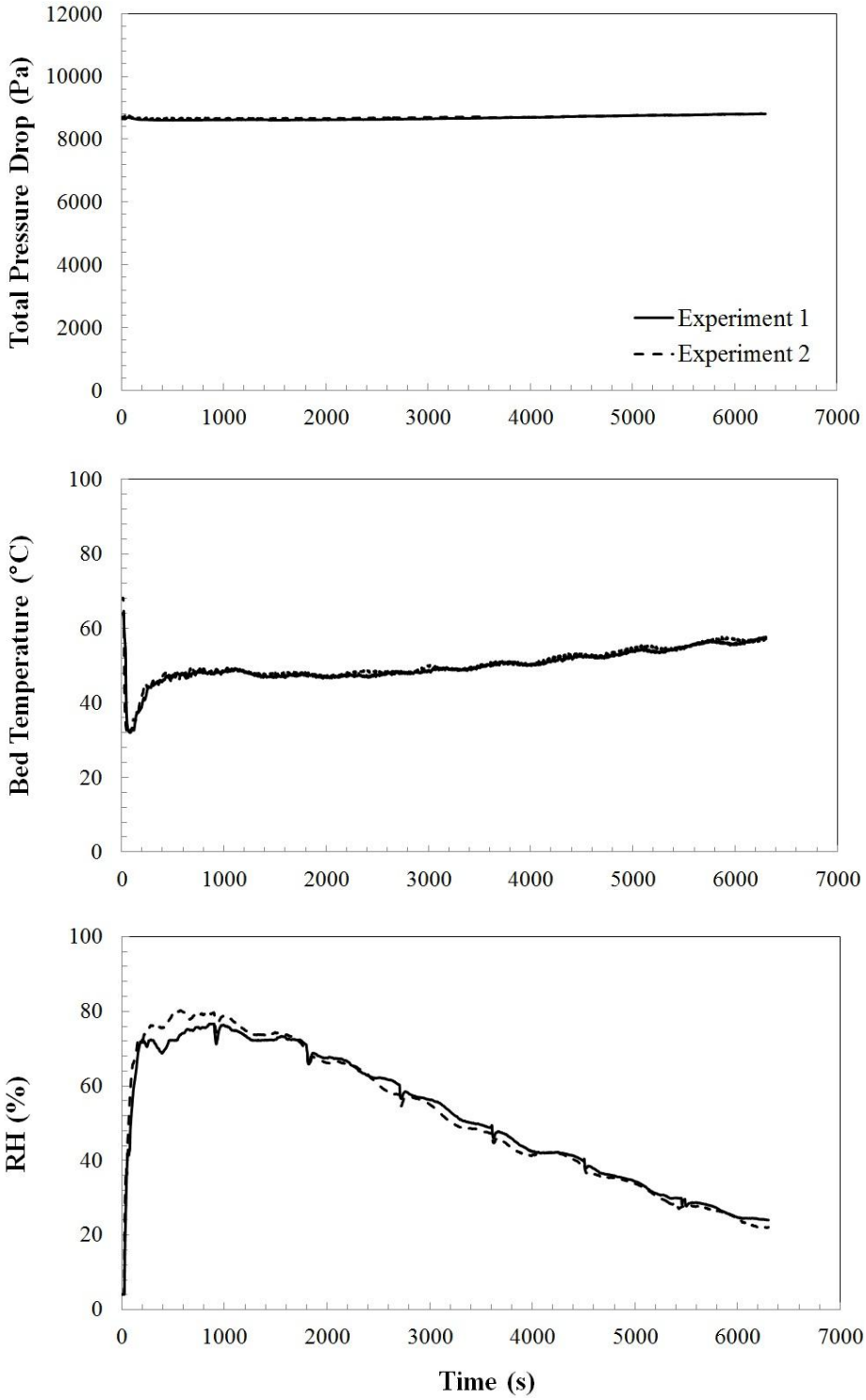

Figure 4.16 Reproducibility of drying tests (T_{in}=60 °C, T_{out}=55°C, U_o=15.8 mm/s)

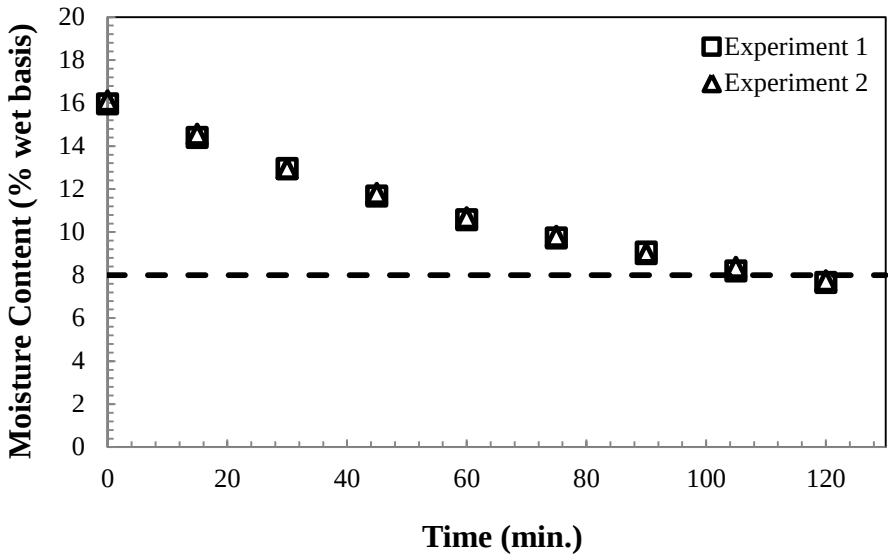

Figure 4.17 Reproducibility of the drying tests in terms of moisture content (T_{in}=60 °C, T_{out}=55°C, U_o=10.5 mm/s)

4.2.2 Determination of Drying Curves

To determine the change of moisture content throughout a drying test, a negligible amount of bed material was sampled out of the fluidized bed at certain time intervals and analyzed by using a moisture analyzer as mentioned in section 3.1.3. Besides, it is possible to determine the moisture content of the bed material without taking samples from the bed during a drying operation. For this purpose, a new moisture content determination technique by using relative humidity measurement data collected at the dryer outlet was used in this study. This technique is explained in detail below.

A vibrated fluidized bed dryer consists of several important subsystems such as air supplier, pre-heater, mechanical vibration system and fluidization chamber (circular or rectangular). However, fluidization chamber where the drying process takes place is of primary importance. Thus, mass balance for a batch drying system can be applied over the fluidization chamber. Considering the fluidized bed chamber as a continuum and assuming that the particles within the bed are perfectly mixed, a moisture balance can be written as:

$$-M_s \frac{d\bar{X}}{dt} = \dot{M}_g (Y_{out} - Y_{in}) \tag{4.1}$$

where M_s is the mass hold-up of dry solid (kg), $\bar{X}$ is the moisture content of material which is uniform through the bed (kg/kg), $\dot{M}_g$ is the mass flow rate of dry air (kg/s), Y_{out} and Y_{in} represent humidity (kg water vapor/kg dry air) of exhaust air and inlet air respectively. In the present study, nitrogen gas is used as fluidization gas. Therefore, eqn. (4.1) reduces to:

$$-M_s \frac{d\bar{X}}{dt} = \dot{M}_g Y_{out} \tag{4.2}$$

To generate the drying curves by using the mass balance given in eqn. (4.2), the experimentally determined operating conditions and continuous measurement data of relative humidity at the exit of the dryer were used. For this purpose, the following steps were followed in finding the change of moisture content of the bed material ($\bar{X}$).

- The transient relative humidity of the exhaust gas at the exit of the dryer is measured, (RH).
- The temperature at the exit of the dryer (T_{out}) is measured and kept constant throughout the experiment.
- The room temperature (T) and pressure (P) is measured.
- Saturation vapor pressure (P_{sat}) is calculated by using ITS-90 formula [95].
- Partial pressure of water vapor (P_v) is calculated by

$$P_v = (RH)\, P_{sat} \tag{4.3}$$

  where P_{sat} is saturated water vapor pressure (Pa).
- The humidity of exhaust gas, Y_{out} (kg water vapor/kg dry gas) is calculated by

$$Y_{out} = \frac{P_v V / R_v T}{P_g V / R_g T} = \frac{R_g}{R_v} \frac{P_v}{P - P_v} \tag{4.4}$$

  where R_g and R_v are the specific gas constants of drying gas and water vapor, respectively.
- Transient drying rate ($N = -d\bar{X}/dt$) is calculated by using eqn. (4.2).
- As the drying rate data are available at every 2 seconds, it is possible to monitor the moisture content results at the end of each progressing 4 seconds utilizing a numerical integration method. Therefore, the change in moisture content of the bed material ($\bar{X}$) at each 4-second time interval is calculated by Simpson's 1/3 rule.

To apply the procedure above, a MATLAB code (Appendix B) was written and used. Figures 4.18, 4.19 and 4.20 reveal that the calculated results agreed well with the sampling results. Therefore, transient relative humidity measurements of the exhaust gas were used to determine the moisture content of the solids and are reported in the following sections of this thesis.

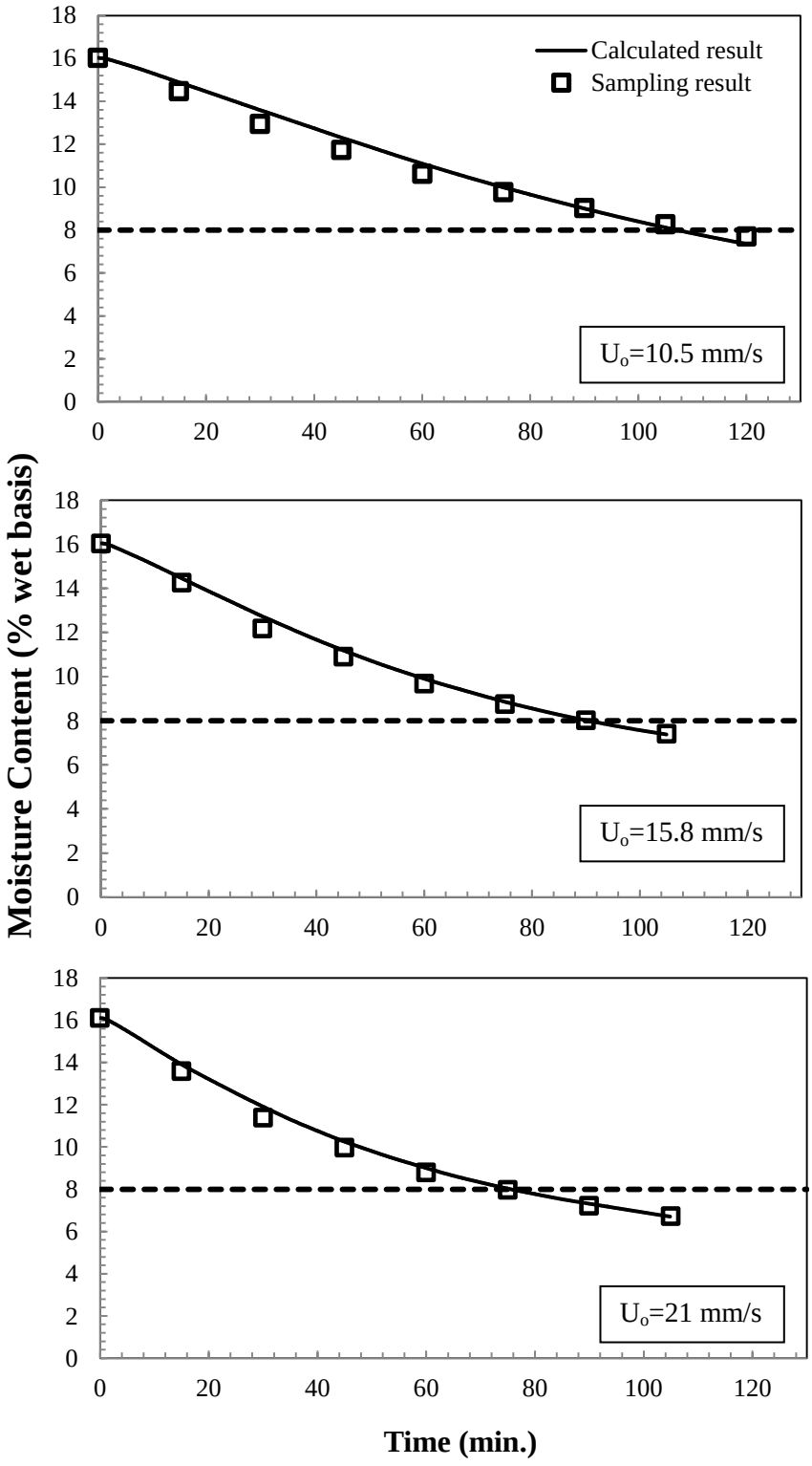

Figure 4.18 Comparison of drying curves obtained from intermittent bed material sampling and continuous exhaust *RH* measurements (T_{in}=60 °C)

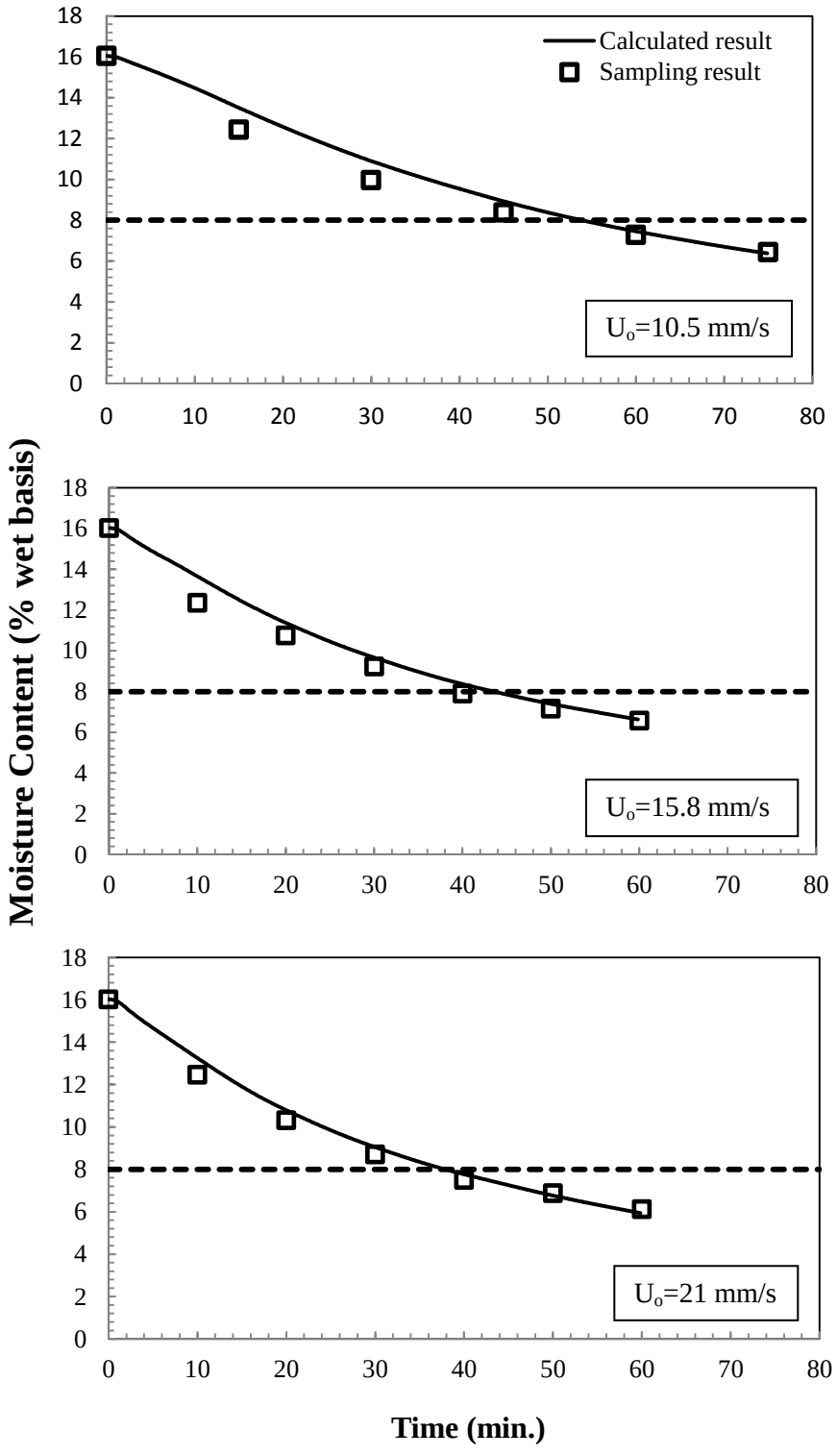

Figure 4.19 Comparison of drying curves obtained from intermittent bed material sampling and continuous exhaust *RH* measurements (T_{in}=80 °C)

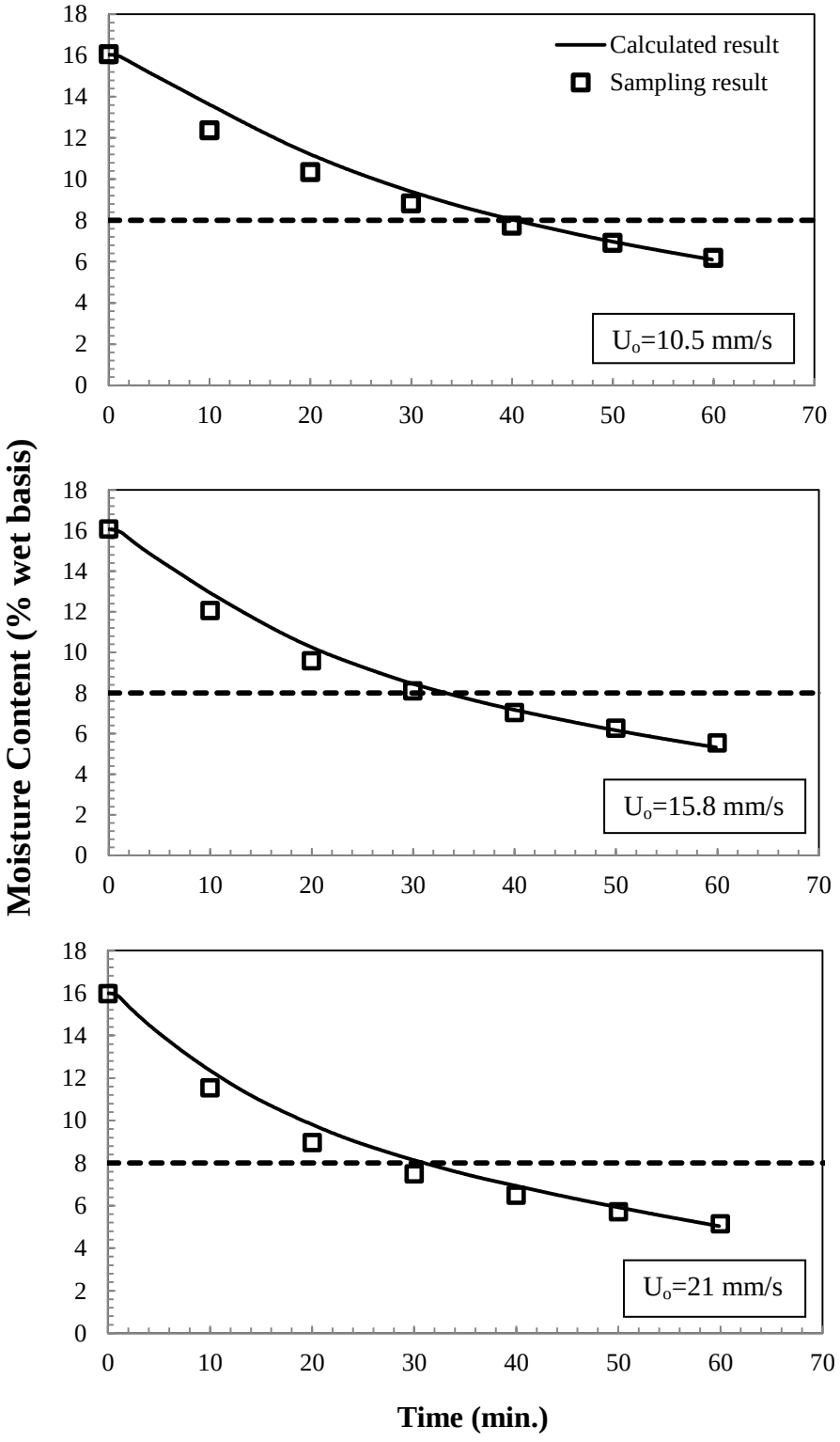

Figure 4.20 Comparison of drying curves obtained from intermittent bed material sampling and continuous exhaust *RH* measurements (T_{in}=90 °C)

4.2.3 Effects of Operating Conditions on Drying Curves

4.2.3.1 Superficial Gas Velocity

The objective of the drying experiments conducted in this study is to dry the bed material to 8% (wet basis) moisture content as economically as possible.

Figure 4.21, 4.22 and 4.23 show the effect of superficial gas velocity on the drying curves obtained by using the exhaust gas relative humidity measurements carried out with three different inlet gas temperatures (60 °C, 80 °C and 90 °C), respectively. Bed temperatures measured during each experiment are also given in these figures. As illustrated, increasing drying gas velocity decreases drying time at each gas inlet temperature. In addition, the temperature of the clinoptilolite bed nearly reaches the inlet gas temperature towards the end of the experiments.

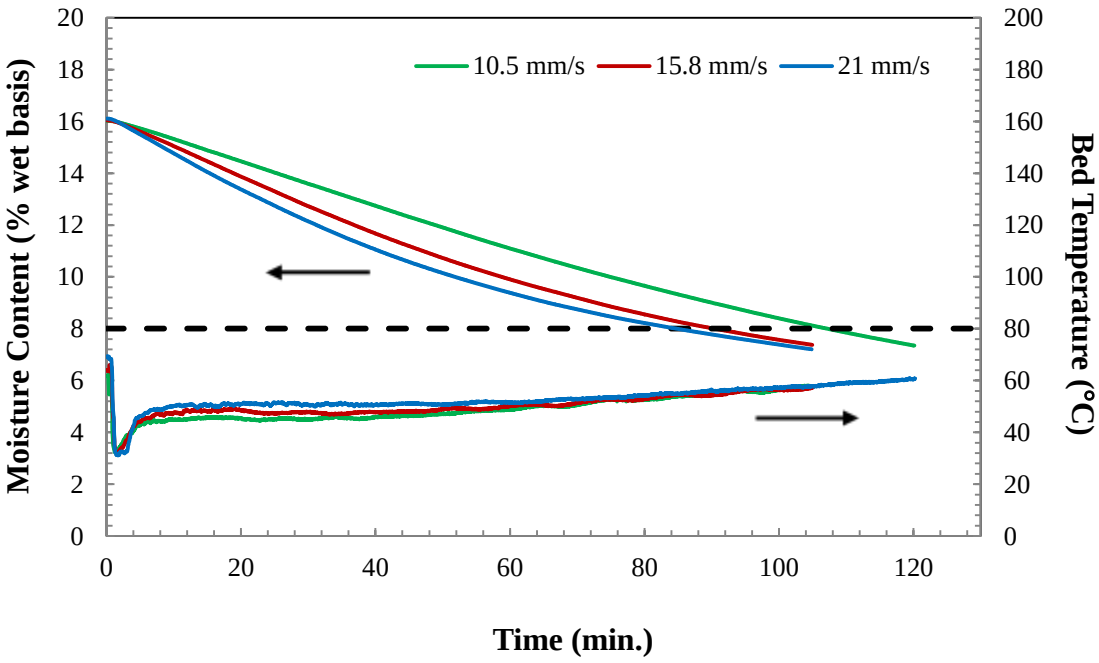

Figure 4.21 Moisture content and bed temperature profiles (T_{in}=60 °C)

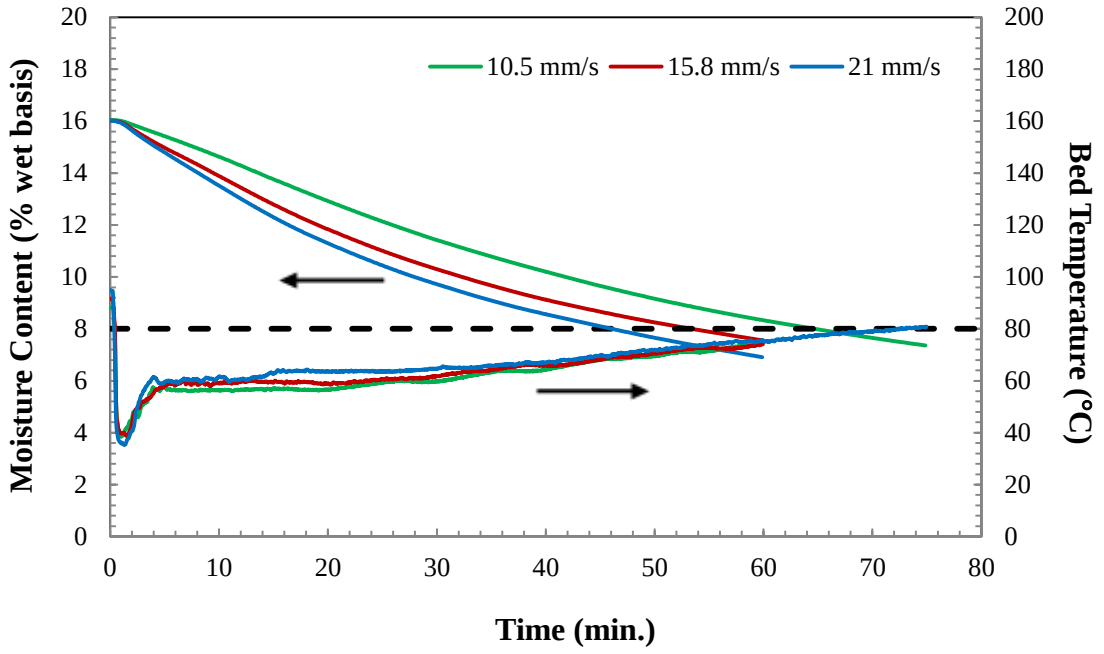

Figure 4.22 Moisture content and bed temperature profiles (T_{in}=80 °C)

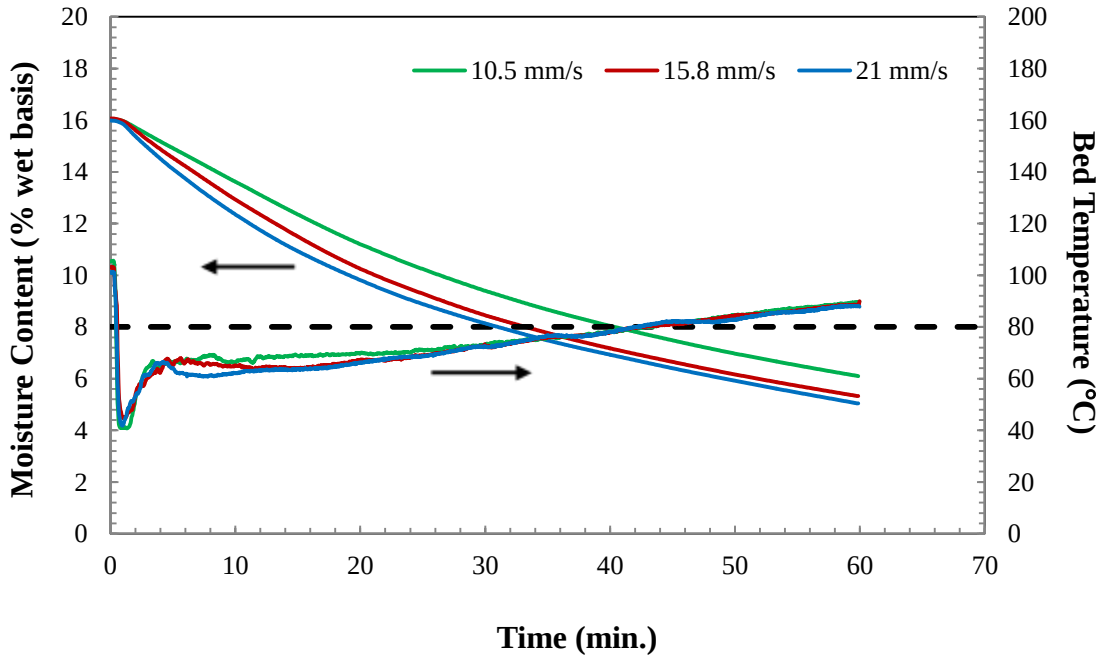

Figure 4.23 Moisture content and bed temperature profiles (T_{in}=90 °C)

As explained in section 1.4 with Figure 1.6, in a fluidized bed drying process of wet particles, drying rate remains almost constant at the initial period of drying due to the removal of surface moisture. When the moisture content reaches a critical point, drying rate starts to decrease gradually towards the end of drying process. These two distinct time intervals are called as constant-rate period and falling-rate period respectively. An example of drying rate curve exhibiting the change in moisture content of the bed material with respect to time is illustrated in Figure 4.24. As can be seen, a characteristic drying curve of convective drying (Figure 1.6) was obtained during the drying process of clinoptilolite from 16 % to 8 %. This curve also showed that the drying process was carried out within both constant and falling rate periods.

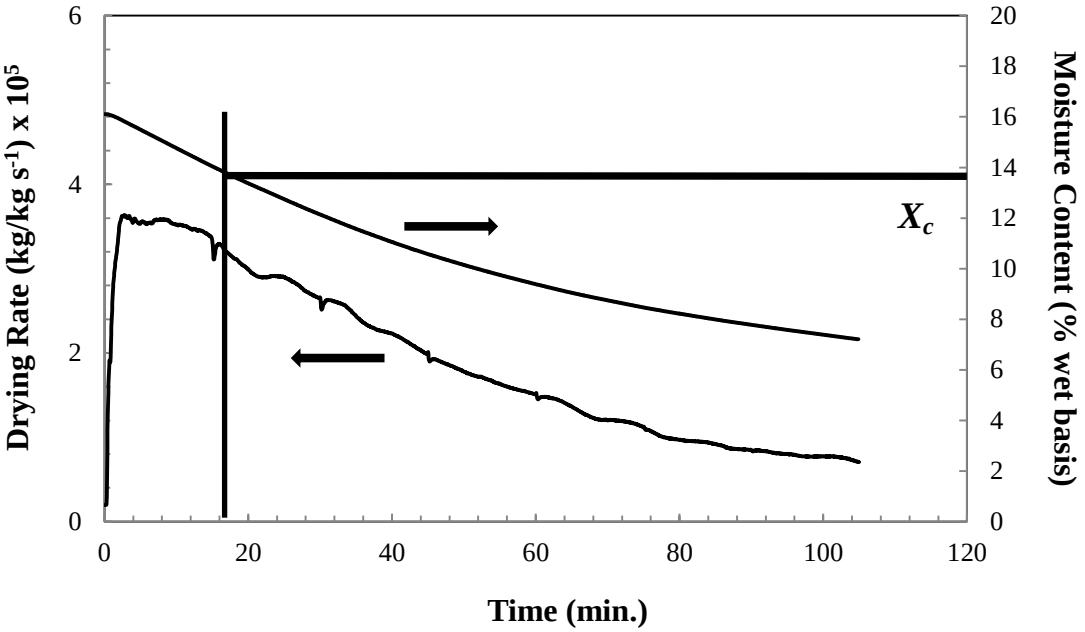

Figure 4.24 Drying curves of clinoptilolite (T_{in}=60 °C, U_0=21 mm/s)

Effect of superficial gas velocity on drying rate and moisture content of the material obtained at T_{in}=60 °C are given in Figure 4.25. It can be observed that increasing gas velocity results in higher drying rates at 60 °C inlet gas temperature. During the constant drying rate period, moisture evaporates from the surface of the solids until about 13 % (X_c) moisture content. During this period, bed temperature also remains constant after rapid heating up of the particles to drying temperature (Figure 4.21). As drying is faster and critical moisture content (X_c) is reached earlier, constant drying rate period becomes shorter with increasing gas velocity. Negative peaks observed on the drying curves are due to the disruptions during a drying test when bed material was being sampled.

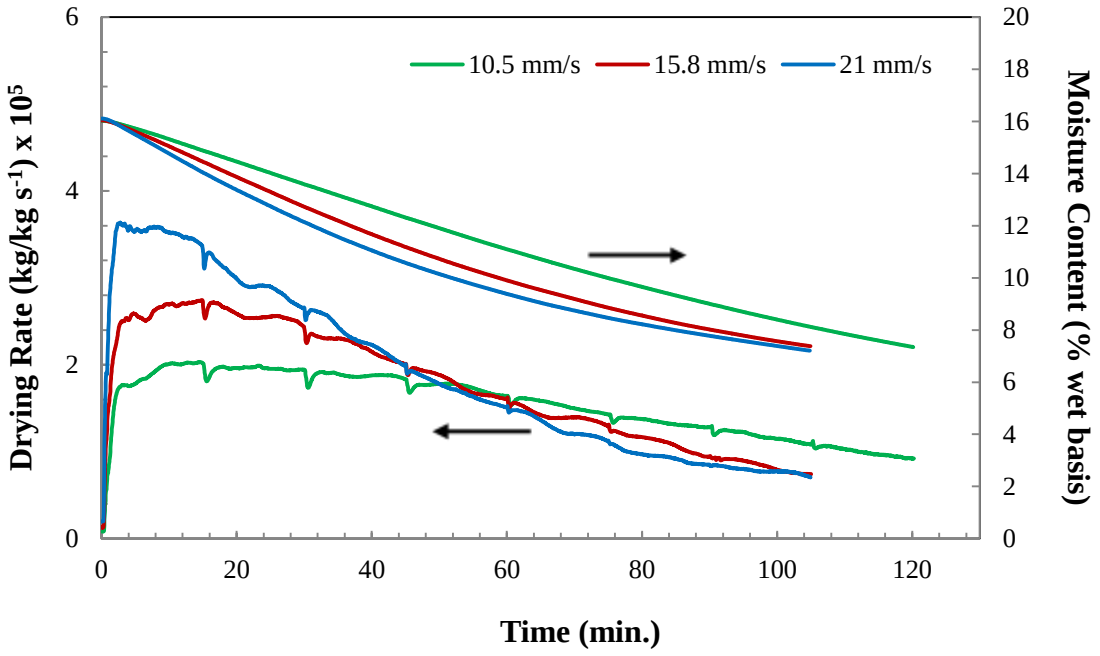

Figure 4.25 Effect of gas velocity on drying rate (T_{in}=60 °C)

Similar analyses were also made for the experiments conducted with 80 °C and 90 °C inlet gas temperatures and the results are illustrated in Figure 4.26 and 4.27, respectively. As can be seen in these figures, higher drying rate values are observed when gas velocity is increased. Different from the previous case (Figure 4.25), a clear constant drying rate period could not be observed with 15.8 and 21 mm/s gas velocities. After a rapid increase, drying rate first decreased and then flattened out just before reaching critical moisture content (X_c).

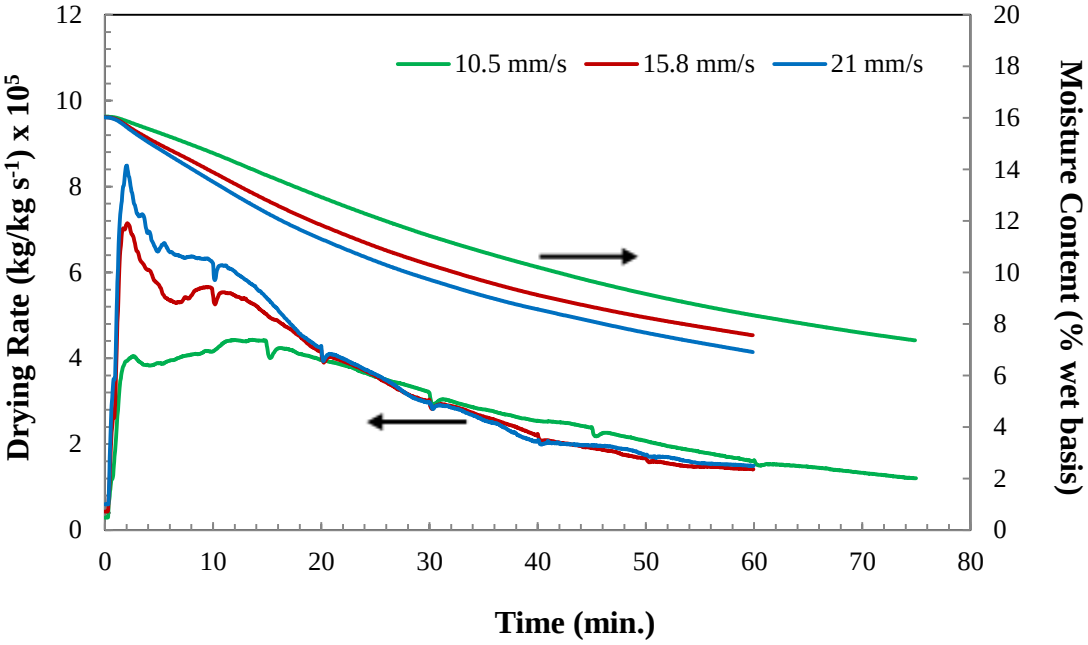

Figure 4.26 Effect of gas velocity on drying rate (T_{in}=80 °C)

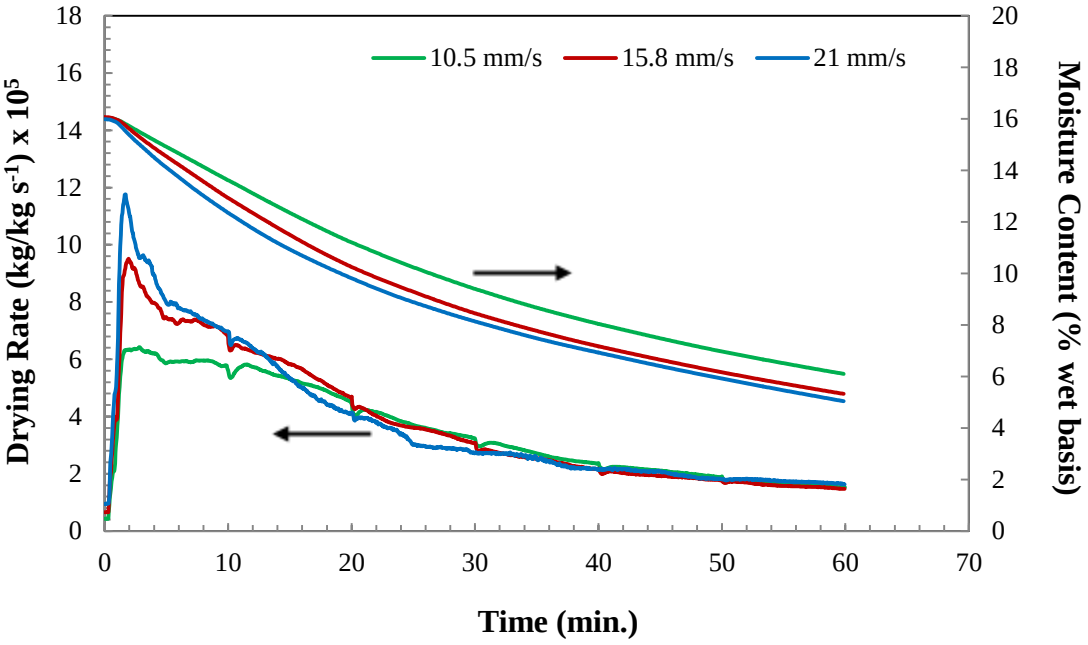

Figure 4.27 Effect of gas velocity on drying rate (T_{in}=90 °C)

4.2.3.2 Inlet Gas Temperature

In view of the fact that the major heating load is the evaporation of moisture during the drying operation, it can be easily predicted that evaporation rate increases with increasing inlet gas temperature. Besides, it is known that temperature has a strong influence on effective diffusivity and hence on drying rate especially in falling rate period.

Figure 4.28 indicates the significant change in drying curves and drying times as a result of different inlet drying gas temperatures. Higher inlet gas temperature values resulted in faster drying operations. As compared with the effect of drying gas velocity, the effect of temperature on drying was found to be more pronounced.

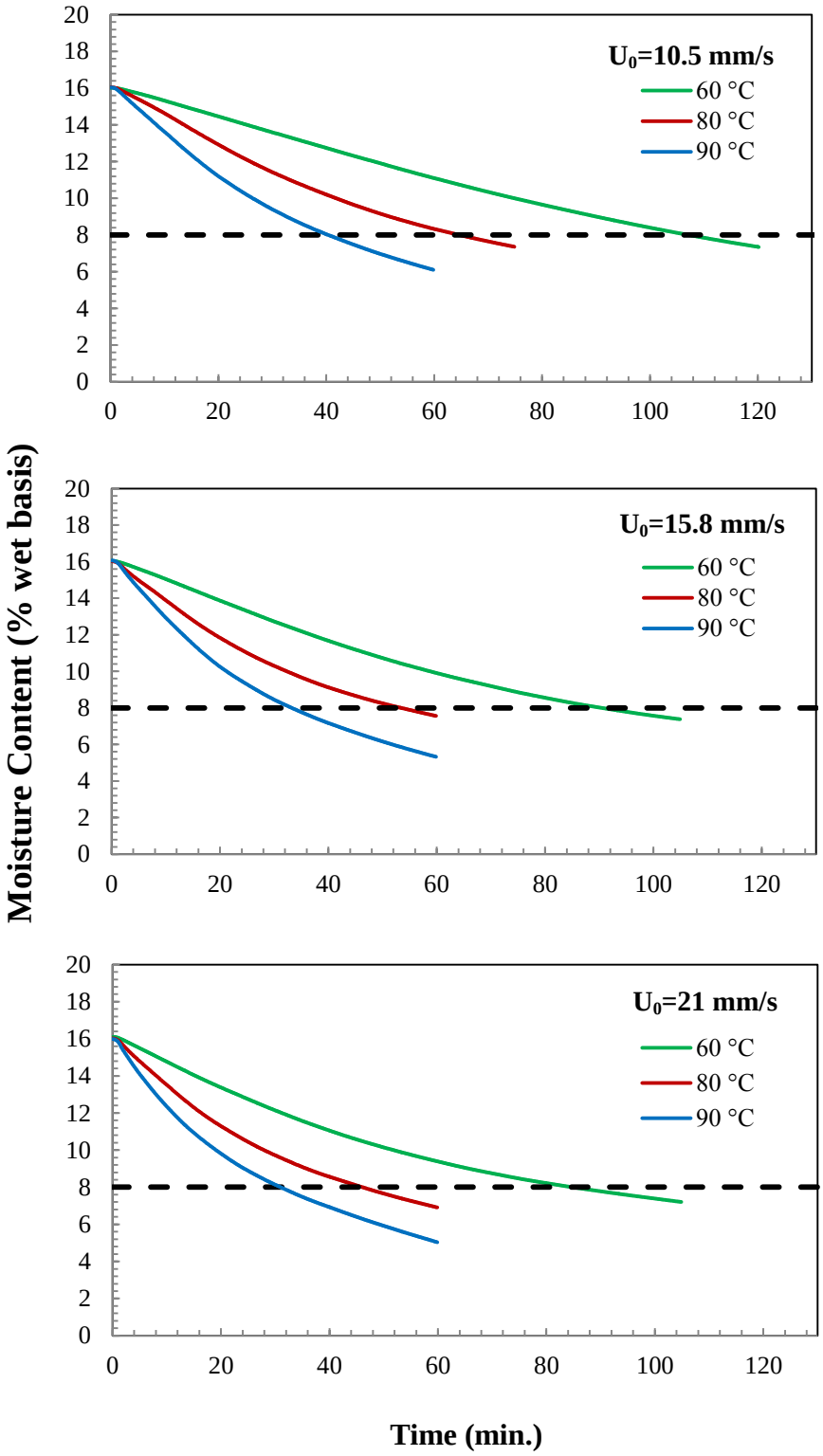

Figure 4.28 Effect of temperature on moisture content profiles

4.2.4 Drying Time and Cost Analysis

Determination of effective operating conditions for a drying process is very important in order to obtain high product quality, good energy efficiency and desired performance. From this point of view, drying time, a cost-determining parameter, is affected by drying gas velocity and temperature as well as the properties of the bed material.

The effect of operating conditions on drying time is given in Table 4.1 It can be seen that drying time was reduced significantly by increasing temperature and gas velocity. Within the range of operating conditions considered in this study, temperature effect was found to be more pronounced than the effect of gas velocity in terms of drying time.

Table 4.1 Effect of operating conditions on drying times to obtain dry product with 8% (w.b.) moisture content

U_o (mm/s) / T_{in} (°C)	**10.5**	**15.8**	**21**
60 °C	111.4 min	90 min	75 min
80 °C	50.2 min	39.2 min	35.3 min
90 °C	37.2 min	31.2 min	26.3 min

Within the range of operating conditions applied in this study, an approximate calculation for the daily operating cost of each experiment was carried out to determine the cost-effective conditions considering the electrical energy need for heating the drying air. Based on the electrical energy cost for industrial site (22.73 Kr/kW-h, June 2013) in Turkey [96], the daily cost for heating ambient air was calculated and the results are tabulated in Table 4.2. For the calculation of mass flow rate of dry air in a continuous well-mixed dryer, wet clinoptilolite particles (1000 kg/h) with an initial moisture content of 16 % (wet basis) at 20 °C were used to be dried to moisture content of 8 % (wet basis). The drying times given in Table 4.1 were used as mean particle residence times. The bed depth was selected as 14 cm and the apparent density of the bed was selected as 426.3 kg/m^3 which are equal to ones applied in the drying experiments. A sample calculation made for operating cost determination is given in Appendix D.

Table 4.2 Daily cost of drying operation to obtain dry product with 8% (w.b.) moisture content in a continuous VFB dryer of 1000 kg/h capacity (Bed area results are given in parenthesis)

U_o (mm/s) / T_{in} (°C)	**10.5**	**15.8**	**21**
60 °C	59.79 TL ($26.09\ m^2$)	72.66 TL ($21.08\ m^2$)	80.52 TL ($17.57\ m^2$)
80 °C	40.26 TL ($11.76\ m^2$)	47.46 TL ($9.18\ m^2$)	56.95 TL ($8.27\ m^2$)
90 °C	35.13 TL ($8.71\ m^2$)	44.30 TL ($7.31\ m^2$)	49.26 TL ($6.16\ m^2$)

The results show that the most economical condition is obtained with the gas velocity of 10.5 mm/s at 90 °C inlet gas temperature. When the bed areas of the dryers are investigated, this condition is also found to be advantageous among others. Therefore, it can be concluded that the conditions of 90 °C temperature and 10.5 mm/s gas velocity can be chosen for a cost-effective drying operation of clinoptilolite powders.

CHAPTER 5

CONCLUSIONS

5.1 Hydrodynamics

For the adaption of vibrated fluidized bed drying technique to Turkish clinoptilolite, firstly, a laboratory scale vibrated fluidized bed was designed and constructed to study and characterize the gas-solid flow of fine clinoptilolite powders. The effects of vibration parameters and moisture content of the bed material on the hydrodynamics were determined experimentally and the most suitable vibration parameters were chosen to obtain a high quality fluidization during the following drying part of the study. In the light of the reproducible experimental results, the following conclusions can be reached related to hydrodynamic behavior:

- Fluidization of 3 micron clinoptilolite powders could not be achieved without mechanical vibration.
- Vibration eliminated channels and rat holes caused by interparticle cohesive forces and enhanced fluidization quality substantially.
- Moisture content has a reducing effect on fluidization quality and increases minimum fluidization velocity and bed voidage at minimum fluidization condition.
- Fluidization quality increases with both vibration strength and vibration frequency.
- Minimum fluidization velocity and bed voidage at minimum fluidization condition decreased with vibration parameters and increased with moisture content.
- Higher vibration frequencies were required to achieve high quality fluidization when operating with moist powders.
- The best bubbling fluidization quality to utilize in drying experiments was achieved when the bed was vibrated with 40 Hz frequency at 1.8 vibration strength.

5.2 Drying

In the second part of this study, a fully equipped stainless steel vibrated fluidized bed dryer was designed and fabricated in the light of the foregoing findings. Different inlet gas velocities and temperatures were applied and the results were analyzed in terms of moisture content, drying rate and drying time. On the basis of the results, the following conclusions have been reached:

- Considering the properties of the bed material and the advantages of the vibrated fluidization technique, relatively low temperatures (60-90 °C) were found to be sufficient for a drying process with reasonable drying times.
- A perfectly homogenous operation was achieved during the drying tests. Therefore, based on a moisture balance applied over the fluidization chamber, a new technique using relative humidity data collected at the dryer outlet could be used to generate the drying curves.
- Drying rate increased significantly by both temperature and superficial velocity of the drying gas. On the other hand, based on drying rate and drying time results, the temperature effect was found to be more pronounced than velocity.
- During the vibrated fluidized bed drying operation of wet clinoptilolite powders from 16 % to 8%, both of the constant and falling drying rate periods were observed. Being a transition point between these two periods, critical moisture content value was in the order of 13 %.
- After a rough estimate of electrical energy cost made on the basis of heating the drying gas, 90 °C temperature and 10.5 mm/s gas velocity were chosen for a cost-effective continuous drying operation of clinoptilolite.

5.3 Suggestions for Future Work

Based on the experience gained in the present study, the following recommendations for future extension of the work can be suggested:

- The vibration system can further be improved and a wider range of vibration parameters can be applied for the investigation of hydrodynamics of different types of bed materials.
- In the light of the findings obtained from drying tests, a detailed design study of a continuous vibrated fluidized bed dryer consisting of vibration system, fluidization chamber and control system can be carried out.
- After the design and scale-up studies of a continuous drying operation system, an industrial scale vibrated fluidized bed dryer can be constructed for the purpose of drying natural zeolite powders.

REFERENCES

[1] H. Basmacıoğlu, M. Ergül, Yemlerde bulunan toksinler ve kontrol yolları, Hayvansal Üretim. 44 (2003) 9-17.

[2] M. Peraica, A.M. Domijan, Z. Jurjevic, B. Cvjetkovic, Prevention of exposure to mycotoxins from food and feed, Arh Hig Rada Toksikol. 53 (2002) 229-237.

[3] S.A. Sabuncuoğlu, T. Baydar, B. Giray, G. Şahin, Mikotoksinler: Toksik etkileri, degredasyonları, oluşumlarının önlenmesi ve zararlı etkilerinin azaltılması, Hacettepe Üniversitesi Eczacılık Fakültesi Dergisi. 28 (2008) 63-92.

[4] T.D. Phillips, Dietary clay in the chemoprevention of aflatoxin-induced disease., Toxicological Sciences: An Official Journal of the Society of Toxicology. 52 (1999) 118-126.

[5] S.S. Parlat, A.O. Yildiz, H. Oguz, Effect of clinoptilolite on performance of Japanese quail (Coturnix coturnix japonica) during experimental aflatoxicosis, British Poultry Science. 40 (1999) 495-500.

[6] H. Oguz, V. Kurtoglu, Effect of clinoptilolite on performance of broiler chickens during experimental aflatoxicosis, British Poultry Science. 41 (2000) 512-517.

[7] F.A. Mumpton, La roca magica: Uses of natural zeolites in agriculture and industry, Proc. Natl. Acad. Sci. USA. 96 (1999) 3463-3470.

[8] J.L. White, A.J. Ohlrogge, Ion exchange materials to increase consumption of non-protein nitrogen by rumitants, United States Patent. (1983).

[9] F.A. Mumpton, P.H. Fishman, The application of natural zeolites in animal science and aquaculture, Journal of Animal Science. 45 (1977) 1188-1203.

[10] T. Armbruster, Clinoptilolite-heulandite: applications and basic research, Studies In Surface Science And Catalysis. 135 (2001) 13-27.

[11] DPT, Madencilik özel ihtisas komisyonu endüstriyel hammaddeler alt komisyonu diğer endüstri mineralleri çalışma grubu raporu, T. C. Başbakanlık Devlet Planlama Teşkilatı Müsteşarlığı. Cilt 1 (1996).

[12] Personal communications with Rota Mining Corporation, September (2011).

[13] R.E. Treybal, Mass-transfer operations, 3rd ed., McGraw-Hill, Inc., Tokyo, 1981.

[14] C.L. Law, A.S. Mujumdar, Handbook of industrial drying, 3rd ed., CRC Press: Boca Raton, 2007.

[15] W.-C. Yang, Handbook of fluidization and fluid-particle systems, CRC Press. (2003) 469-485.

[16] D. Kunii, O. Levenspiel, Fluidization Engineering, 2nd ed., Butterworth-Heinemann, Boston, 1991.

[17] D. Geldart, Types of gas fluidization, Powder Technology. 7 (1973) 285-292.

[18] J.R. Grace, Contacting modes and behaviour classification of gas-solid and other two-phase suspensions, The Canadian Journal of Chemical Engineering. 64 (1986) 353-362.

[19] K. Rietema, Powders, what are they?, Powder Technology. 37 (1984) 5-23.

[20] W.-C. Yang, Modification and re-interpretation of Geldart's classification of powders, Powder Technology. 171 (2007) 69-74.
[21] D. Liu, M. Kwauk, H. Li, Aggregative and particulate fluidization—The two extremes of a continuous spectrum, Chemical Engineering Science. 51 (1996) 4045-4063.
[22] D. Geldart, N. Harnby, A.C. Wong, Fluidization of cohesive powders, Powder Technology. 37 (1984) 25-37.
[23] J. Visser, Van der Waals and other cohesive forces affecting fluidization, Powder Technology. 58 (1989) 1-10.
[24] L.F. Hakim, J.L. Portman, M.D. Casper, A.W. Weimer, Aggregation behavior of nanoparticles in fluidized beds, Powder Technology. 160 (2005) 149-160.
[25] C.T. Crowe, Multiphase flow handbook, CRC Press, Boca Raton, 2005.
[26] H.W. Piepers, E.J. Cottaar, A.H.M. Verkooijen, K. Rietema, Effects of pressure and type of gas on particle-particle interaction and the consequences for gas—solid fluidization behaviour, Powder Technology. 37 (1984) 55-70.
[27] A.G. Bailey, Electrostatic phenomena during powder handling, Powder Technology. 37 (1984) 71-85.
[28] E. Charlaix, J. Crassous, Adhesion forces between wetted solid surfaces., The Journal of Chemical Physics. 122 (2005) 184701.
[29] D. Geldart, A.C.Y. Wong, Fluidization of powders showing degrees of cohesiveness-I. Bed expansion, Chemical Engineering Science. 39 (1984) 1481-1488.
[30] D. Geldart, A.C.Y. Wong, Fluidization of powders showing degrees of cohesiveness-II. Experiments on rates of de-aeration, Chemical Engineering Science. 40 (1985) 653-661.
[31] C.J. Geankoplis, Transport processes and unit operations, 3rd ed., Prentice-Hall, Inc., U.S.A, 1993.
[32] M.C.B. Ambrosio, O.P. Taranto, The drying of solids in a modified fluidized bed, Brazilian Journal of Chemical Engineering. 19 (2002) 355-358.
[33] A. Reyes, G. Diaz, F.H. Marquardt, Analysis of mechnanically agitated fluid-particle contact dryers, Drying Technology: An International Journal. 19 (2001) 2235-2259.
[34] S. Alavi, B. Caussat, Experimental study on fluidization of micronic powders, Powder Technology. 157 (2005) 114-120.
[35] N.J.M. Kuipers, E.J. Stamhuis, A.A.C.M. Beenackers, Fluidization of potato starch in a stirred vibrating fluidized bed, Chemical Engineering Science. 51 (1996) 2727-2732.
[36] W.R.W. Daud, Fluidized bed dryers — Recent advances, Advanced Powder Technology. 19 (2008) 403-418.
[37] R. Gupta, Aerodynamic and drying characteristics of a vibrated fluidized bed, M.Sc. Thesis, McGill University, Quebec, Canada. (1979).
[38] L.F. Hakim, J.L. Portman, M.D. Casper, A.W. Weimer, Aggregation behavior of nanoparticles in fluidized beds, Powder Technology. 160 (2005) 149-160.
[39] C.K. Gupta, D. Sathiyamoorthy, Fluid bed technology in materials processing, CRC Press, Boca Raton, 1998.

[40] D. Geldart, Gas fluidization technology, John Wiley & Sons, New York, (1986).
[41] E. Bratu, G.I. Jinescu, Effect of vertical vibrations on the pressure drop in a fluidised layer, British Chemical Engineering. 16 (1971) 691-695.
[42] R. Gupta, A.S. Mujumdar, Aerodynamics of a vibrated fluid bed, The Canadian Journal of Chemical Engineering. 58 (1980) 332-338.
[43] D.U. Ringer, A.S. Mujumdar, Analysis of aerodynamics and heat transfer in vibro-fluidized beds, Drying Technology: An International Journal. 2 (1983) 449-470.
[44] K. Malhotra, L. Law-Kwet-Cheong, A.S. Mujumdar, Pressure-drop charateristics for vibrated beds of dry and sticky particles, Powder Technology. 39 (1984) 101-105.
[45] K. Erdesz, A.S. Mujumdar, Hydrodynamic aspects of conventional and vibrofluidized beds- A comparative evaluation, Powder Technology. 46 (1986) 167-172.
[46] S. Satija, I.L. Zucker, Hydrodynamics of vibro-fluidized beds, Drying Technology: An International Journal. 4 (1986) 19-43.
[47] E. Marring, A.C. Hoffmann, L.P.B.M. Janssen, The effect of vibration on the fluidization behaviour of some cohesive powders, Powder Technology. 79 (1994) 1-10.
[48] K. Noda, Y. Mawatari, S. Uchida, Flow patterns of fine particles in a vibrated fluidized bed under atmospheric or reduced pressure, Powder Technology. 99 (1998) 11-14.
[49] J.R. Wank, S.M. George, A.W. Weimer, Vibro-fluidization of fine boron nitride powder at low pressure, Powder Technology. 121 (2001) 195-204.
[50] S.M. Tasirin, N. Anuar, Fluidization behavior of vibrated and aerated beds of starch powders, Journal of Chemical Engineering of Japan. 34 (2001) 1251-1258.
[51] Y. Mawatari, T. Koide, Y. Tatemoto, S. Uchida, K. Noda, Effect of particle diameter on fluidization under vibration, Powder Technology. 123 (2002) 69-74.
[52] B.Y. Mawatari, T. Akune, Y. Tatemoto, K. Noda, Bubbling and bed expansion behavior under vibration in a gas-solid fluidized bed, Chemical Engineering and Technology. 25 (2002) 1095-1100.
[53] Y. Mawatari, Y. Tatemoto, K. Noda, Prediction of minimum fluidization velocity for vibrated fluidized bed, Powder Technology. 131 (2003) 66-70.
[54] V.A. Silva-Moris, S.C.S. Rocha, Development of a vibrofluidized bed and fluid-dynamic study with dry and wet adipic acid, Brazilian Journal of Chemical Engineering. 20 (2003) 423-434.
[55] C.H. Nam, R. Pfeffer, R.N. Dave, S. Sundaresan, Aerated vibrofluidization of silica nanoparticles, AIChE Journal. 50 (2004) 1776-1785.
[56] R.V. Daleffe, J.T. Freire, Analysis of the fluid-dynamic behavior of fluidized and vibrofluidized bed containing glycerol, Brazilian Journal of Chemical Engineering. 21 (2004) 35-46.
[57] H. Jin, Z. Tong, J. Zhang, B. Zhang, Homogeneous fluidization characteristics of vibrating fluidized beds, The Canadian Journal of Chemical Engineering. 82 (2004) 1048-1053.

[58] Y. Mawatari, M. Tsunekawa, Y. Tatemoto, K. Noda, Favorable vibrated fluidization conditions for cohesive fine particles, Powder Technology. 154 (2005) 54-60.
[59] C. Xu, J. Zhu, Parametric study of fine particle fluidization under mechanical vibration, Powder Technology. 161 (2006) 135-144.
[60] H. Jin, J. Zhang, B. Zhang, The effect of vibration on bed voidage behaviors in fluidized beds with large particles, Brazilian Journal of Chemical Engineering. 24 (2007) 389-397.
[61] F.P.R. Brod, K.J. Park, R.G.D.E. Almeida, Image analysis to obtain the vibration amplitude and the residence time distribution of a vibro-fluidized dryer, Food and Bioproducts Processing. 82 (2004) 157-163.
[62] D. Barletta, G. Donsì, G. Ferrari, M. Poletto, P. Russo, The effect of mechanical vibration on gas fluidization of a fine aeratable powder, Chemical Engineering Research and Design. 86 (2008) 359-369.
[63] R.V. Daleffe, M.C. Ferreira, J.T. Freire, Effects of binary particle size distribution on the fluid dynamic behaviour of fluidized, vibrated and vibrofluidized beds, Brazilian Journal of Chemical Engineering. 25 (2008) 83-94.
[64] C.C. Xu, J. Zhu, Prediction of the minimum fluidization velocity for fine particles of various degrees of cohesiveness, Chemical Engineering Communications. 196 (2009) 499-517.
[65] J. Yang, T. Zhou, L. Song, Agglomerating vibro-fluidization behavior of nano-particles, Advanced Powder Technology. 20 (2009) 158-163.
[66] S. Kaliyaperumal, S. Barghi, L. Briens, S. Rohani, J. Zhu, Fluidization of nano and sub-micron powders using mechanical vibration, Particuology. 9 (2011) 279-287.
[67] R.D.A.B. Lima, M.D.C. Ferreira, Fluidized and vibrofluidized shallow beds of fresh leaves, Particuology. 9 (2011) 139-147.
[68] J.F. Nunes, F.C.A.D. Alcântara, V.A.D.S. Moris, S.C.D.S. Rocha, Fluid dynamics and coating of sodium bicarbonate in a vibrofluidized bed, Chemical Engineering and Processing: Process Intensification. 52 (2012) 34-40.
[69] L. Zhang, J. Hou, X.T. Bi, J.R. Grace, T. Janke, C. Arato, Fluidization characteristics and charging behavior of fly ash in a vibro-fluidized bed, Powder Technology. 215-216 (2012) 235-241.
[70] D. Barletta, M. Poletto, Aggregation phenomena in fluidization of cohesive powders assisted by mechanical vibrations, Powder Technology. 225 (2012) 93-100.
[71] M. Sadeghi, M.H. Khoshtaghaza, Vibration effect on particle bed aerodynamic behavior and thermal performance of black tea in fluidized bed dryers, J. Agr. Sci. Tech. 14 (2012) 781-788.
[72] X.J. Zhu, D. Jun, Y.F. Li, Hydrodynamic Characteristic of Large Particles in Vibrated Fluidization Bed, Applied Mechanics and Materials. 170-173 (2012) 2454-2457.
[73] M. Leva, Fluidization, McGraw-Hill, New York, 1959.
[74] C.Y. Wen, Y.H. Yu, A generalized method for predicting the minimum fluidization velocity, AIChE Journal. 12 (1966) 610-612.

[75] K. Suzuki, H. Hosaka, R. Yamazaki, G. Jimbo, Drying characteristics of particles in a constant drying rate period in vibro-fluidized bed, Journal of Chemical Engineering of Japan. 13 (1980) 117-122.
[76] K. Suzuki, A. Fujigami, R. Yamazaki, G. Jimbo, Characteristics of vibro-fluidized bed for drying of wetted and agglomerated particles, Journal of Chemical Engineering of Japan. 13 (1980) 495-498.
[77] M. Hasatani, N. Arai, K. Hori, Drying of granular particles in a multistage inclined fluidized bed with mechanical vibration, Drying Technology: An International Journal. 3 (1985) 39-62.
[78] L. Nilsson, R. Wimmerstedt, Drying in longitudinal-flow vibraiting fluid-beds, Drying Technology: An International Journal. 5 (1987) 337-361.
[79] Z.X. Dong, Y.K. Pan, W.Y. Deng, Z. Wei, A.S. Mujumdar, Effect of vibration on the drying rate during the falling rate period, Drying Technology: An International Journal. 9 (1991) 723-733.
[80] Y.K. Pan, Y.M. Gan, X.D. Liu, Z. Wei, A.S. Mujumdar, Drying of sticky granular materials during the constant rate period in a vibrated fluidized bed, Drying Technology: An International Journal. 9 (1991) 1067-1079.
[81] M.N. Ramesh, P.N.S. Rao, Drying studies of cooked rice in a vibrofluidised bed drier, Journal of Food Engineering. 27 (1996) 389-396.
[82] Y.K. Pan, J.Z. Pang, Z.Y. Li, A.S. Mujumdar, T. Kudra, Drying of photosynthetic bacteria in a vibrated fluid bed of solid carriers, Drying Technology: An International Journal. 13 (1995) 395-404.
[83] Y.K. Pan, Z.Y. Li, A.S. Mujumdar, T. Kudra, Drying of a root crop in vibro-fluidized beds, Drying Technology. 15 (1997) 215-223.
[84] Y.K. Pan, H. Wu, Z.Y. Li, A.S. Mujumdar, T. Kudra, Effect of a tempering period on drying of carrot in a vibro-fluidized bed, Drying Technology. 15 (1997) 2037-2043.
[85] Y.K. Pan, L.J. Zhao, Z.X. Dong, A.S. Mujumdar, T. Kudra, Intermittent drying of carrot in a vibrated fluid bed : Effect on product quality, Drying Technology. 17 (1999) 2323-2340.
[86] R. Moreno, R. Rios, H. Calbucura, Batch vibrating fluid bed dryer for sawdust particles : experimental results, Drying Technology. 18 (2000) 1481-1493.
[87] S. Soponronnarit, S. Wetchacama, S. Trutassanawint, W. Jariyatontivaitt, Design, testing, and optimization of vibro-fluidized bed paddy dryer, Drying Technology. 19 (2001) 1891-1908.
[88] Y.K. Pan, J.G. Li, L.J. Zhao, W.H. Ye, A.S. Mujumdar, T. Kudra, Performance characteristics of the vibrated fluid bed of inert particles for drying of liquid feeds, Drying Technology: An International Journal. 19 (2001) 2003-2018.
[89] M.A.A. Cruz, M.L. Passos, W.R. Ferreira, B. Horizonte, Final drying of whole milk powder in vibrated-fluidized beds, Drying Technology. 23 (2005) 2021-2037.
[90] P.I. Alvarez, R. Blasco, J. Gomez, A first principles – Neural networks approach to model a vibrated fluidized bed dryer : Simulations and experimental results, Drying Technology: An International Journal. 23 (2005) 187-203.
[91] V.A. Silva-Moris, S.C.S. Rocha, Vibrofluidized bed drying of adipic acid, Drying Technology. 24 (2006) 303-313.

[92] L. Meili, R.V. Daleffe, M.C. Ferreira, J.T. Freire, Analysis of the influence of dimensionless vibration number on the drying of pastes in vibrofluidized beds, Drying Technology. 28 (2010) 402-411.

[93] M. Stakić, T. Urošević, Experimental study and simulation of vibrated fluidized bed drying, Chemical Engineering and Processing: Process Intensification. 50 (2011) 428-437.

[94] D. Kunii, O. Levenspiel, Fluidization Engineering, Butterworth-Heinemann. E.U.A., 1991.

[95] B. Hardy, ITS-90 Formulations for Vapor Pressure, Frostpoint Temperature, Dewpoint Temperature, and Enhancement Factors in the Range –100 to +100 C, in: The Proceedings of the Third International Symposium on Humidity & Moisture, 1998: pp. 1-8.

[96] Enerji Enstitüsü, URL: http://enerjienstitusu.com/2011/01/11/2011-yili-yeni-elektrik-tarifesi/, June (2013).

APPENDIX A

CALIBRATION

Pressure Transducers

The pressure source was chosen as the fluidized bed system for the calibration of pressure transducers. Pressure difference between the plenum and ambient air was generated by increasing gas flow rate resulting in higher pressure drop of the gas distributor. During a pressure transducer calibration, leaks are a potential source of error. Therefore, Teflon tape was used on all pressure connections. The pressure drop in the plenum was measured by a manometer filled with colored water. The pressure transducer and the manometer were connected to the system alternately while keeping the gas velocity constant. The height of the water column was read from the mm scale attached to the plastic pipe, and then the results were converted to Pascal. The pressure transducers used in this work have an electric voltage output (*V*). This way the output voltage of the transducers and the pressure measured by the manometer could be related. The calibration results of the pressure transducers are given in Figure A.1 and Figure A.2.

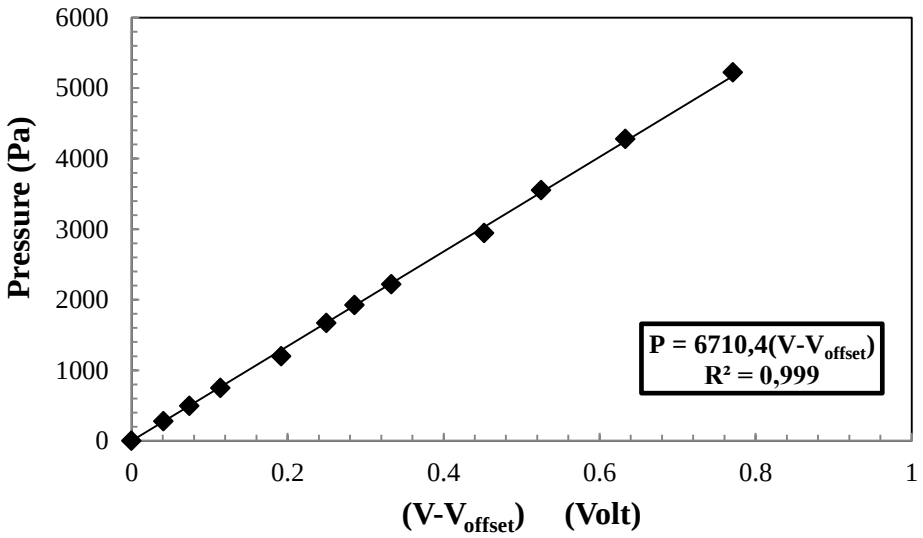

Figure A.1 Calibration graph of PX142-005D5V model pressure transducer (V_{offset} =1.018)

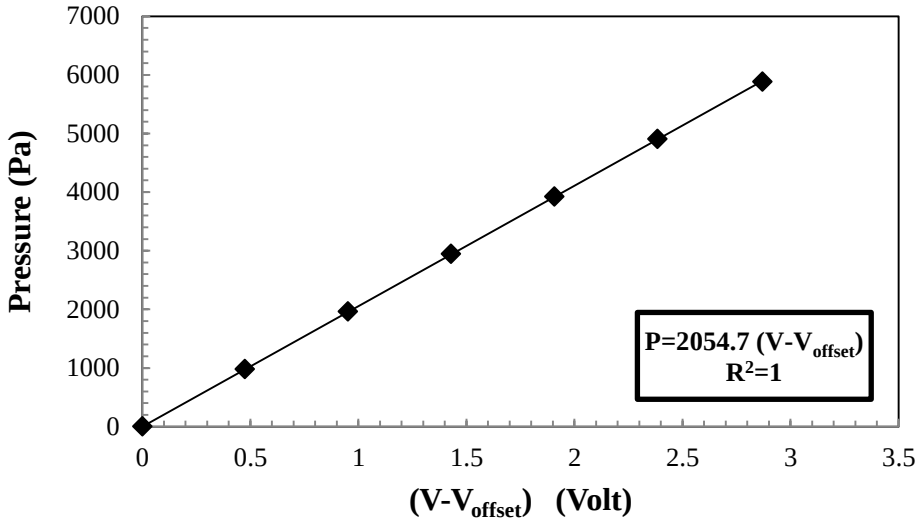

Figure A.2 Calibration graph of Keller 0-160mbar model pressure transducer (V_{offset} =1.918 Volt)

Relative Humidity and Temperature Sensors

The relative humidity sensor was calibrated by using saturated salt solutions and pure nitrogen gas. At a given temperature, it is known that special saturated salt solutions have always a specific humidity value in the atmosphere above. For a three point calibration process of the relative humidity sensor, two data points were obtained by using Potassium Chloride and Potassium Iodide saturated salt solutions. These solutions were put into two different glass bottles with sealable tops. The sensor was firmly placed in the atmosphere above the salt solutions. Then, it was left stabilizing for two hours at a constant temperature. The output voltage was read and recorded. The last output voltage data was recorded at a relative humidity value of zero. For this purpose, the sensor was placed into a duct and pure nitrogen gas was passed through it.

The calibration of temperature sensor was conducted in the fluidized bed dryer system. The sensor was placed in the exhaust duct and the exiting gas temperature was adjusted at different values. The exhaust gas temperature was measured by a J type thermocouple and a mercury thermometer while the output voltage was recorded simultaneously. The calibration graphs of relative humidity and temperature sensors are given below.

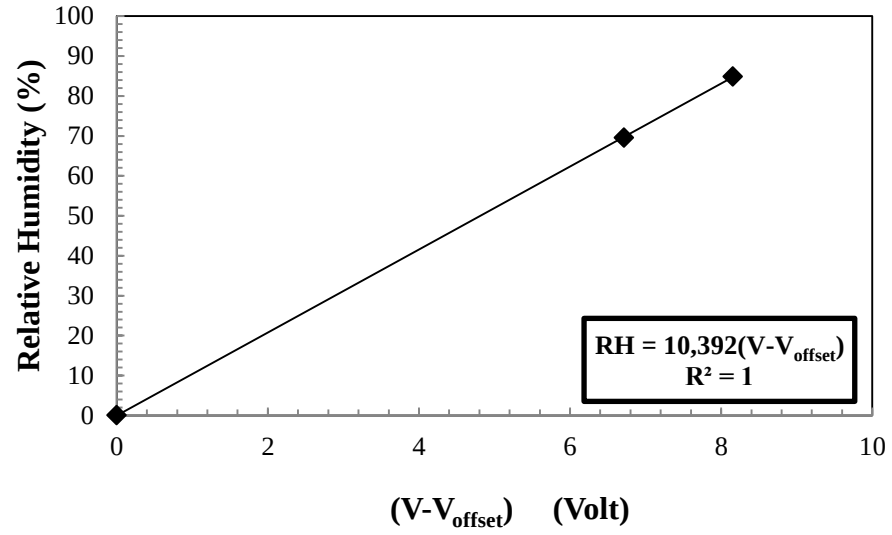

Figure A.3 Calibration graph of PCMini52 model relative humidity sensor (V_{offset}=0.007 Volt)

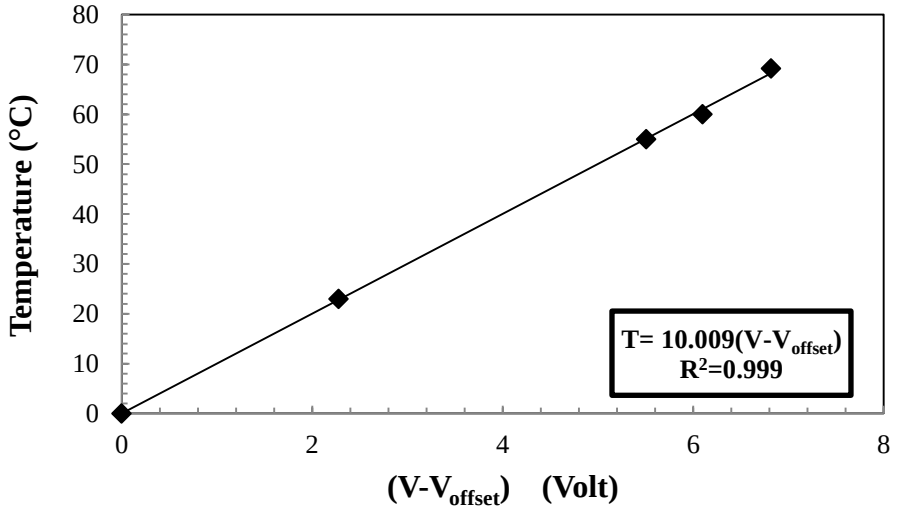

Figure A.4 Calibration graph of PCMini52 model temperature sensor (V_{offset}=2.152 Volt)

MEMS Accelerometer

To calculate the vibration amplitude accurately by measuring the vibration acceleration, the single-axis MEMs accelerometer was calibrated and the result is given in Figure A.5. It is known that an accelerometer positioned stationary on the Earth with its sensitive axis pointing vertically gives an output signal equal to one g. Therefore, rotating the sensitive axis of the accelerometer to the position 0, -90 and +90 degrees from the horizontal, the

accelerometer produced output voltage indicating 0, -g and +g respectively. This operation yielded a three point calibration result.

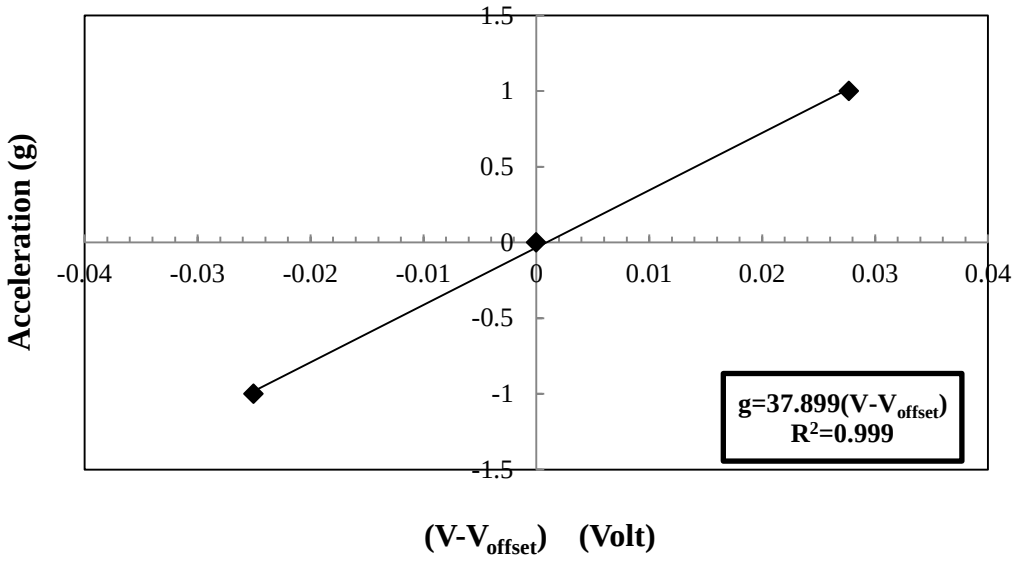

Figure A.5 Calibration graph of MEMs accelerometer (V_{offset}=2.38 Volt)

APPENDIX B

DRYING CURVE GENERATION CODE IN MATLAB

```
clear
clc
format long
disp("""VFB DRYING""");
F=input('Rotameter Reading(mm):');
Mt=input('Initial Mass of Moist Solid(g):');
Ms=input('Mass of Dry Solid(g):');
T1=input('Temperature(C):'); % temperature at the outlet
t=input('Drying Time(s):');
load data.txt
RH=data(:,1);
Rg=296.8;Rv=461.5;Patm=101325;
%ITS-90 Coefficients(g0-g7)
g0=-2.8365744e3;g1=-6.028076559e3;g2=19.54263612;g3=-2.737830188e-2;
g4=1.6261698e-5;g5=7.0229056e-10;g6=-1.8680009e-13;g7=2.7150305;
T=T1+273; % T(C)-->T(K)
%Calculation of Saturation Vapor Pressure(Psat) with Hardy ITS-90 Formula
Psat=exp((g0*T^-2)+(g1*T^-
1)+(g2*T^0)+(g3*T)+(g4*T^2)+(g5*T^3)+(g6*T^4)+(g7*log(T)));
Pv=((RH/100)*Psat);
for k=1:1:((t/2)+1);
Y(k,1)=((Rg/Rv)*(Pv(k,1)/(Patm-(Pv(k,1))))); %Y:Nitrogen humidity(Mixing ratio)
end
R=8314462.1;M=28.02;q=(Patm*M)/(R*T); %q:Density of nitrogen(g/cm3)
Mg=(F*0.13137*pi*4^2)*q; %Mg:Mass flow rate of nitrogen(g/s)
Dd(:,1)=Y(:,1)*(Mg/Ms); %Dd:Drying Rate (dX/dt)in dry basis
for m=1:1:((t/2)+1);
   Dw(m,1)=((Dd(m,1))/(Dd(m,1)+1)); %Dw:Drying Rate (dX/dt)in wet basis
end
x=0:2:t;x=x';
L=[x,Dw];
xlswrite('Dryingrate.xls',L);
subplot(2,1,1)
plot(x,Dw)
xlabel('time(s)')
```

```
ylabel('Drying Rate(dX/dt)')
grid off
%SYMPSON'S RULE
h=2;   % value of the sub-interval for sympson’s rule
for i=1:2:((t/2)-1);
   Dd(i+2,2)=(h/3)*(Dd(i,1)+4*Dd(i+1,1)+Dd(i+2,1));
end
SYMPSONdrybasis=sum(Dd(:,2))
%DRYING CURVE
K=(Mt-Ms)/Ms;
for j=1:2:((t/2)-1);
   %cumulative summation of fraction values obtained by SYMPSON's RULE at every 4
seconds (As data are avaliable at 0,2,4--4,6,8..intervals)
   Dd(j+2,3)=sum(Dd((1:(j+2)),2));
   Dd(j+2,4)=K-Dd(j+2,3);
   O(j,1)=Dd(j+2,4);
   %Conversion of dry basis to wet basis--
   %PERCENTAGE(results are multiplied by 100)
   X((j+1)/2,1)=((O(j,1))/((O(j,1))+1)*100);
end
p=0:4:(4*(length(X(:,1)))-1);p=p';
U=[p,X];
xlswrite('Dryingcurve.xls',U);
subplot(2,1,2)
plot(p,X)
xlabel('time(s)')
ylabel('Moisture Content (%w.b.)')
grid off
```

APPENDIX C

REPRODUCIBILITY OF DRYING TESTS

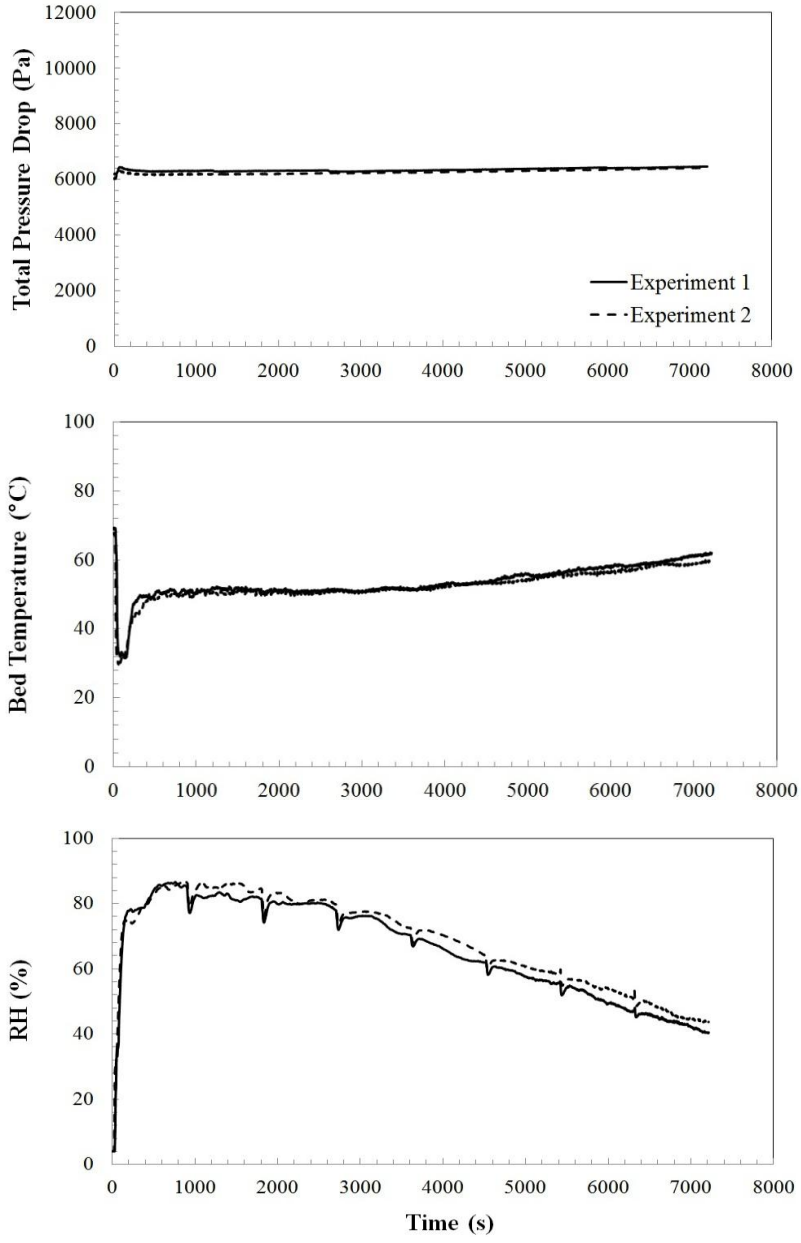

Figure C.1 Reproducibility of drying tests (T_{in}=60 °C, T_{out}=55°C, U_o=10.5 mm/s)

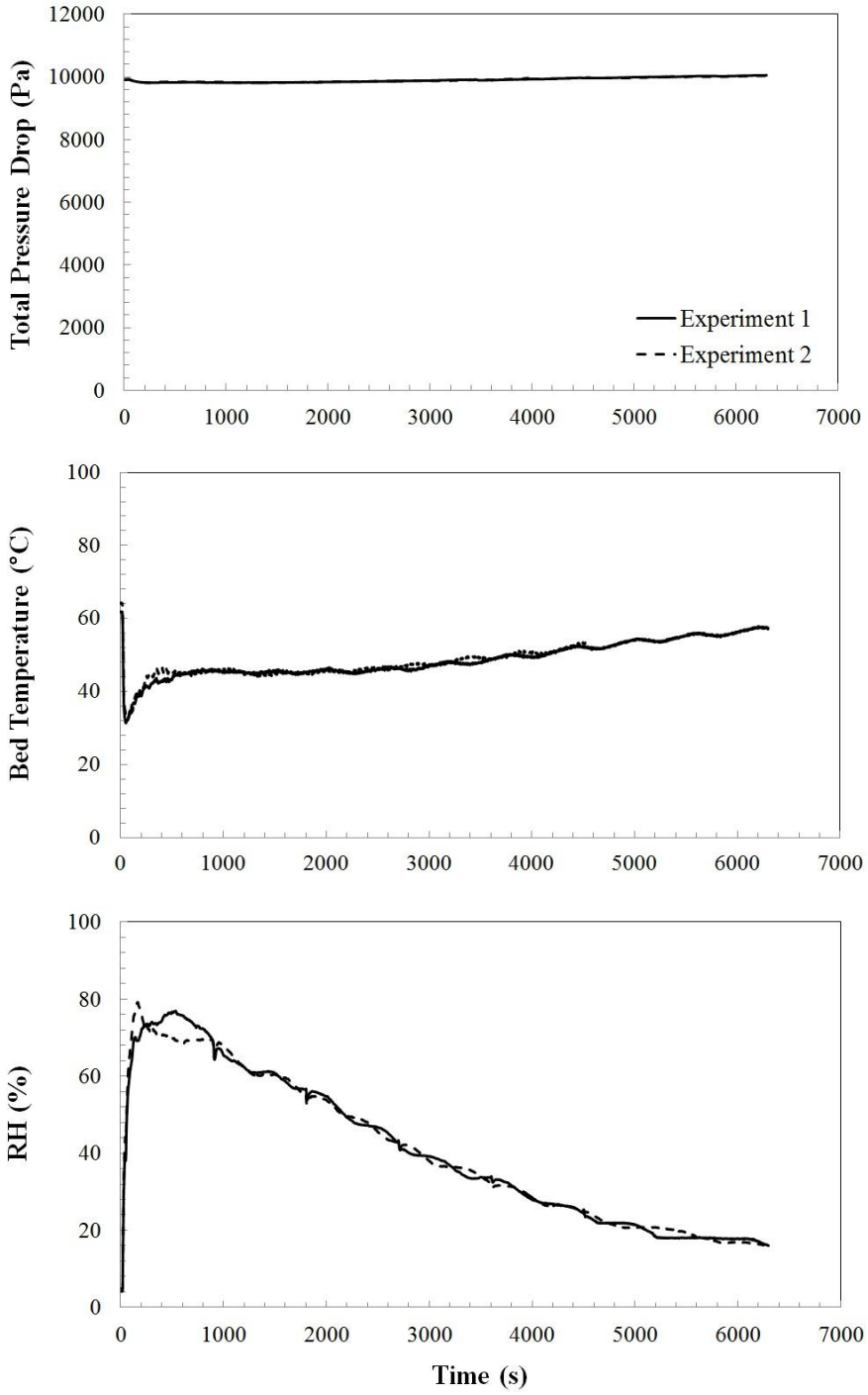

Figure C.2 Reproducibility of drying tests (T_{in}=60 °C, T_{out}=55°C, U_o=21 mm/s)

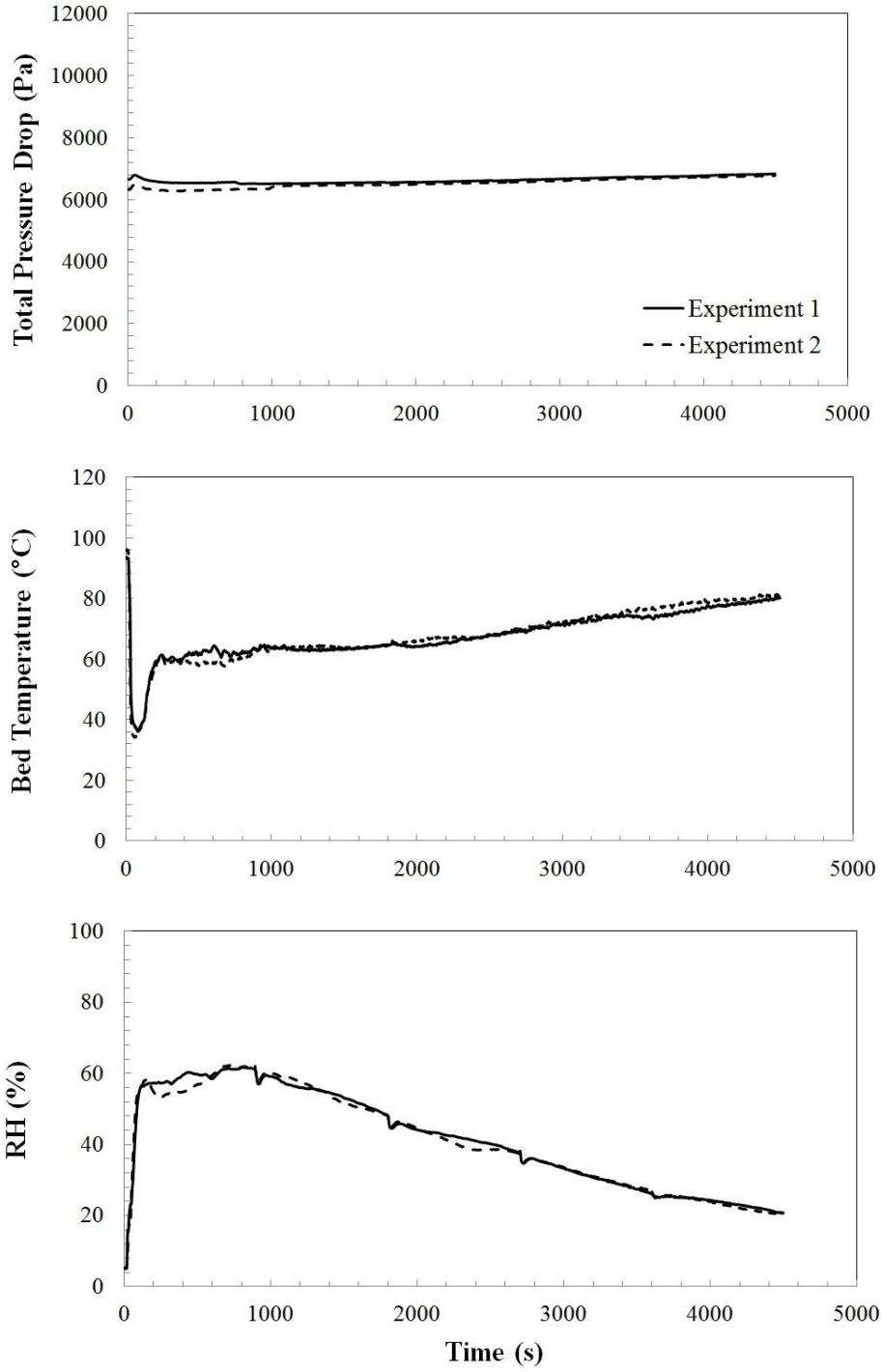

Figure C.3 Reproducibility of drying tests (T_{in}=80 °C, T_{out}=77°C, U_o=10.5 mm/s)

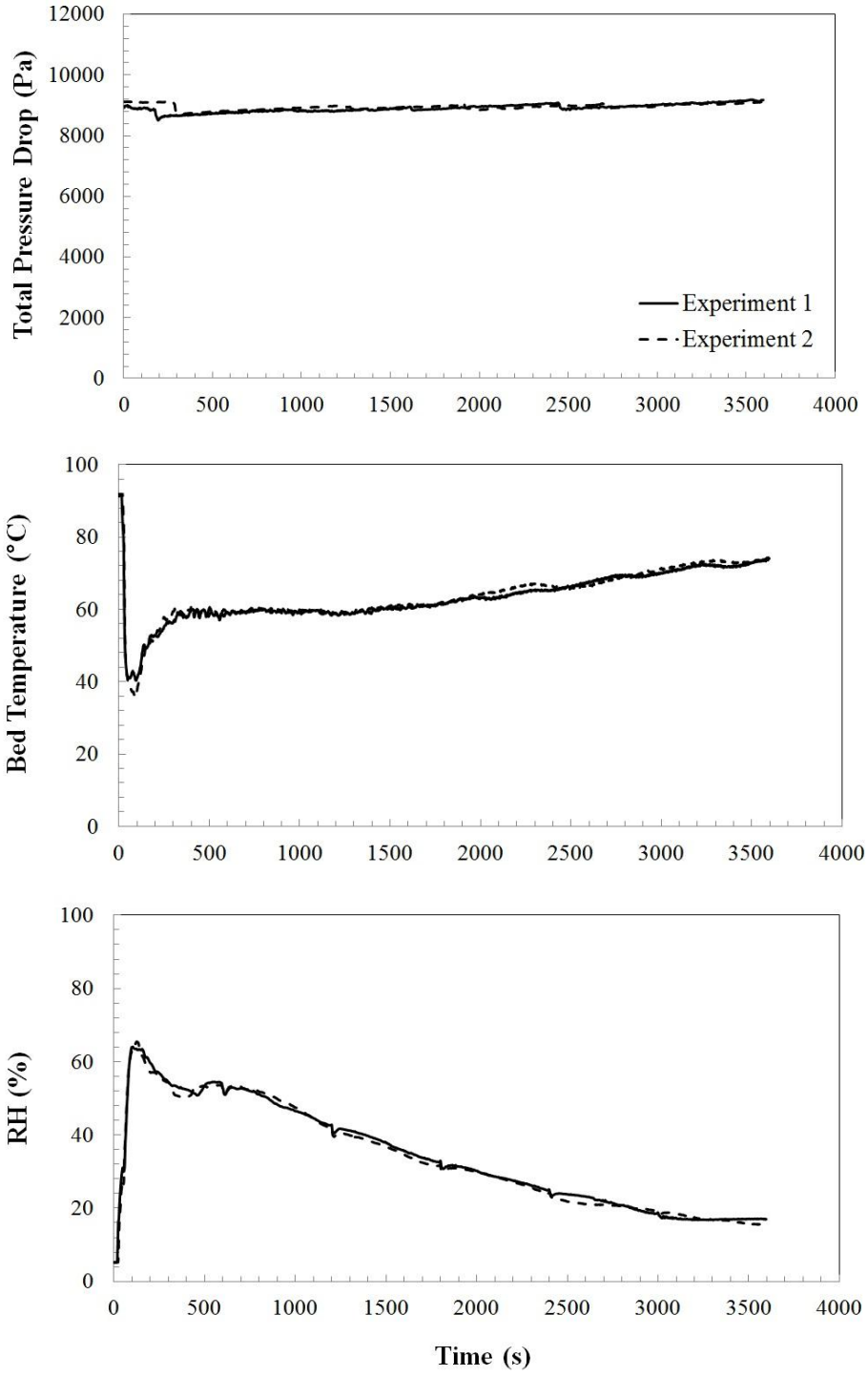

Figure C.4 Reproducibility of drying tests (T_{in}=80 °C, T_{out}=77°C, U_o=15.8 mm/s)

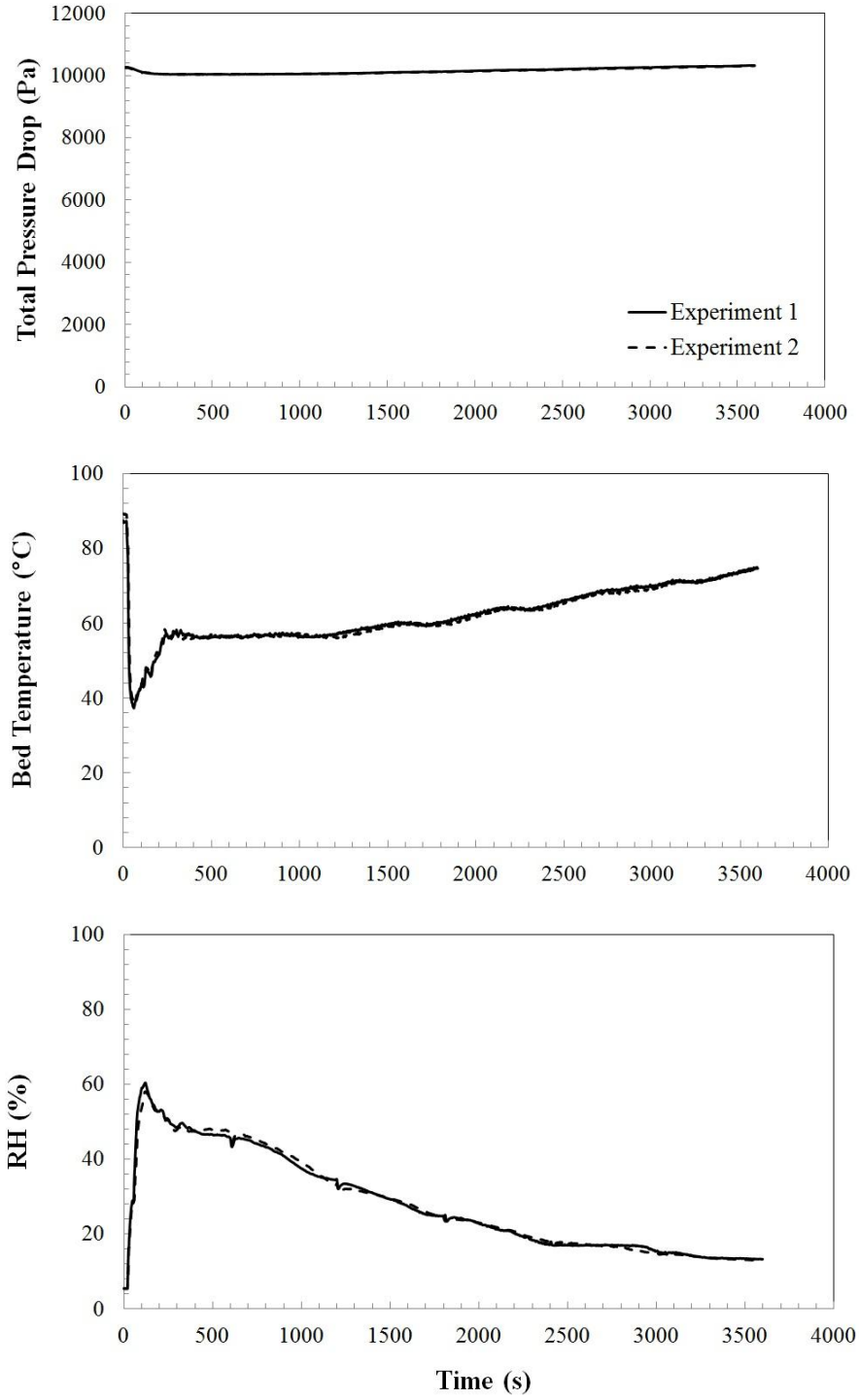

Figure C.5 Reproducibility of drying tests (T_{in}=80 °C, T_{out}=77°C, U_o=21 mm/s)

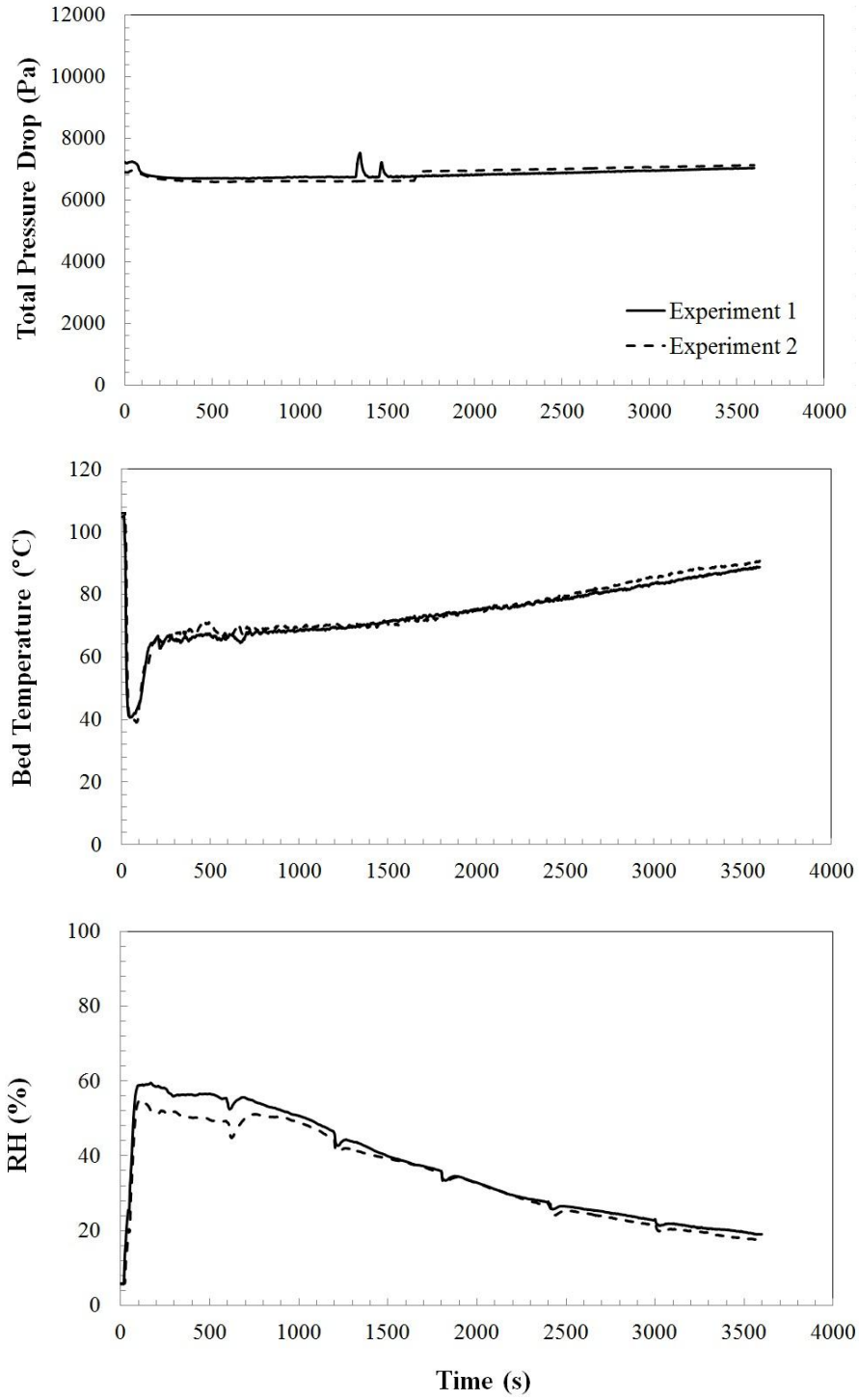

Figure C.6 Reproducibility of drying tests (T_{in}=90 °C, T_{out}=85.5°C, U_o=10.5 mm/s)

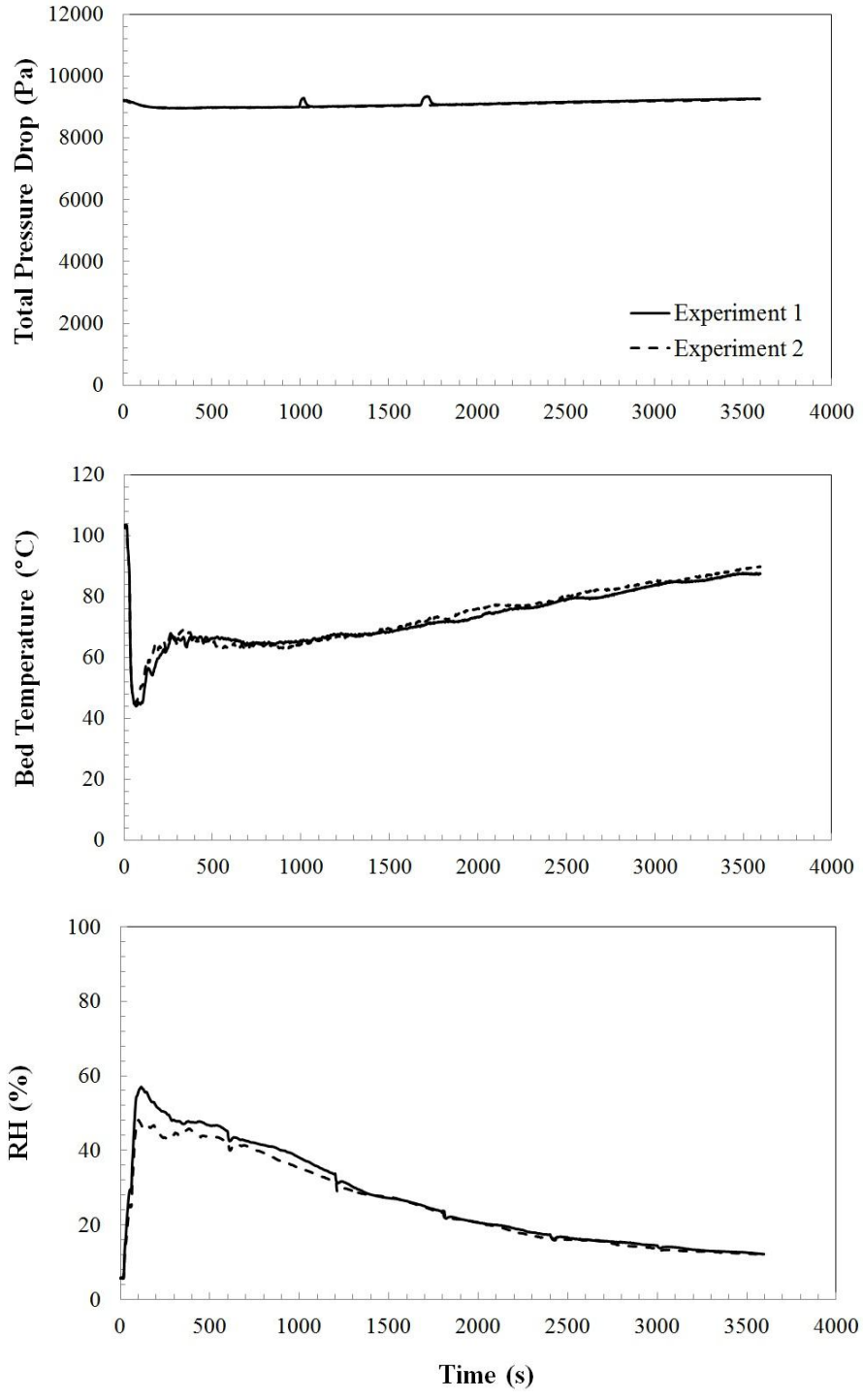

Figure C.7 Reproducibility of drying tests (T_{in}=90 °C, T_{out}=85.5°C, U_o=15.8 mm/s)

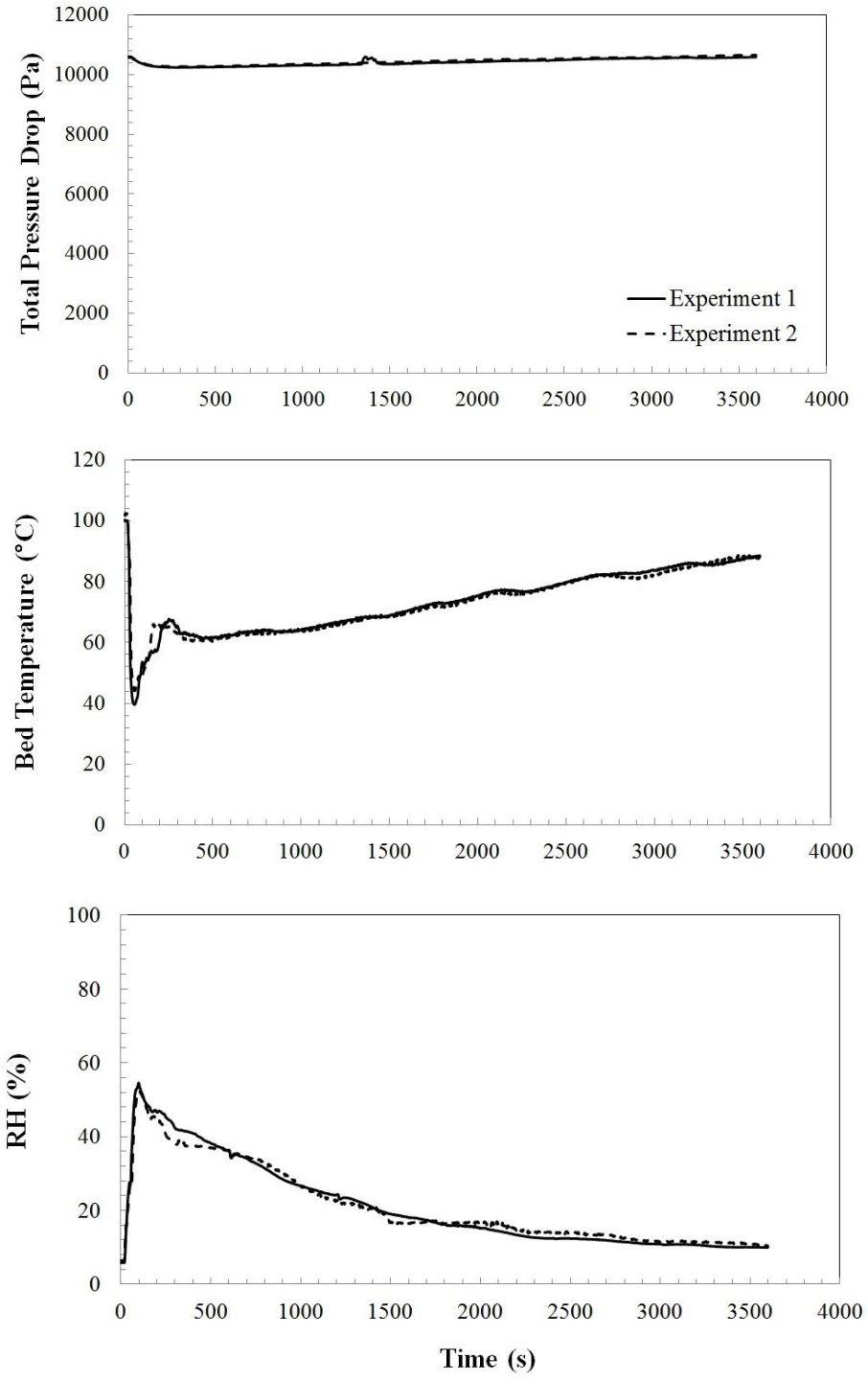

Figure C.8 Reproducibility of drying tests (T_{in}=90 °C, T_{out}=85.5°C, U_o=21 mm/s)

APPENDIX D

SAMPLE CALCULATION FOR COST ANALYSIS

Wet clinoptilolite powders with a mass flow rate of 1000 kg/h and an initial moisture content of 16 % (w.b.) at 20 °C are to be dried to moisture content of 8 % (w.b.). The expanded bed height (H) is 14 cm and the apparent bed density (ρ_a) is 426.3 kg/m^3 throughout the operation. The equations used for the calculation are:

$$A = \frac{\dot{M}_s \; t_R}{H \; \rho_a} \tag{D.1}$$

$$\dot{M}_g = \rho_g \; U_0 \; A \tag{D.2}$$

$$Q = \dot{M}_g C_{pg} (T - T_{amb.}) \tag{D.3}$$

$$Cost = (Q)\;(W)\;(t) \tag{D.4}$$

where A is bed area of the dryer (m^2), $\dot{M}_s$ is mass flow rate of solids (kg dry solid/s), t_R is mean particle residence time, Q is heat transfer rate (kJ/s), $T_{amb.}$ is the ambient temperature of drying gas (K), $Cost$ is the electrical energy cost for heating ambient air (TL), W is the electrical energy cost for industrial site (Kr/kW-h) and t is the drying time (24 h for a daily operation).

For a continuous well-mixed vibrated fluidized bed drying operation at the conditions of 90 °C air inlet temperature and 10.5 mm/s air velocity, a sample calculation procedure is explained step by step below:

Mass flow rate of dry solid is calculated from mass flow rate of wet solid:

$$\dot{M}_s = 1000 \; \frac{kg \; wet \; solid}{h} \; \frac{1 \; kg \; dry \; solid}{1.19 \; kg \; wet \; solid} \; \frac{1 \; h}{3600 \; s}$$

$$\dot{M}_s = 0.233 \; kg \; dry \; solid/s$$

For the selected conditions, mean particle residence time is 37.2 min. (Table 4.1). Then, bed area of the dryer is given by

$$A = \frac{(0.233\ kg\ dry\ solid/s)(2232\ s)}{(0.14\ m)(426.3\ kg/m^3)} = 8.71\ m^2$$

Mass flow rate of drying air is calculated as

$$\dot{M}_g = (1\ kg/m^3)\ (0.0105\ m/s)\ (8.71\ m^2)\ \cong 0.092\ kg/s$$

Heat transfer rate can be obtained by

$$Q = (0.092\ kg/s)(1\ kJ/kg\ K)(363\ K - 293\ K)\ = 6.44\ kJ/s$$

Finally, assuming the system is well-insulated, the specific operating cost for a daily operation of 24 hours can be given as

$$Cost = (6.44\ kW)\ (0.2273\ TL/kW - h)\ (24\ h)\ \cong 35.13\ TL$$